CHAPTER 5   RESULTS

5.1   Surface Characterization

5.1.1   Chemical Composition

The chemical composition of the surfaces of samples was determined using XPS. The quantitative measurements of detected elements were presented as Atomic Percent Concentration while the qualitative measurements were determined by high-resolution scans in terms of peak fittings of detected elements.

5.1.1.1   Atomic Percent Concentration

Table 5-1 (see, p75) shows the different samples with their atomic percent composition. The dominant signals are Carbon, Oxygen and Titanium with weaker contributions from Aluminium and Sodium. Other occasional smaller signals from Calcium, Zinc, Lead, Nitrogen, Zirconium and Vanadium were observed.

Carbon, Oxygen and Titanium were found in varying amounts on samples. Oxygen was observed to have the highest atomic percent concentration for most samples. Aluminium was found on all except the cpTi machined control samples. Sodium was detected on all cast, but only Ti6Al4V machined (SI) samples. Though in small amounts, Calcium was detected on all samples, with the exception of RFGDT machined cpTi and Ti6Al4V control samples. Lead was present only on machined cpTi and Ti6Al4V control surfaces and disappeared with RFGDT. Zinc and Nitrogen were present mostly on untreated samples and disappeared with RFGDT. Vanadium was detected on Ti6Al4V (machined and cast) control samples before RFGDT. Enhanced samples had no Vanadium detected. Zirconium showed up after the RFGDT of all cast samples and some machined samples.

Table 5-1: A summary of the elemental composition of sample surfaces (At %)

Element	C	O	Ti	Al	Na	Zn	Pb	Ca	N	V	Zr
cpTi machined control surface	37.7	45.8	11.2	0.0	0.0	2.7	0.5	0.6	1.4	0.0	0.0
cpTi machined control surface RFGDT	20.8	56.4	21.6	0.0	0.0	0.0	0.0	0.0	0.8	0.0	0.4
cpTi machined SI Enhanced	41.5	43.6	7.2	5.2	0.0	0.5	0.0	0.4	0.0	0.0	0.0
cpTi machined SI Enhanced RFGDT	19.9	52.7	12.9	9.7	0.0	0.0	0.0	0.3	0.0	0.0	0.0
cpTi machined ES Enhanced	29.5	51.4	8.8	5.8	0.0	1.4	0.0	0.9	0.0	0.0	0.0
cpTi machined ES Enhanced RFGDT	15.1	55.9	14.7	7.5	0.0	0.0	0.0	0.4	0.0	0.0	0.0
Ti6Al4V machined control surface	36.8	48.7	10.3	1.1	0.0	2.1	0.3	0.3	0.5	0.9	0.0
Ti6Al4V machined control surface RFGDT	21.8	56.7	18.8	1.1	0.0	0.0	0.0	0.0	0.0	0.0	0.7
Ti6Al4V machined SI Enhanced	36.7	43.8	4.2	8.7	5.9	0.0	0.0	0.2	0.5	0.0	0.0
Ti6Al4V machined SI Enhanced RFGDT	14.9	55.3	12.9	9.8	6.2	0.2	0.0	0.3	0.0	0.0	0.4
Ti6Al4V machined ES Enhanced	29.2	52.2	5.5	9.5	0.0	0.7	0.0	0.8	0.0	0.0	0.0
Ti6Al4V machined ES Enhanced RFGDT	16.1	55.5	13.7	9.2	0.0	0.0	0.0	0.3	0.0	0.0	0.0
cpTi cast control surface	23.6	53.6	5.3	12.7	4.6	0.0	0.0	0.2	0.0	0.0	0.0
cpTi cast control surface RFGDT	15.1	57.9	9.2	12.9	4.7	0.0	0.0	0.4	0.0	0.0	0.2
cpTi cast SI Enhanced	37.3	43.9	4.3	10.5	2.2	0.2	0.0	0.5	1.1	0.0	0.0
cpTi cast SI Enhanced RFGDT	15.5	56.3	14.6	8.2	4.5	0.0	0.0	0.4	0.0	0.0	0.5
cpTi cast ES Enhanced	25.6	52.9	7.1	9.8	3.3	0.7	0.0	0.5	0.0	0.0	0.0
cpTi cast ES Enhanced RFGDT	23.1	51.3	12.9	7.9	3.0	0.0	0.0	0.5	0.9	0.0	0.3
Ti6Al4V cast control surface	28.7	51.4	5.6	9.6	3.3	0.0	0.0	0.4	0.8	0.2	0.0
Ti6Al4V cast control surface RFGDT	25.3	55.4	6.2	10.5	1.5	0.0	0.0	1.0	0.0	0.0	0.1
Ti6Al4V cast SI Enhanced	32.7	47.7	8.4	8.0	2.2	0.1	0.0	0.2	0.7	0.0	0.0
Ti6Al4V cast SI Enhanced RFGDT	14.9	55.5	9.9	15.1	3.5	0.0	0.0	0.1	0.0	0.0	0.4
Ti6Al4V cast ES Enhanced	28.9	52.3	4.8	10.1	2.4	0.5	0.0	0.6	0.4	0.0	0.0
Ti6Al4V cast ES Enhanced RFGDT	15.9	56.6	12.6	10.9	3.2	0.0	0.0	0.4	0.0	0.0	0.4

XPS survey spectra

A typical XPS survey spectrum of a cpTi cast sample before RFGDT is shown in Fig 5-1 and after RFGDT in Fig 5-2 (see p77). XPS spectra for all other samples are given in Addendum H (see p200-209). The spectrum depicts elements with binding energies from 0 to 1100eV that are detected from the surface layer of samples. Every element has its own binding energy value and detected peaks were identified by the computer database in most instances and counterchecked (Moulder et al, 1992). Major lines identified were Carbon (1s), Titanium (2p) and Oxygen (1s). Associated weaker lines were also identified but not further monitored.

ESCA SURVEY   4/10/91   ANGLE= 65 deg   ACQ TIME=9.17 min
FILE: f27I1 Carneiro - Ti F
SCALE FACTOR= 0.759 k c/s,   OFFSET= 0.004 k c/s   PASS ENERGY= 44.750 eV   Al   300 W
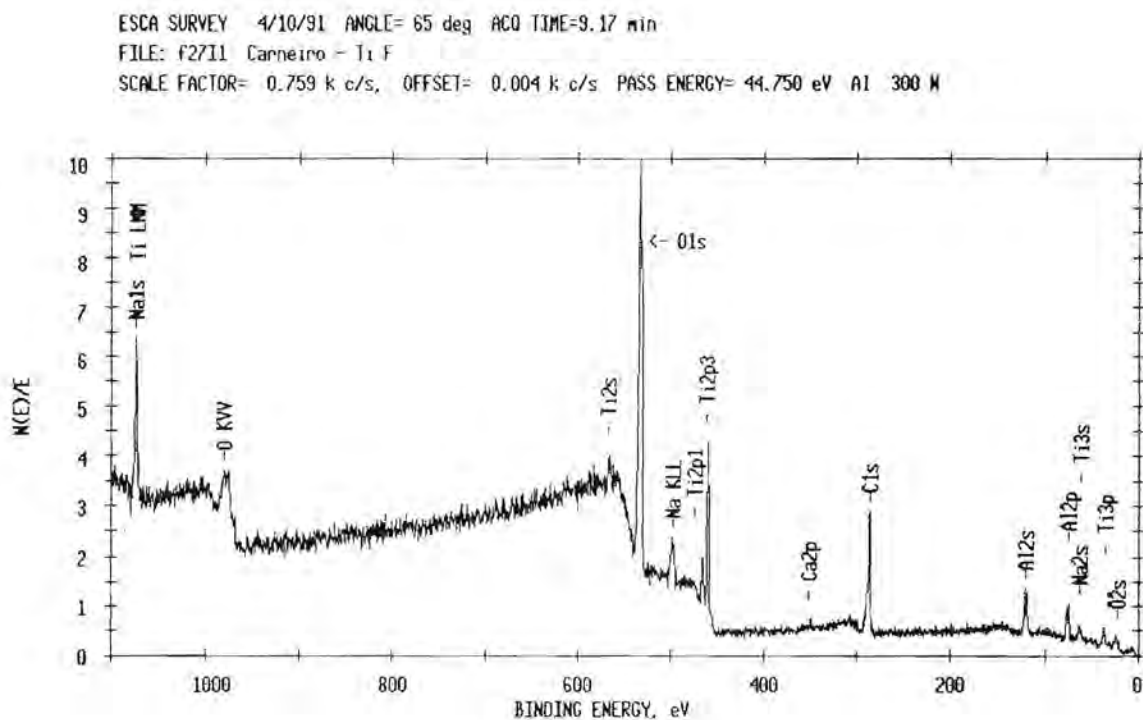
Fig 5-1: XPS survey spectra for cpTi cast control sample surface before RFGDT

ESCA SURVEY   4/10/91   ANGLE= 65 deg   ACQ TIME=9.17 min
FILE: f27H1 Carneiro - Ti FG
SCALE FACTOR= 0.903 k c/s,   OFFSET= 0.004 k c/s PASS ENERGY= 44.750 eV Al 300 W
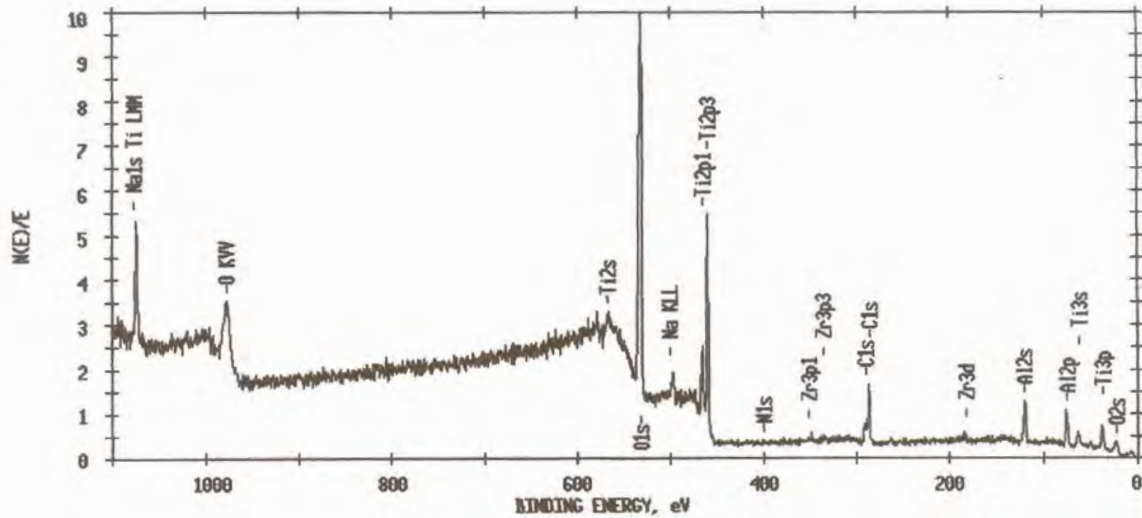
Fig 5-2: XPS survey spectra for cpTi cast control sample surface after RFGDT

Differences in the survey spectra of RFGDT cpTi machined and cast and Ti6Al4V machined and cast samples of control surfaces are shown in Fig 5-3 and Fig 5-4 (see p78), respectively.

ESCA SURVEY   4/10/91   ANGLE= 65 deg   ACQ TIME=9.17 min
FILE: f27H1 Carneiro - Ti FG
SCALE FACTOR= 0.903 k c/s,   OFFSET= 0.004 k c/s PASS ENERGY= 44.750 eV Al 300 W
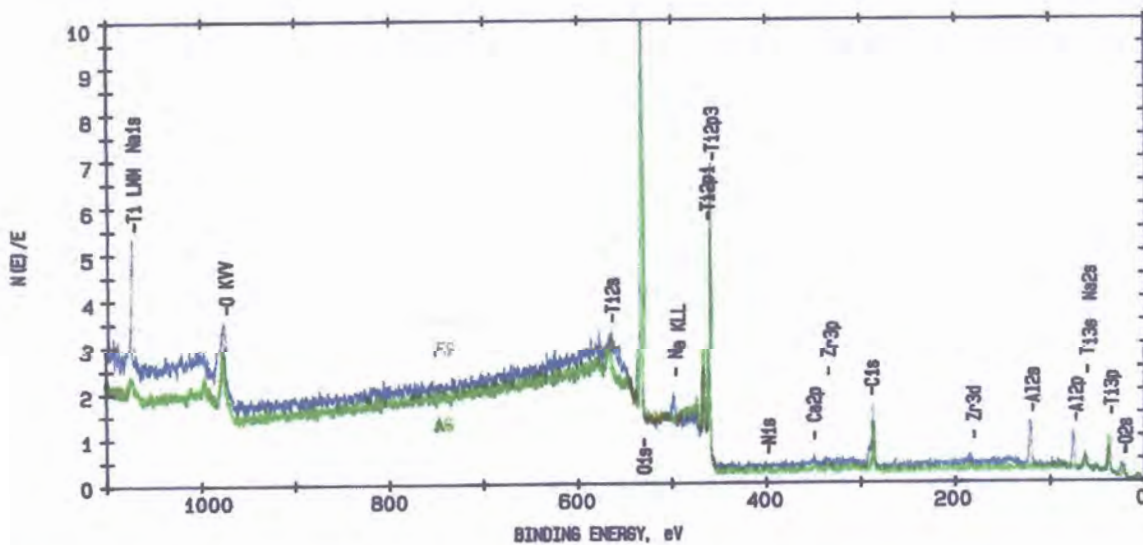
Fig 5-3: XPS survey spectra of cpTi machined RFGDT sample (AG=green) and cpTi cast RFGDT sample (FG=blue) of control surfaces

ESCA SURVEY   4/15/91   ANGLE= 65 deg   ACQ TIME=14.67 min
FILE: f32C3   Carneiro - Ti alloy cast H6
SCALE FACTOR= 0.682 k c/s,   OFFSET= 0.005 k c/s   PASS ENERGY= 44.750 eV   Al   300 W
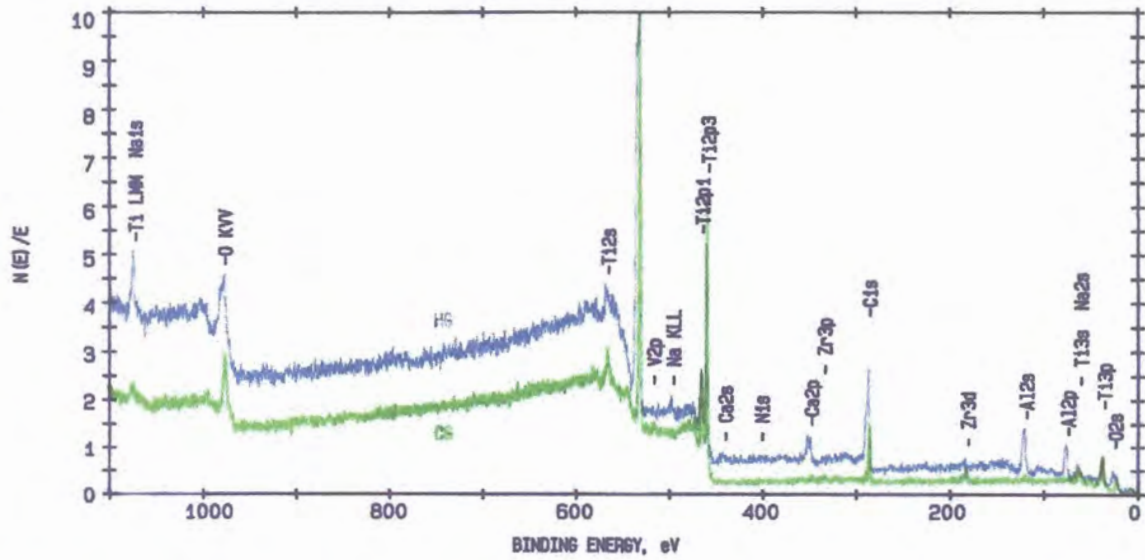
Fig 5-4: XPS survey spectra of Ti6Al4V machined RFGDT sample (CG=green) and Ti6Al4V cast RFGDT sample (HG=blue) of control surfaces

Carbon

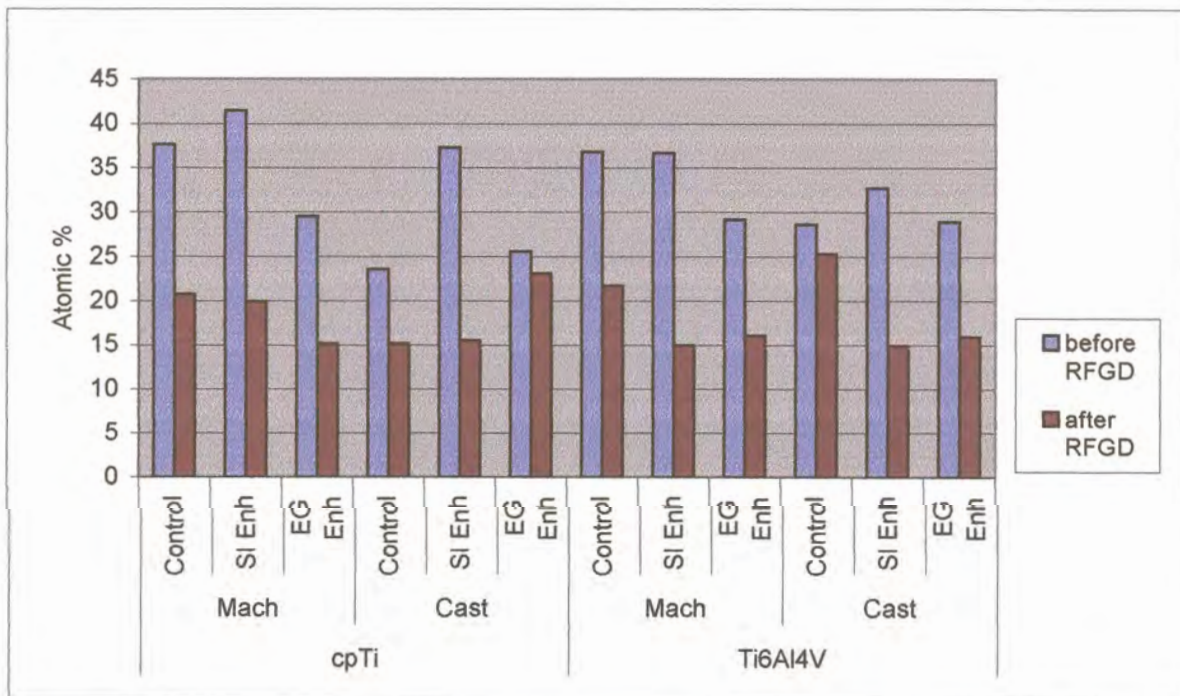Data of the atomic percent concentration of Carbon for all samples before and after RFGDT is shown in Fig 5-5.

Fig 5-5: Atomic percent concentration of Carbon before and after RFGDT of sample surfaces

On average RFGDT significantly reduced the surface Carbon atomic percent concentration from 32.4% to 18.2% ($p<0.05$). An interaction between RFGDT and surface enhancement showed that the untreated control and SI enhanced samples had significantly higher surface Carbon content than treated samples ($p=0.02$).

No significant differences were observed in Carbon atomic percent concentration between the different materials used, method of fabrication employed or surface enhancement procedures other than RFGDT.

Oxygen

The surface Oxygen atomic concentration percent of samples before and after RFGDT is shown in Fig 5-6 (see p80).

A significant difference in surface Oxygen atomic percent concentration was observed between samples that were differently enhanced ($p=0.0025$). On average the SI enhanced samples had significantly lower surface Oxygen atomic percent (49.9%) compared to ES enhanced and control samples (53.5% and 53.2% respectively).

RFGDT significantly enhanced the average surface Oxygen level from 49.0% to 55.4 % ($p<0.05$). A significant interaction was observed between surface enhancement and RFGDT ($p=0.0045$) depicting that enhanced surfaces that were treated had significantly higher surface Oxygen content than untreated enhanced samples.

No significant difference in the Oxygen content was observed between materials used or fabrication procedures adopted.
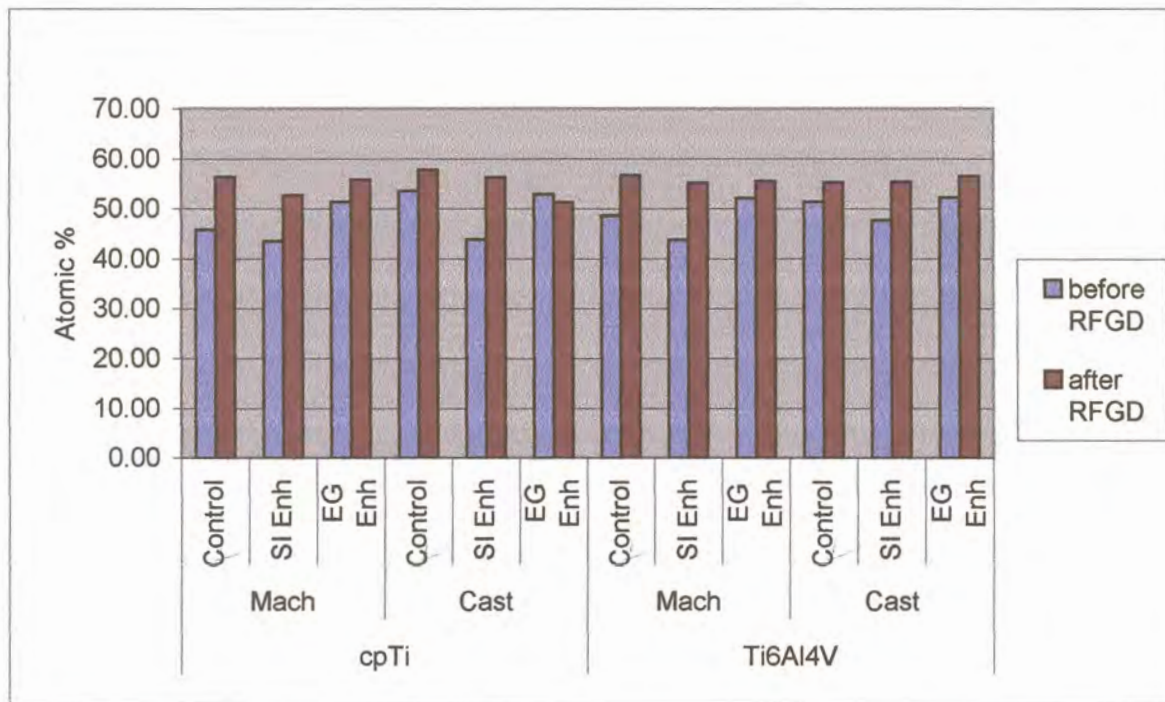
Fig 5-6: Atomic percent concentration of Oxygen before and after RFGDT of sample surfaces

Titanium

Fig 5-7 (see p81) shows the atomic percent concentration of Titanium for the different samples.

The fabrication procedure significantly decreased Titanium levels (p-0.0004). On average higher Titanium atomic percent concentration was measured on the surfaces of machined samples (11.8%) than cast samples (8.4%). RFGDT samples had on average significantly higher measured Titanium percentages on their surfaces (13.3%) compared to untreated samples (6.9%). There was an interaction between the method of fabrication and surface enhancement (p-0.0005) and machined control samples had on average significantly higher measured surface Titanium percentages (15.5%) than the enhanced machined surfaces (SI and ES) or cast samples.
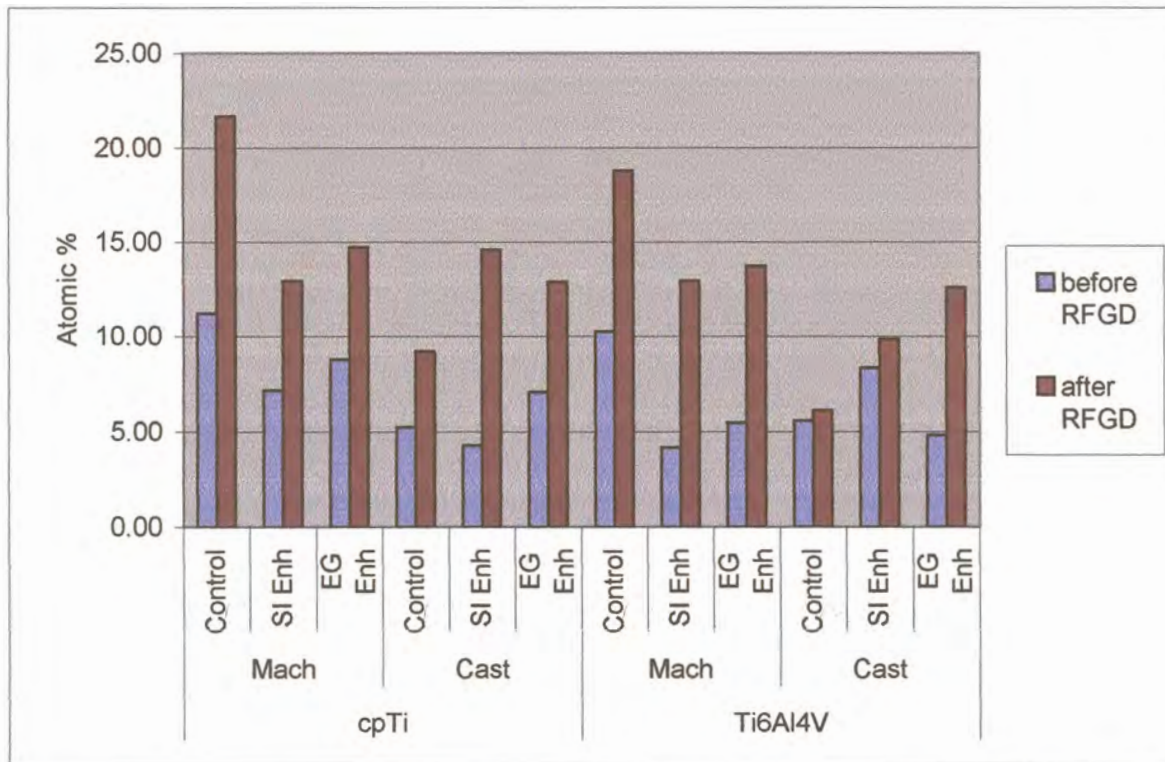
Fig 5-7: Atomic percent concentration of Titanium before and after RFGDT of sample surfaces

Aluminium

The observed XPS values for the Aluminium atomic percent concentration of samples are shown in Fig 5-8 (see p82).

The surface Aluminium atomic percent concentration increased significantly with method of fabrication ($p<0.05$). On average cast sample surfaces (10.5%) showed significantly higher Aluminium concentrations than machined sample surfaces (5.6%). Surface enhancement significantly affected the Aluminium surface concentration ($p=0.005$). Enhanced surfaces recorded significantly higher Aluminium than control surfaces. Interaction between method of fabrication and surface enhancement ($p=0.0002$) showed that on average machined control surfaces (0.6%) have significantly lower Aluminium content compared to cast control sample (11.4%) and other sample surfaces. Material used for fabrication or RFGDT did not have any significant effect on the surface Aluminium content in samples.
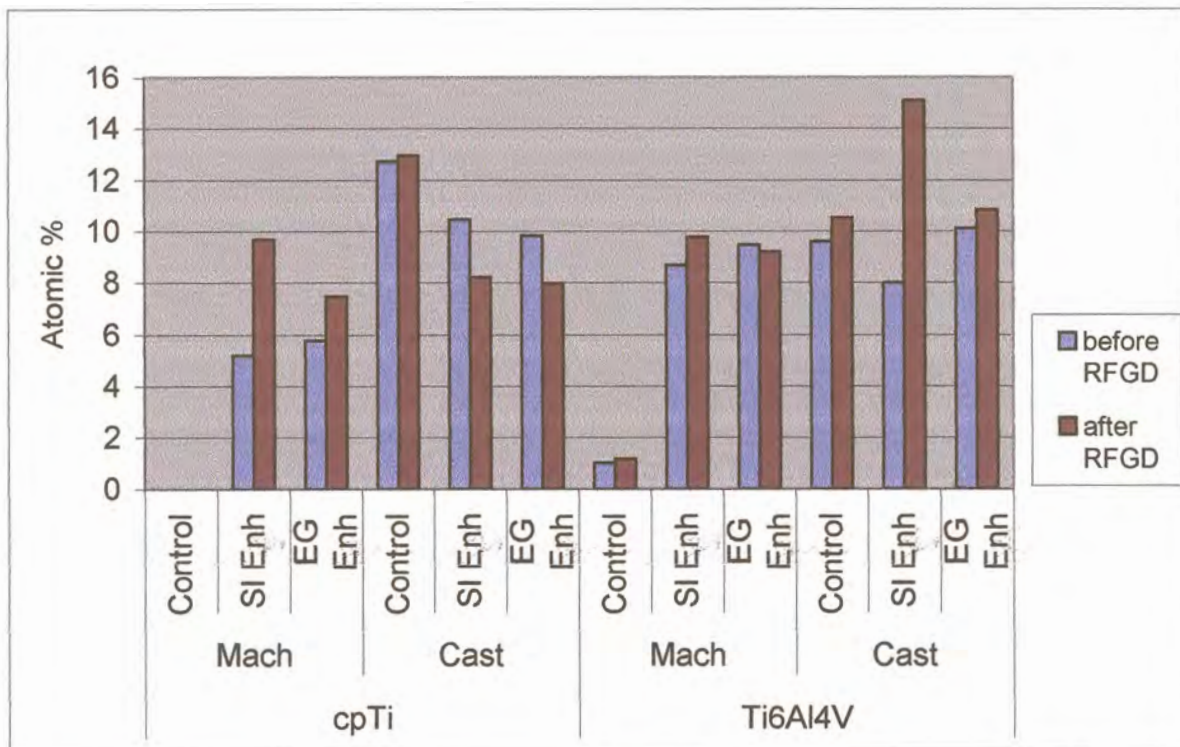
Fig 5-8: Atomic percent concentration of Aluminium before and after RFGDT of sample surfaces

Sodium

Fig 5-9 (see p83) shows the atomic percent concentration of Sodium for the different samples.

The method of fabrication of samples significantly increased the Sodium surface concentration. On average cast samples (3.1%) had significantly higher surface Sodium content than machined samples (1.0%) (p=0.0002). SI enhanced samples (3.1%) had significantly higher surface Sodium concentration compared to other enhanced samples (p=0.02). There was an interaction between material used and fabrication procedure adopted (p=0.0039). On average cpTi machined samples were observed to have significantly lower surface Sodium concentration (0.0%) compared to Ti6Al4V machined and cast samples (3.7%). The interaction between material employed and surface enhancement showed that on average Ti6Al4V SI enhanced surfaces (4.4%) had significantly higher surface Sodium concentration compared to other samples (p=0.0079). When the fabrication process was related to surface enhancement it was significant that

machined control and experimental enhanced samples had lower surface Sodium concentration compared to other samples (p=0.0147).
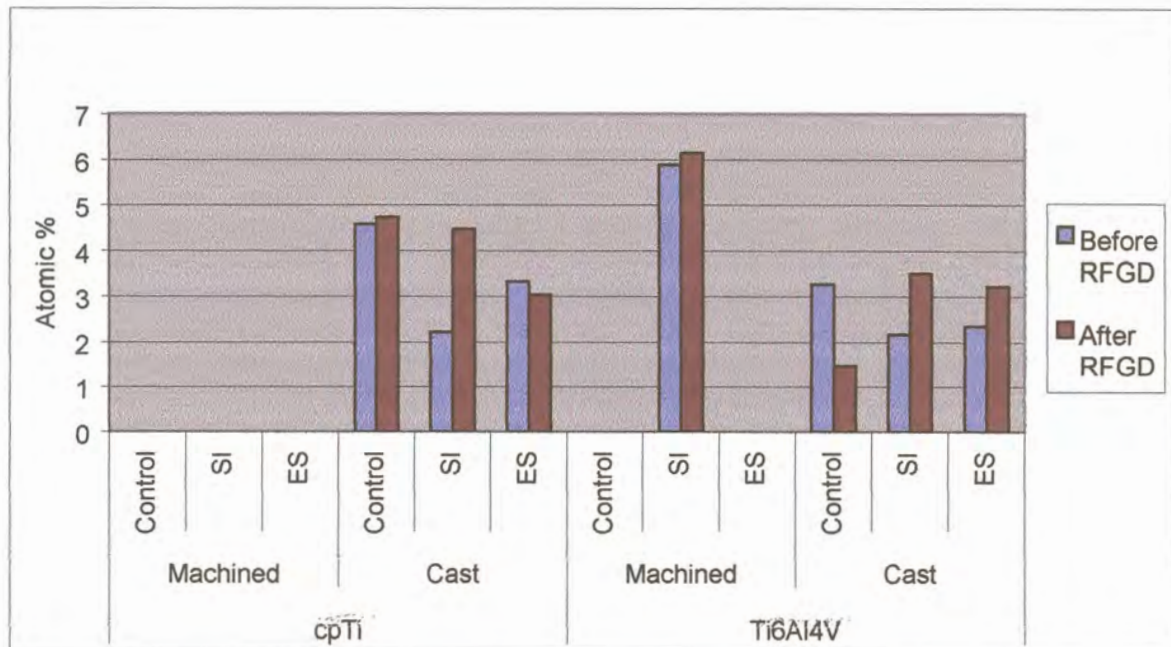

Fig 5-9: Atomic percent concentration of Sodium before and after RFGDT of sample surfaces

5.1.1.2 Curve Fitting

Carbon sub peaks

Deconvolution of high-resolution spectra of the Carbon 1s peak revealed four components for most samples. Table 5-2 (see p84) shows the contribution of each individual sub peak to the Carbon envelope for samples.

The major sub peak of Carbon for most sample surfaces was at ~285eV indicating adventitious Carbon. The remaining sample surfaces had peaks at ~286eV that can be assigned to Carbon bonded with Oxygen or Nitrogen (Moulder et al, 1992). Other sub peaks were recorded between ~287 and 290eV. The peak at ~286eV can also be assigned to hydroxyls (C-OH), while the peaks between ~288-290eV can be assigned to carboxyl (Louw, 1997).

Table 5-2: Deconvoluted Carbon 1s envelope with respective sub peak positions (Bold figures indicate highest peak).

Element	Peak I	Peak II	Peak III	Peak IV
cpTi machined control surface	**286.0**	287.3	289.8	
cpTi machined control surface RFGDT	**285.8**	287.2	289.6	
cpTi machined SI Enhanced	**285.7**	286.7	288.1	289.6
cpTi machined SI Enhanced RFGDT	**285.7**	286.9	288.6	289.8
cpTi machined ES Enhanced	**285.9**	287.4	289.7	
cpTi machined ES Enhanced RFGDT	**285.9**	287.5	289.8	
Ti6Al4V machined control surface	**285.8**	287.3	289.7	
Ti6Al4V machined control surface RFGDT	**285.8**	287.4	289.7	
Ti6Al4V machined SI Enhanced	**285.9**	286.9	288.3	290.2
Ti6Al4V machined SI Enhanced RFGDT	**285.5**	286.6	288.6	289.9
Ti6Al4V machined ES Enhanced	**285.9**	287.4	288.6	289.8
Ti6Al4V machined ES Enhanced RFGDT	**285.6**	286.6	288.4	289.9
cpTi cast control surface	**286.4**	287.8	290.3	
cpTi cast control surface RFGDT	**286.4**	287.8	290.4	
cpTi cast SI Enhanced	**286.0**	287.0	288.3	289.9
cpTi cast SI Enhanced RFGDT	**285.7**	286.7	288.3	289.8
cpTi cast ES Enhanced	**285.7**	286.9	287.9	289.6
cpTi cast ES Enhanced RFGDT	**285.7**	286.8	288.4	289.7
Ti6Al4V cast control surface	**286.1**	287.4	288.8	289.9
Ti6Al4V cast control surface RFGDT	**286.2**	287.3	288.4	289.6
Ti6Al4V cast SI Enhanced	**285.8**	286.4	287.4	289.3
Ti6Al4V cast SI Enhanced RFGDT	**285.5**	286.7	288.1	289.7
Ti6Al4V cast ES Enhanced	**285.7**	287.0	288.2	289.5
Ti6Al4V cast ES Enhanced RFGDT	**285.5**	286.7	288.5	290.0

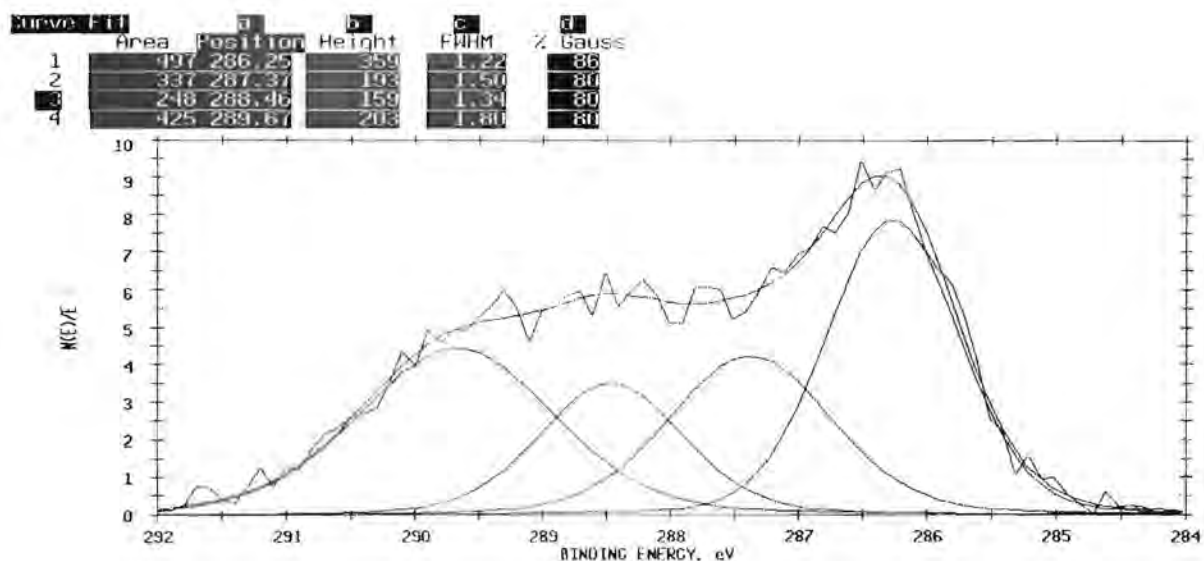Fig 5-10 shows a representative plot of the Carbon 1s envelope with its curve fit.

Fig 5-10: Deconvolution of XPS Carbon envelope of Ti6Al4V cast control RFGDT sample surface

Oxygen sub peaks

The respective Oxygen 1s sub peaks within its respective envelope are shown in Table 5-3. Most samples had four components with the exception of Ti6Al4V cast control RFGDT sample that had five component peaks. RFGDT reduced the number of peaks of cpTi and Ti6Al4V machined control samples from three to two.

Table 5-3: Deconvoluted Oxygen 1s envelope with respective sub peak positions (Bold figures indicate highest peak).

Element	Peak I	Peak II	Peak III	Peak IV	Peak V
cpTi machined control surface	**529.8**	531.2	532.1	533.5	
cpTi machined control surface RFGDT	**530.0**	531.4			
cpTi machined SI Enhanced	**529.7**	530.7	531.7	532.9	
cpTi machined SI Enhanced RFGDT	**529.4**	530.3	531.3	532.5	
cpTi machined ES Enhanced	**529.6**	530.6	531.6	532.6	
cpTi machined ES Enhanced RFGDT	**529.3**	530.0	531.0	532.6	
Ti6Al4V machined control surface	**530.0**	531.8	533.2		
Ti6Al4V machined control surface RFGDT	**530.0**	531.3			
Ti6Al4V machined SI Enhanced	529.5	530.9	**531.8**	533.2	
Ti6Al4V machined SI Enhanced RFGDT	**529.4**	530.4	531.4	533.1	
Ti6Al4V machined ES Enhanced	529.5	530.9	**531.9**	533.0	
Ti6Al4V machined ES Enhanced RFGDT	**529.5**	530.4	531.2	532.3	
cpTi cast control surface	**529.6**	530.9	531.9	533.1	
cpTi cast control surface RFGDT	**529.5**	530.5	531.8	533.2	
cpTi cast SI Enhanced	529.4	530.5	**531.7**	532.9	
cpTi cast SI Enhanced RFGDT	**529.3**	530.0	531.2	532.6	
cpTi cast ES Enhanced	529.6	530.7	**531.7**	532.9	
cpTi cast ES Enhanced RFGDT	**529.4**	530.5	531.4	532.9	
Ti6Al4V cast control surface	529.3	530.7	**532.2**	533.8	
Ti6Al4V cast control surface RFGDT	529.7	530.6	531.5	**532.9**	534.6
Ti6Al4V cast SI Enhanced	**529.6**	530.8	531.8	533.2	
Ti6Al4V cast SI Enhanced RFGDT	**529.4**	530.8	531.9	533.6	
Ti6Al4V cast ES Enhanced	529.6	530.8	**531.9**	533.0	
Ti6Al4V cast ES Enhanced RFGDT	**529.4**	530.2	531.4	533.0	

The major sub peak of the different samples varied considerably. For most samples it was at ~529eV, occasionally ~531eV and sometimes ~532eV. Some sub peaks had more or less the same peak height as was observed in Ti6Al4V cast control RFGDT sample. Metal oxides (529-531eV) and hydroxides (531-532eV) mainly contributed to the Oxygen sub peaks. Carbonates could also be present at ~531eV. Besides the different metal oxides of Titanium (TiO_2-529.7-530.2eV; TiO-530.6eV; Ti_2O_3-

529.6eV), Aluminium oxide could also have been contributory (Al_2O_3-528-532eV) to the metal oxide peak detected (Lausmaa et al, 1990).

Deconvoluted high-resolution spectra sub peaks within its respective Oxygen envelope is shown in Fig 5-11.
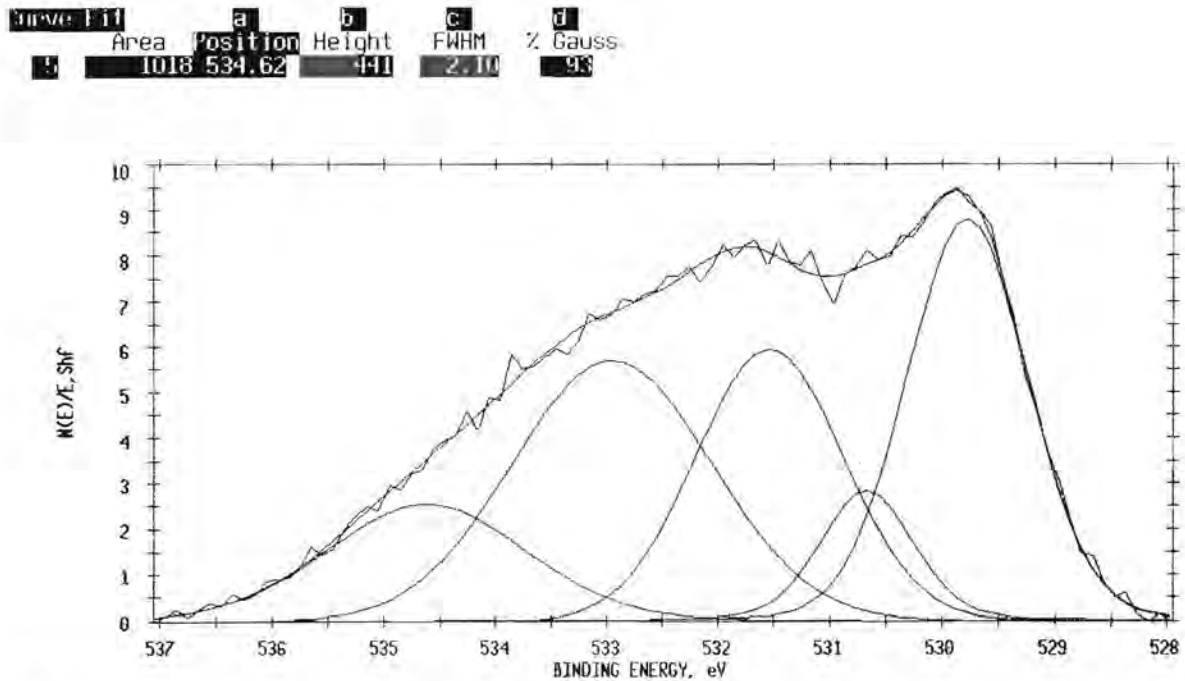
Fig 5-11: Deconvolution of XPS Oxygen envelope of Ti6Al4V cast control RFGDT sample surface

Titanium sub peaks

On most sample surfaces, only one major peak was detected, but deconvolution of the Ti2p peak on cpTi and Ti6Al4V machined control samples revealed two sub peaks, at 458eV and 457eV (see Table 5-4, p87). The major peak detected at 458eV indicates that the sample surfaces constituted mostly of TiO_2. The oxide layer on some samples though, may rather consist of Ti_2O_3 as indicated by the 457eV peak.

A high-resolution spectrum for Titanium is shown in Fig 5-12 (see p87) with the peak centre at 458eV.

Table 5-4: Deconvoluted Titanium 2p envelope with respective sub peak positions (Bold figures indicate highest peak).

Element	Peak I	Peak II
cpTi machined control surface	**458.3**	
cpTi machined control surface RFGDT	**458.6**	457.9
cpTi machined SI Enhanced	**458.2**	
cpTi machined SI Enhanced RFGDT	**458.0**	
cpTi machined ES Enhanced	**458.1**	
cpTi machined ES Enhanced RFGDT	**457.8**	
Ti6Al4V machined control surface	**458.4**	
Ti6Al4V machined control surface RFGDT	**458.5**	457.7
Ti6Al4V machined SI Enhanced	**457.9**	
Ti6Al4V machined SI Enhanced RFGDT	**457.9**	
Ti6Al4V machined ES Enhanced	**458.0**	
Ti6Al4V machined ES Enhanced RFGDT	**458.0**	
cpTi cast control surface	**458.1**	
cpTi cast control surface RFGDT	**458.1**	
cpTi cast SI Enhanced	**457.9**	
cpTi cast SI Enhanced RFGDT	**457.9**	
cpTi cast ES Enhanced	**458.1**	
cpTi cast ES Enhanced RFGDT	**458.0**	
Ti6Al4V cast control surface	**458.1**	
Ti6Al4V cast control surface RFGDT	**458.2**	
Ti6Al4V cast SI Enhanced	**458.1**	
Ti6Al4V cast SI Enhanced RFGDT	**457.9**	
Ti6Al4V cast ES Enhanced	**458.1**	
Ti6Al4V cast ES Enhanced RFGDT	**458.0**	

Curve Fit   a   b   c   d
        Area Position Height FWHM % Gauss
1   1458   458.23   861   1.45   80
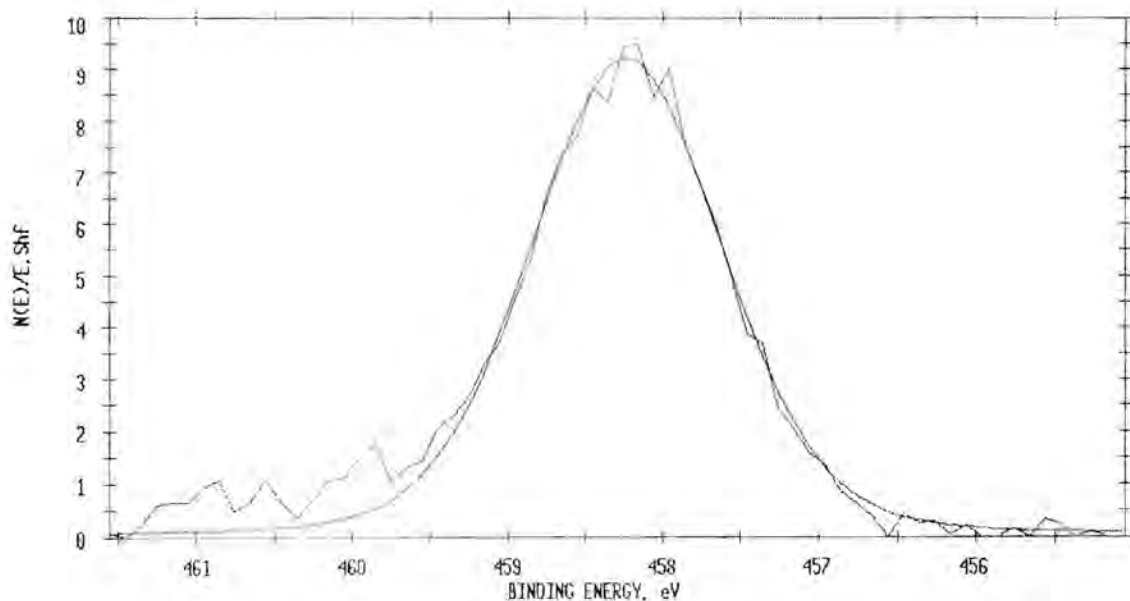
Fig 5-12: Deconvolution of XPS Titanium envelope of Ti6Al4V cast control RFGDT sample surface

Aluminium sub peaks

Fig 5-13 shows the deconvolution of XPS Aluminium envelope for the Ti6Al4V cast control surface.

Curve Fit	a	b	c	d
Area	Position	Height	FWHM	% Gauss
1	138	73.08	93	1.28	80
2	236	74.51	123	1.80	100
3	119	76.07	80	1.37	96
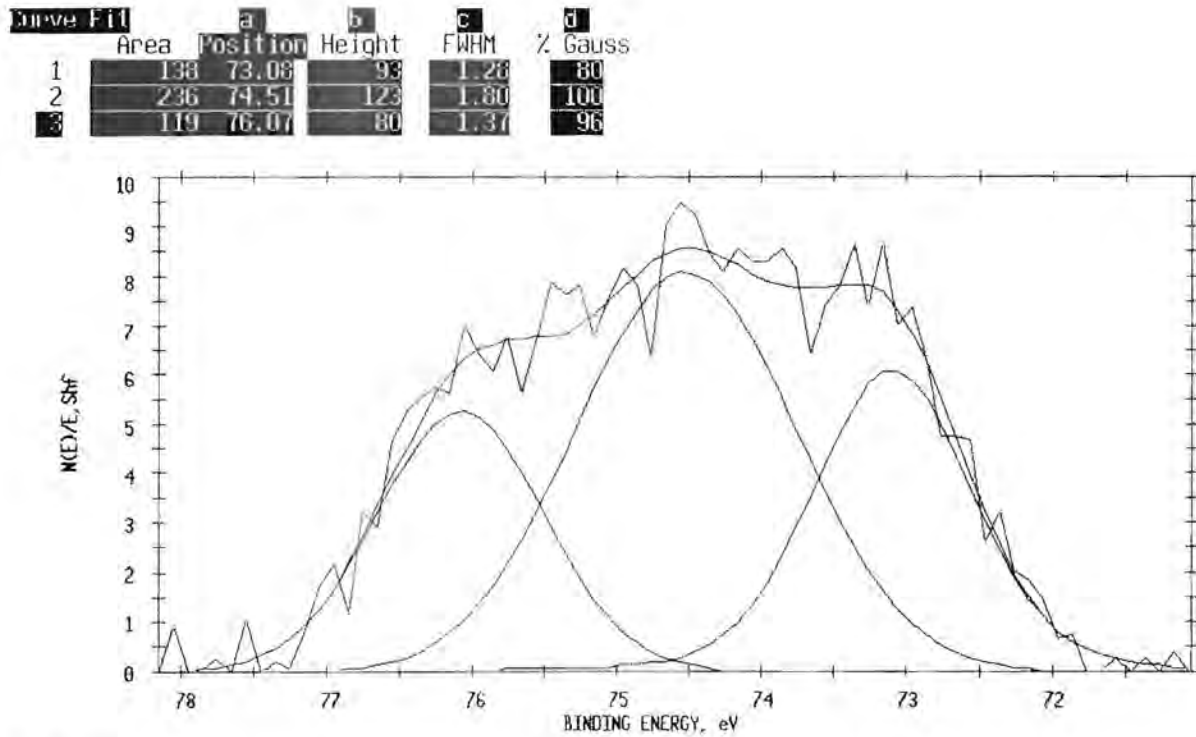
Fig 5-13: Deconvolution of Aluminium envelope for Ti6Al4V cast control surface

A deconvoluted high-resolution spectrum within the Aluminium envelope shows three main sub peaks. The sub peak at 73.03eV was attributed to Aluminium metal while the 74.51eV sub peak was attributed to Aluminium oxides. The 76.07eV peak was probably a Halide form of Aluminium (Moulder et at, 1992).

Sodium sub peaks

The presence of Sodium was detected together with Titanium at 1072eV using the Na (1s) peak and no attempts were made to further deconvolute the Sodium and Titanium peak.

5.1.2 Surface Roughness

5.1.2.1 Area Analysis

Representative 3D images of samples scanned using the Atomic Force Microscope are shown in Fig 5-14 to 5-17 (see p89-90).
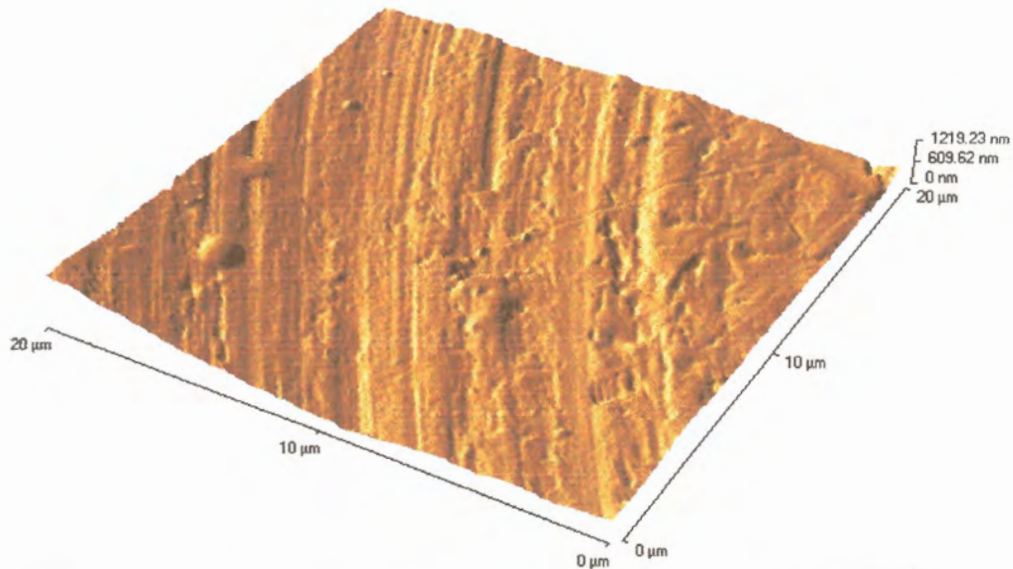
Fig 5-14: AFM 3D images of 20μm scans of cpTi machined control sample surface
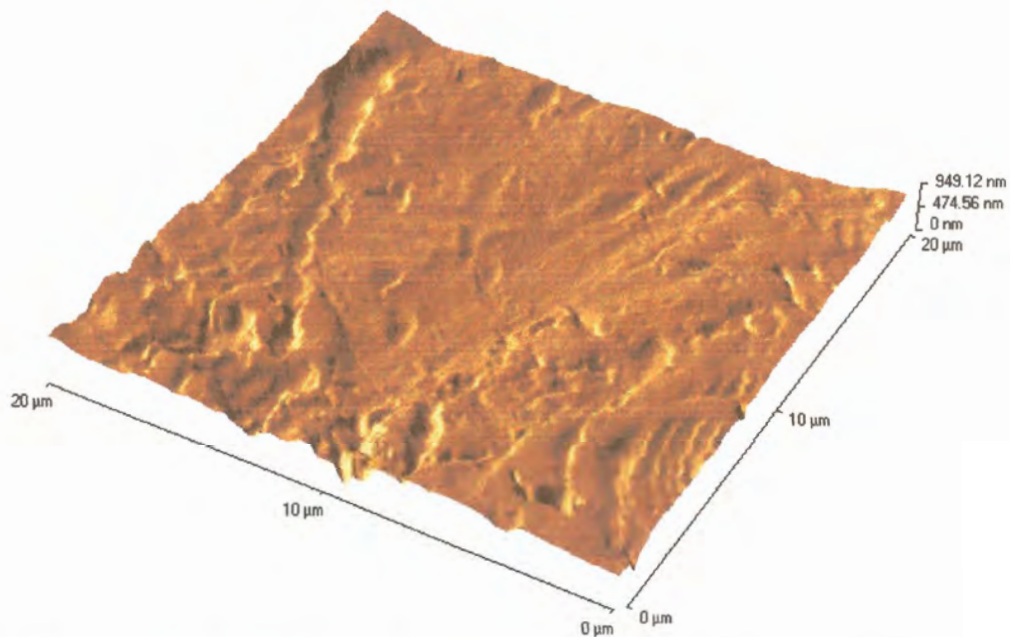
Fig 5-15: AFM 3D images of 20μm scans of Ti6Al4V machined control sample surface
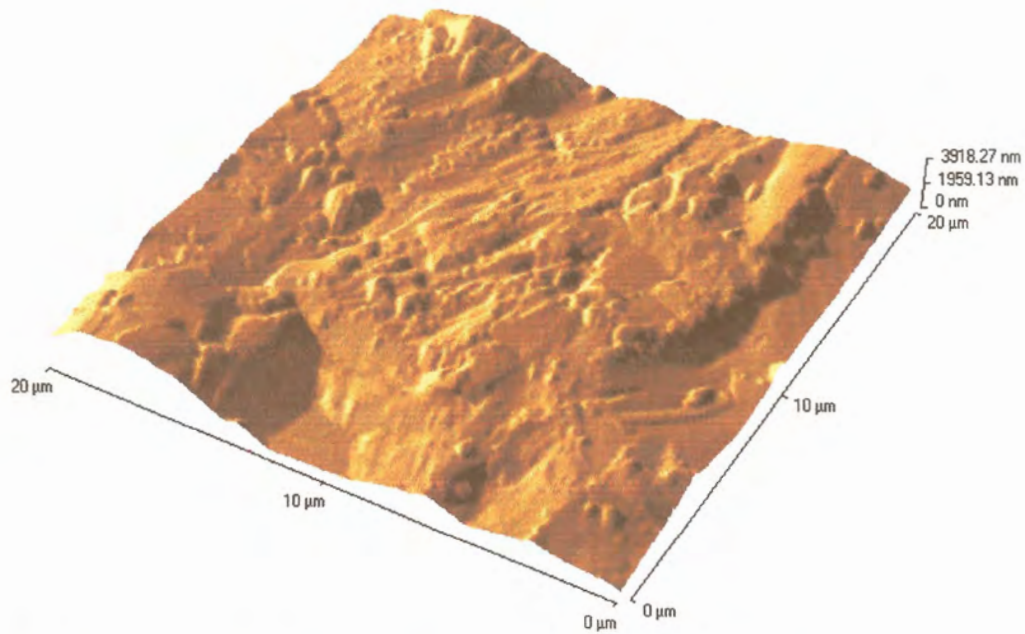
Fig 5-16: AFM 3D images of 20μm scans of cpTi cast control sample surface
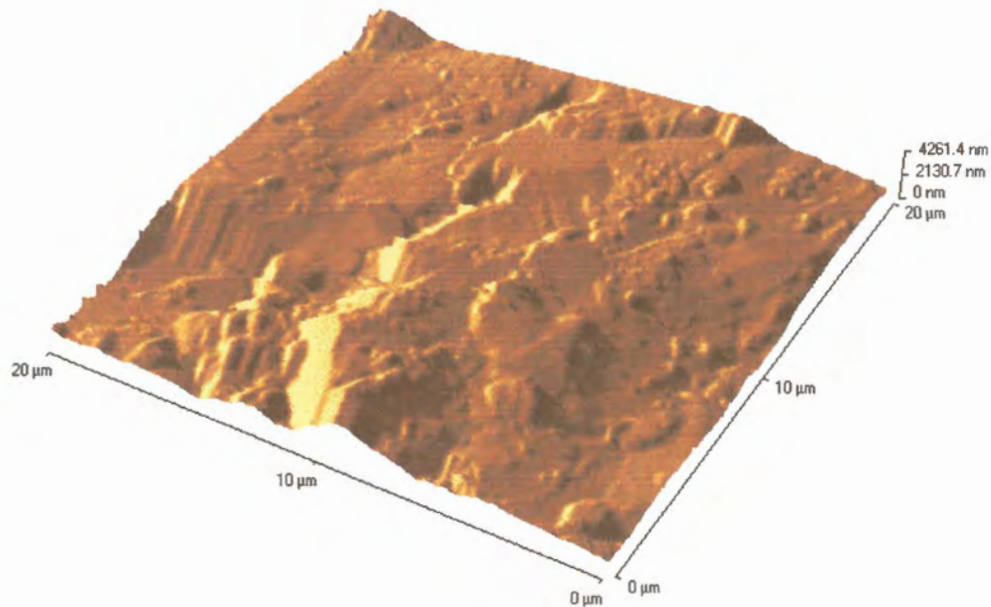
Fig 5-17: AFM 3D images of 20μm scans of Ti6Al4V cast control sample surface

The quantitative data obtained from the surfaces of 3D Atomic Force micrographs were analyzed and averages of the different measures of Area analysis for the 20μm (see Table 5-5, p91) and 5μm (see Table 5-6, p92) are shown (see Addendum C, p180-182)

Table 5-5: Average tabulated values of the surface topography of samples for 20µm scans (N=5).

Material	Ra ± SD	RMS ± SD	Maximum Height ± SD	Average Range ± SD	Surface Area ± SD
CpTi machined control surface	0.14 ± 0.04	0.17 ± 0.05	0.58 ± 0.15	1.04 ± 0.16	416.18 ± 4.09
CpTi machined control surface & RFGDT	0.09 ± 0.02	0.12 ± 0.04	0.43 ± 0.22	0.95 ± 0.29	416.34 ± 5.77
Ti6Al4V machined control surface	0.08 ± 0.03	0.11 ± 0.04	0.63 ± 0.29	0.92 ± 0.35	415.00 ± 3.18
Ti6Al4V machined control surface & RFGDT	0.14 ± 0.02	0.18 ± 0.03	0.53 ± 0.07	1.20 ± 0.14	425.02 ± 6.49
cpTi cast control surface	0.51 ± 0.1	0.65 ± 0.12	1.88 ± 0.52	3.94 ± 0.62	531.92 ± 24.25
cpTi cast control surface & RFGDT	0.64 ± 0.19	0.79 ± 0.22	2.20 ± 1.03	4.55 ± 1.21	559.14 ± 60.88
Ti6Al4V cast control surface	0.44 ± 0.19	0.55 ± 0.24	1.74 ± 0.84	3.30 ± 1.38	508.26 ± 55.34
Ti6Al4V cast control surface & RFGDT	0.41 ± 0.10	0.52 ± 0.14	1.92 ± 0.81	3.67 ± 0.99	535.26 ± 65.83

The mean of the different analyses of surface roughness for both the 20µm and 5µm scans are observed to be higher for the surfaces of cast samples than for the machined samples.

Table 5-6: Average tabulated values of the surface topography of samples for 5µm scans (N=5).

Material	Ra ± SD	RMS ± SD	Maximum Height ± SD	Average Range ± SD	Surface Area ± SD
CpTi machined control surface	0.05 ± 0.02	0.07 ± 0.02	0.26 ± 0.13	0.51 ± 0.16	27.1 ± 0.75
CpTi machined control surface & RFGDT	0.06 ± 0.05	0.08 ± 0.06	0.21 ± 0.12	0.42 ± 0.28	26.56 ± 1.0
Ti6Al4V machined control surface	0.08 ± 0.02	0.10 ± 0.03	0.34 ± 0.24	0.52 ± 0.25	27.31 ± 1.17
Ti6Al4V machined control surface & RFGDT	0.10 ± 0.03	0.12 ± 0.03	0.31 ± 0.06	0.67 ± 0.16	28.04 ± 0.96
cpTi cast control surface	0.26 ± 0.15	0.32 ± 0.17	0.68 ± 0.33	1.61 ± 0.55	32.85 ± 3.32
cpTi cast control surface & RFGDT	0.27 ± 0.14	0.33 ± 0.15	0.80 ± 0.45	1.78 ± 0.53	34.26 ± 4.46
Ti6Al4V cast control surface	0.25 ± 0.11	0.31 ± 0.14	0.75 ± 0.38	1.63 ± 0.73	34.94 ± 5.01
Ti6Al4V cast control surface & RFGDT	0.2 ± 0.13	0.24 ± 0.16	0.58 ± 0.29	1.31 ± 0.79	32.39 ± 5.82

Area Ra and RMS

Surface roughness is representative of both Ra and RMS values and results are reported together. RMS is the root mean square of Ra and therefore predicted to be a more reliable measure of assessment (see 2.6.2.1, p33). Ra and RMS values of samples for the 20µm scan are shown in Fig 5-18 (see p93).

For the 20µm scans the respective average Ra and RMS values of surfaces of cast samples (0.50µm and 0.65µm) were significantly higher than machined samples (0.11µm and 0.14µm).

No significant differences in the Ra or RMS values were observed between material used (cpTi or Ti6Al4V) and treatment rendered.
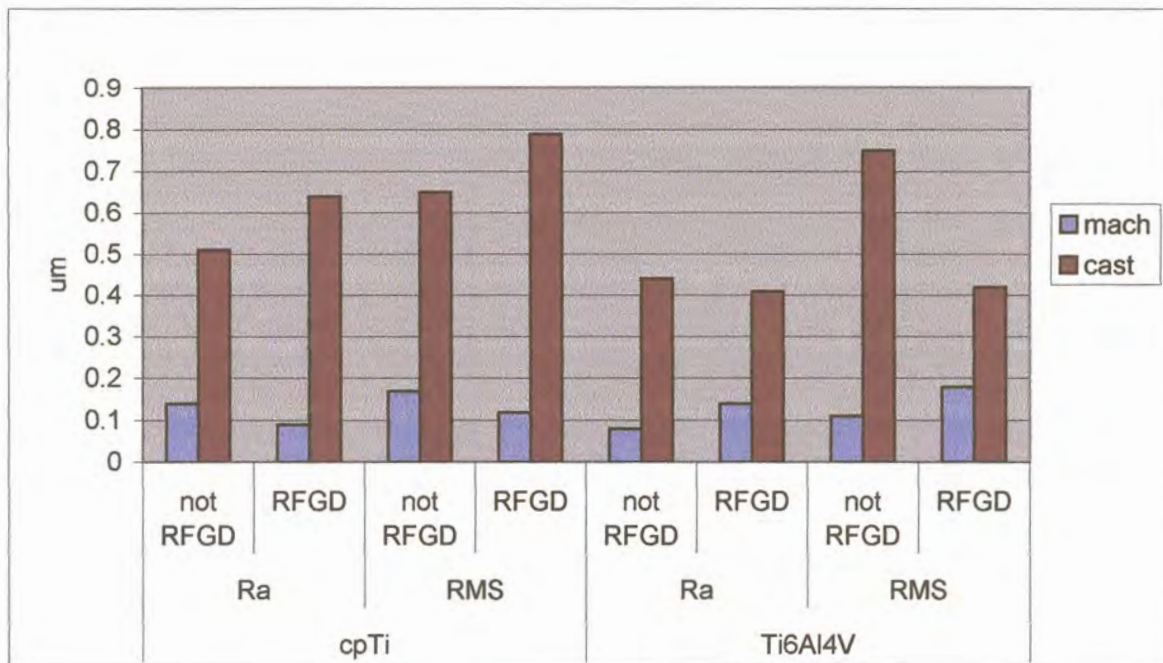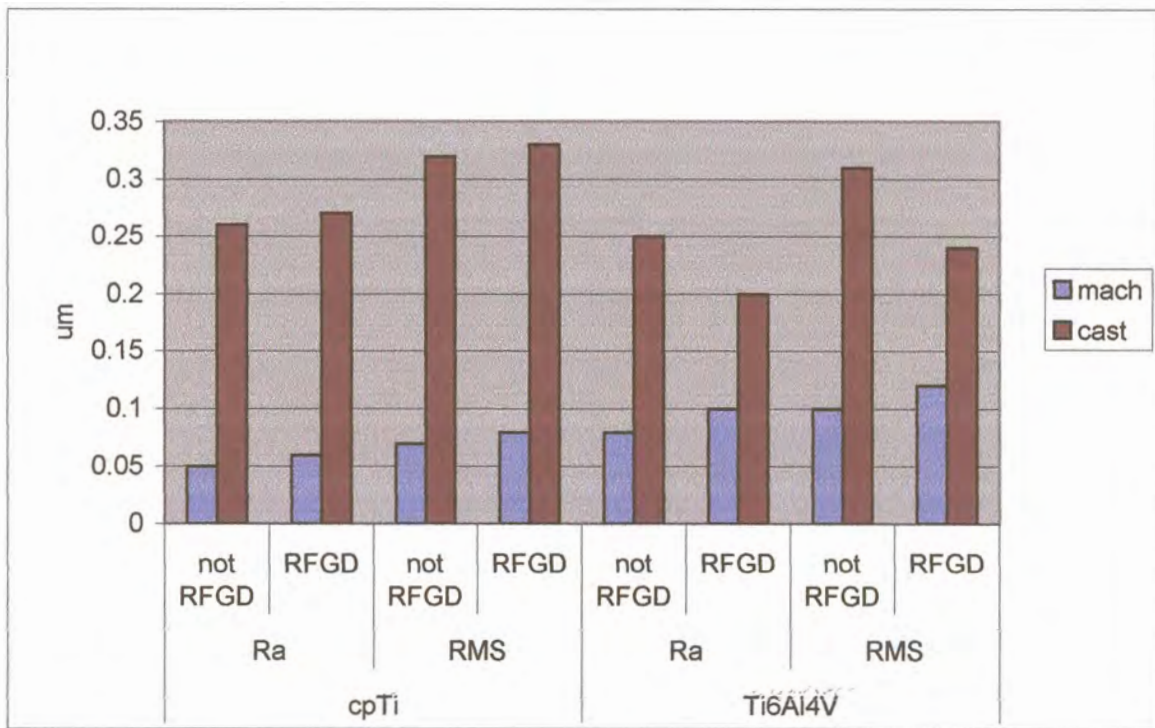

Fig 5-18: Average roughness (Ra and RMS) of the different sample surfaces by material employed and RFGDT for 20µm scan

Ra and RMS values of the 5µm scans are showed in Fig 5-19 (see p94). Surfaces of cast samples showed on average a significantly higher Ra (0.20µm) and RMS (0.30µm) values compared to the machined samples (Ra=0.08µm and RMS=0.09µm). Materials used or treatment rendered was of no significance in terms of Ra or RMS values.

Fig 5-19: Average roughness (Ra and RMS) of the different sample surfaces by material employed and RFGDT for 5μm scan

Average height and Maximum range

Average height is the highest point from the zero value of the surface scanned while the Maximum range reveals how the surface topography is related in terms of highest and lowest point of scanned surface (see 2.6.2.1, p33). The Average height and Maximum range for the 20μm scans and 5μm scans are shown in Fig 5-20 and 5-21 (see p95).
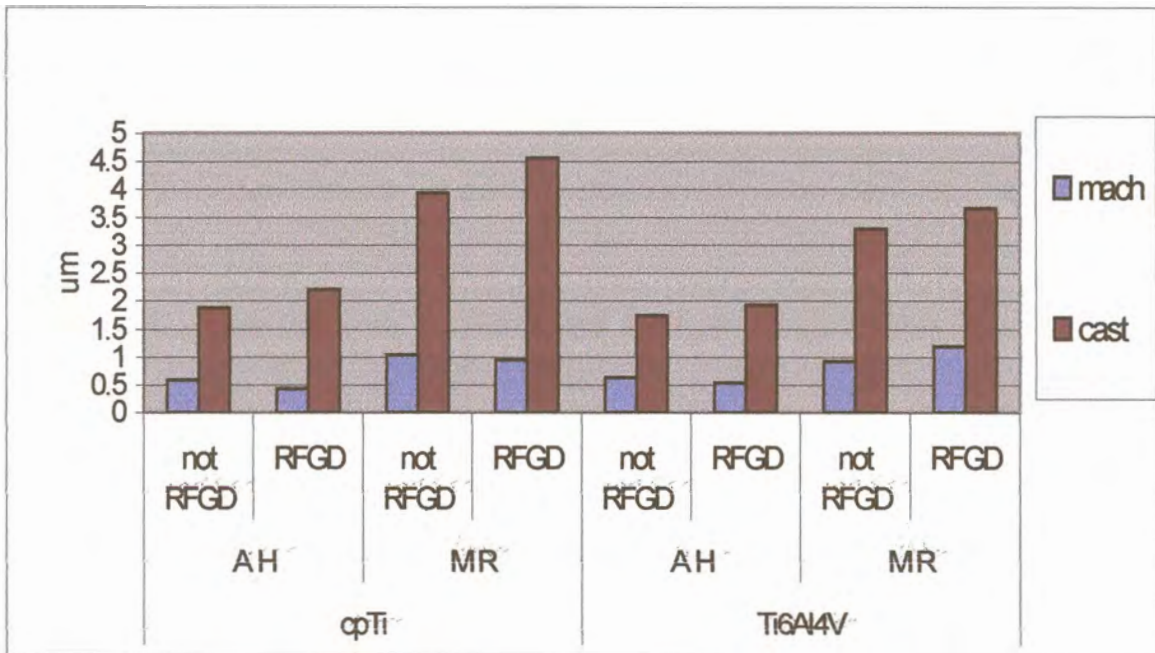
Fig 5-20: Average height and Maximum range for 20µm scans of sample surfaces

For the 20µm scan the respective Average height and Maximum range on average were significantly higher for the surfaces of cast samples (1.93µm and 3.86µm) than that observed for the machined samples (0.54µm and 1.03µm).
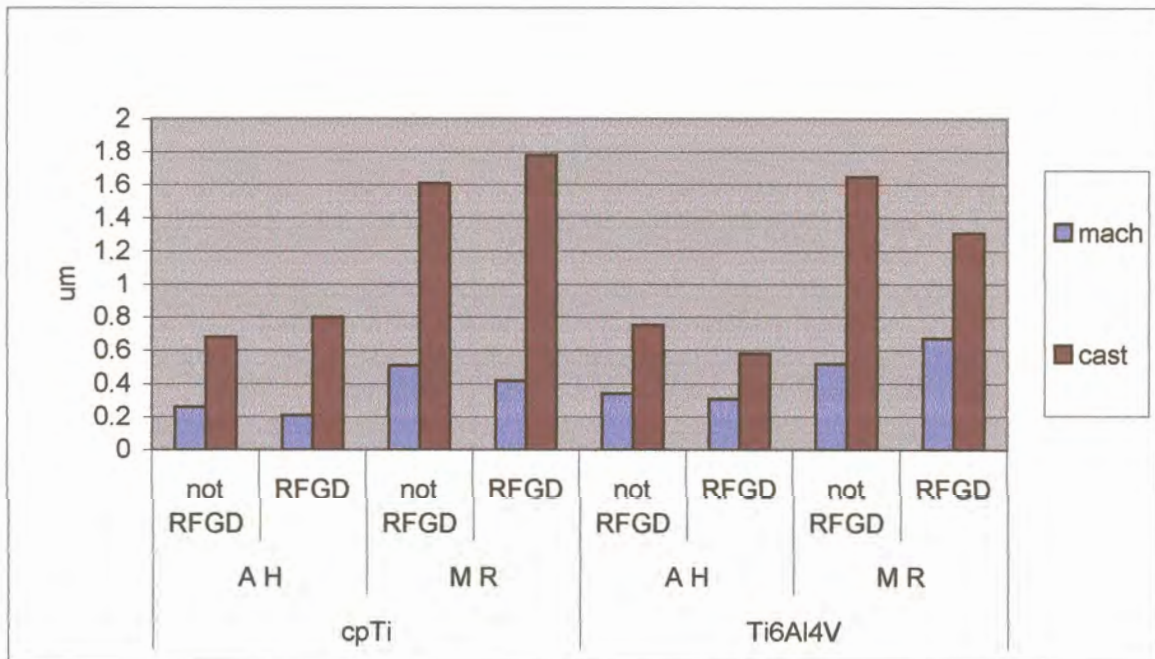
Fig 5-21: Average height and Maximum range for 5µm scans of sample surfaces

For the 5µm scans the Maximum range on average for the surfaces of cast samples (1.59µm) was significantly higher than machined samples (0.53µm) and similarly the Average range was significantly higher for surfaces of cast (0.70µm) than machined (0.28µm) samples.

Surface Area

Surface area or the projected area denotes the probable contact area of the sample surface (see 2.6.2.1, p33) and the projected surface area is the increase in area as a result of surface topography.
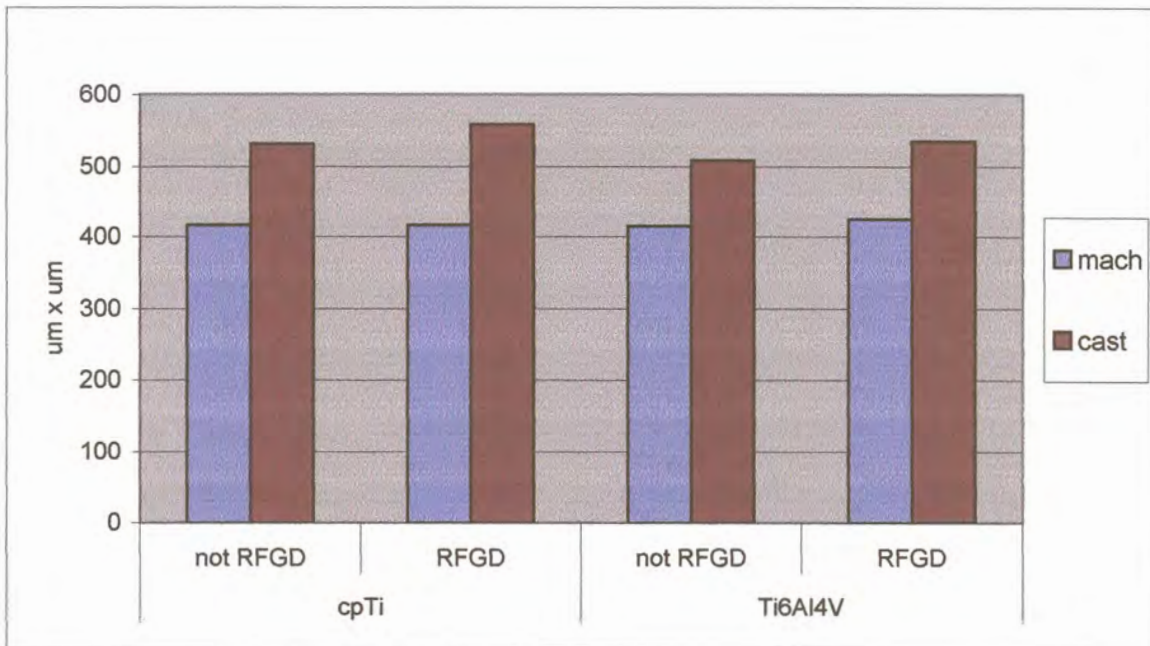
Fig 5-22: Average projected surface area of the 20µm scans for sample surfaces

Fig 5-22 shows the average surface area for the 20µm scan and surfaces of cast samples display on average a significant surface area increase (533.65µm^2) compared to machined samples (418.14µm^2) (p<0.05). RFGDT significantly increased the surface area from 467.84µm^2 to 483.94µm^2 (p=0.03). Material used for fabrication did not significantly modify the projected surface area.
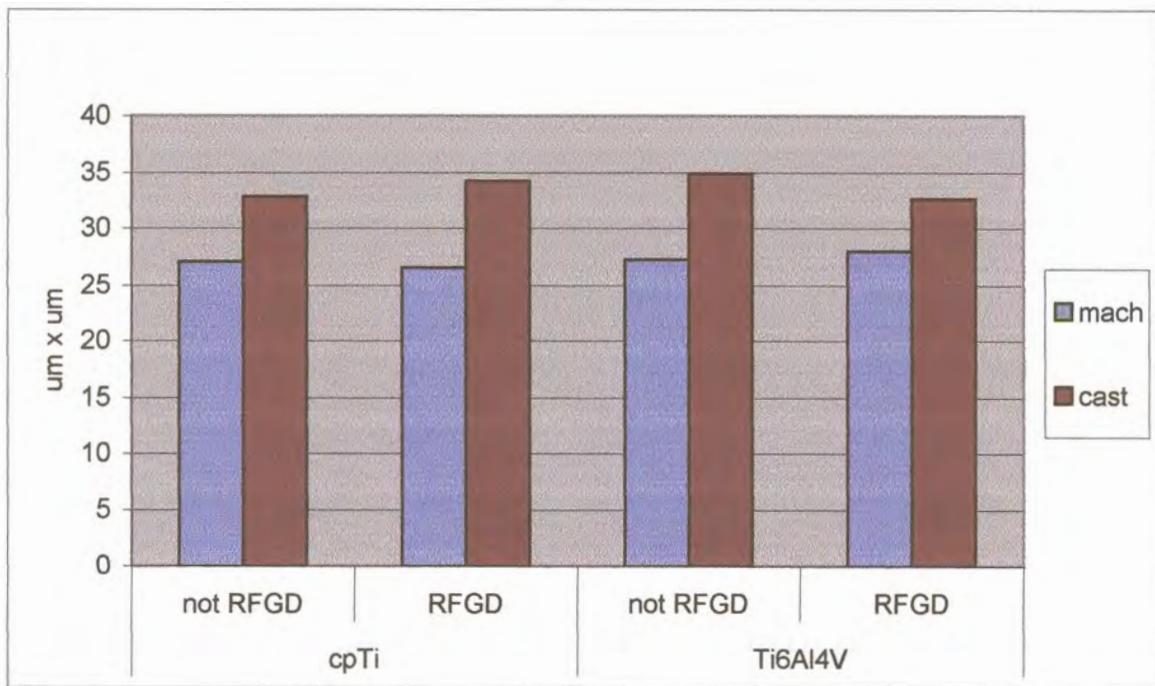
Fig 5-23: Average Projected surface area of the 5μm scans for sample surfaces

Average surface area for the 5μm scans is shown in Fig 5-23. The effect of RFGDT or material used was not obvious but on average surfaces of cast samples ($33.59 \mu m^2$) had a significantly higher projected surface area than machined samples ($27.26 \mu m^2$) ($p=0.0001$).

For a smooth surface with an absolute flat surface topography the projected surface area for a 20x20μm scan is assumed to be $400 \mu m^2$ and is equated to a 100% projected surface area. Table 5-7 (see p98) shows the projected surface area of samples as a percentage increase in terms of the projected surface area of the 20X20μm scans.

Table 5-7: Projected surface area of samples with their relative percent increase.

Material	Surface area (μm^2)	Percentage increase
cpTi machined control surface	416.18 ± 4.09	4.04
cpTi machined control surface & RFGDT	416.34 ± 5.77	4.08
Ti6Al4V machined control surface	415.00 ± 3.18	3.75
Ti6Al4V machined control surface & RFGDT	425.02 ± 6.49	6.25
cpTi cast control surface	531.92 ± 24.25	32.75
cpTi cast control surface & RFGDT	559.14 ± 60.88	39.78
Ti6Al4V cast control surface	508.26 ± 55.34	27.06
Ti6Al4V cast control surface & RFGDT	535.26 ± 65.83	33.81

Fig 5-24 shows the percentage increase of the projected surface area for the different samples.
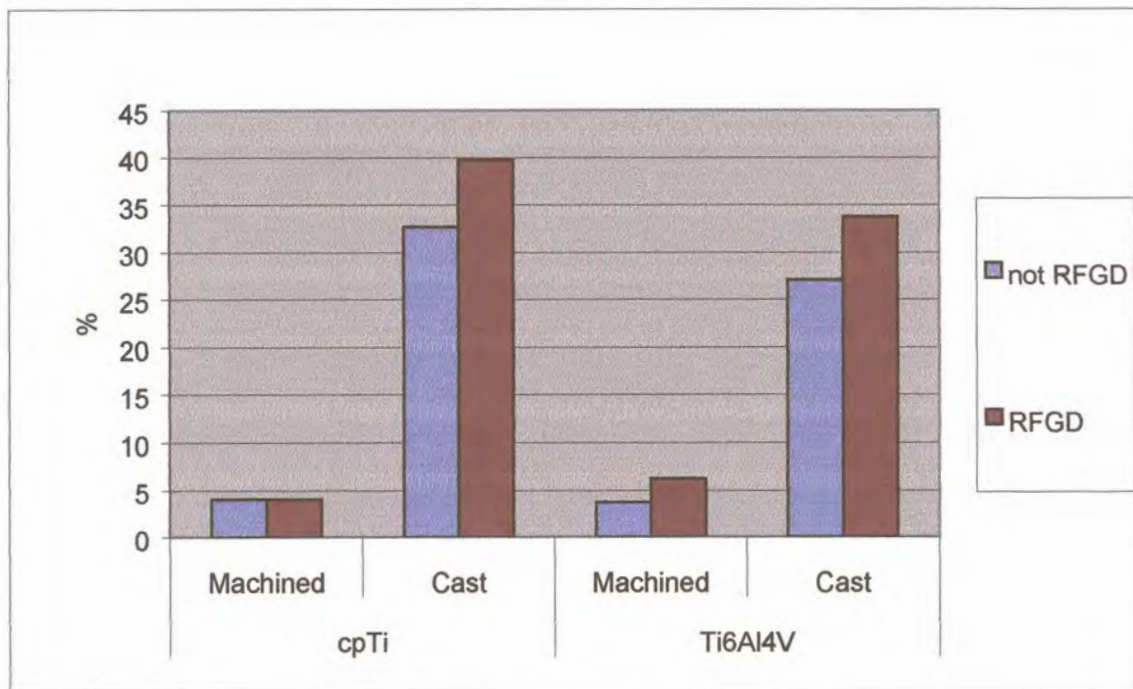
Fig 5-24: Percentage increase in Projected surface area of samples for 20μm scans

The percentage increase of 33.4% in Projected surface area for surfaces of cast samples was significantly higher than the 4.5% increase in Projected surface area for machined samples ($p < 0.05$). RFGDT on average significantly increased the surface area of samples from 116.90% to 120.98% ($p = 0.03$). Material

used or treatment rendered did not significantly change the percent increase in surface area.

5.1.2.2   Line Analysis

The 20µm scan line analysis of for the different sample surfaces of the three predetermined lines drawn on the 2D images are shown in Figures 5-25 to 5-28 (see p99-101).
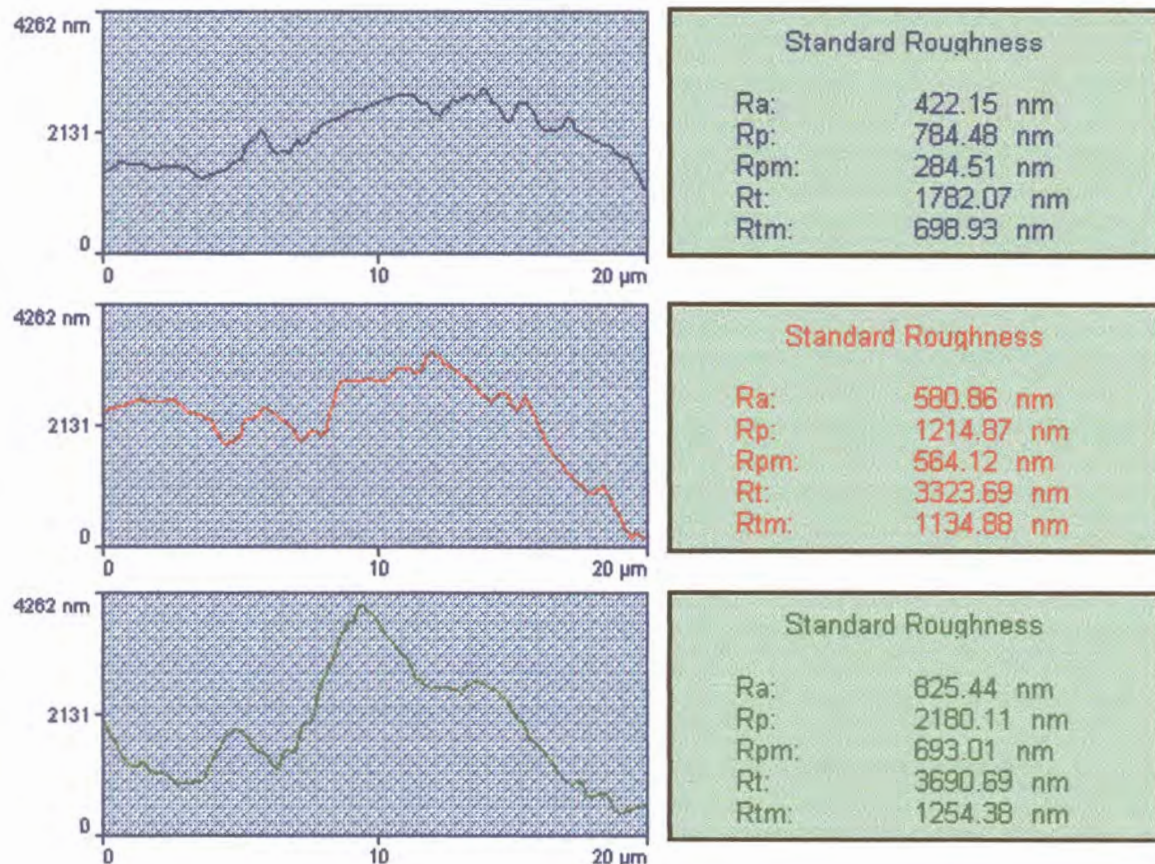

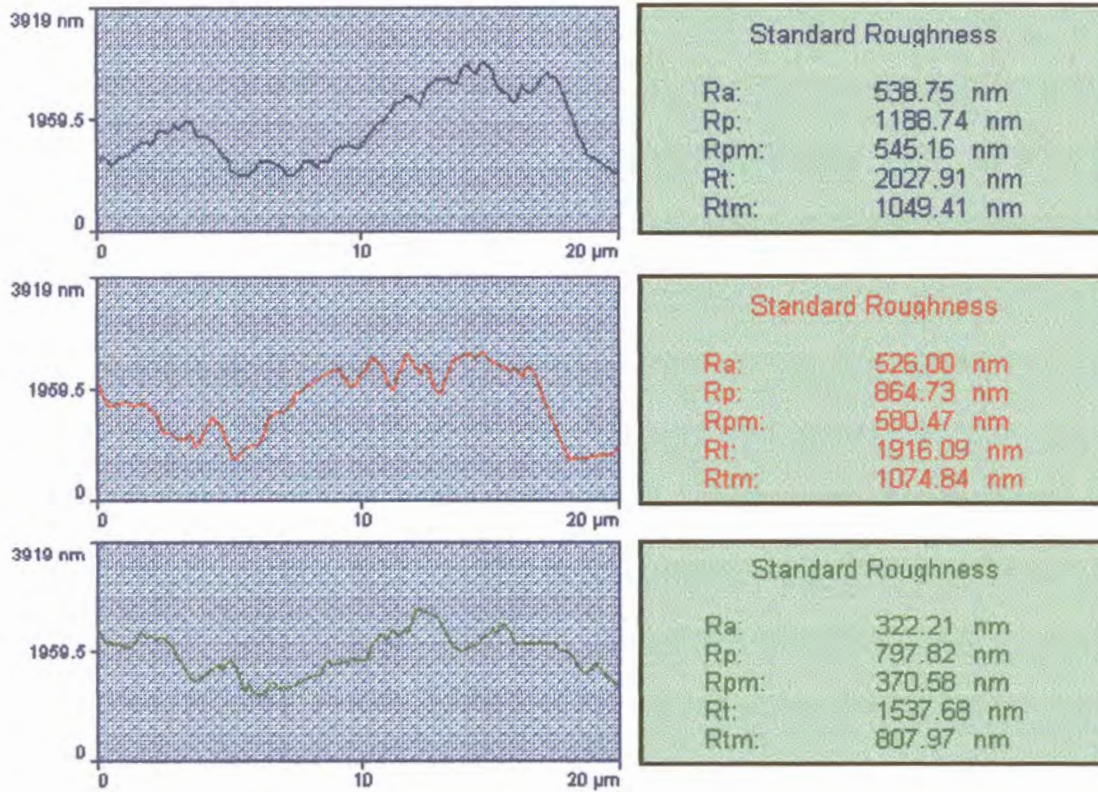Fig 5-25: Line analysis of the 20µm scans of cpTi machined control sample surface

Standard Roughness	
Ra:	538.75 nm
Rp:	1188.74 nm
Rpm:	545.16 nm
Rt:	2027.91 nm
Rtm:	1049.41 nm

Standard Roughness	
Ra:	526.00 nm
Rp:	864.73 nm
Rpm:	580.47 nm
Rt:	1916.09 nm
Rtm:	1074.84 nm

Standard Roughness	
Ra:	322.21 nm
Rp:	797.82 nm
Rpm:	370.58 nm
Rt:	1537.68 nm
Rtm:	807.97 nm

Fig 5-26: Line analysis of the 20µm scans of cpTi cast control sample surface

Standard Roughness	
Ra:	99.39 nm
Rp:	251.42 nm
Rpm:	110.27 nm
Rt:	446.04 nm
Rtm:	226.13 nm

Standard Roughness	
Ra:	88.09 nm
Rp:	166.79 nm
Rpm:	82.86 nm
Rt:	347.70 nm
Rtm:	167.09 nm

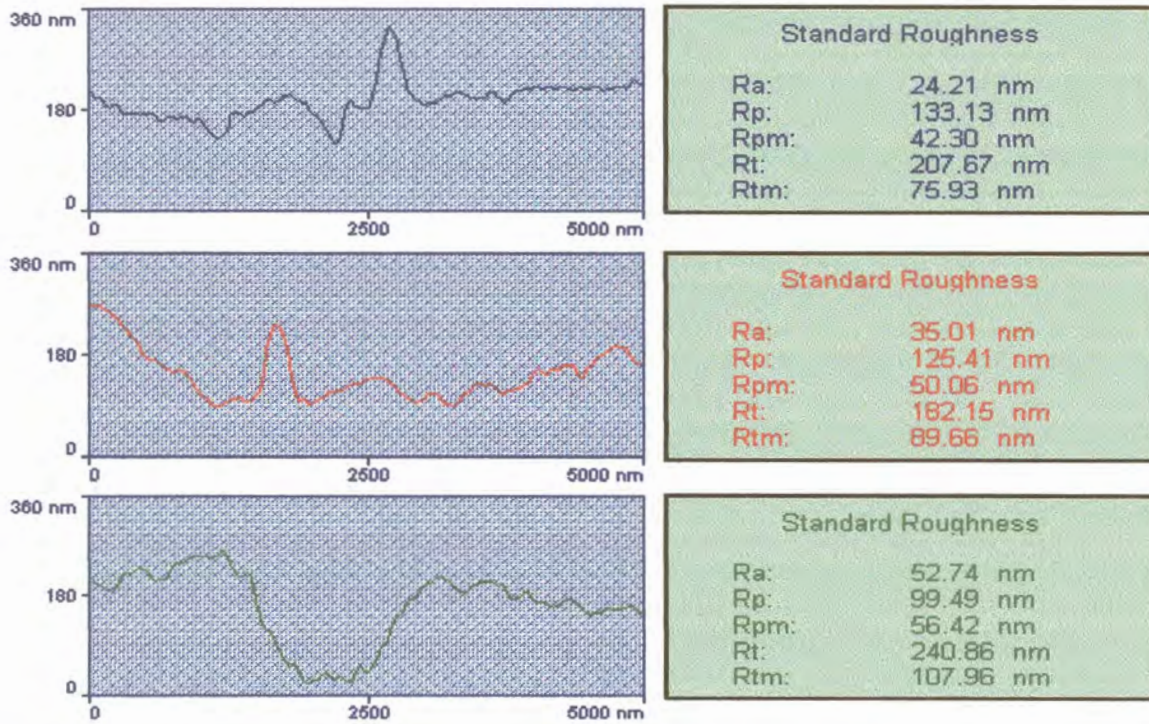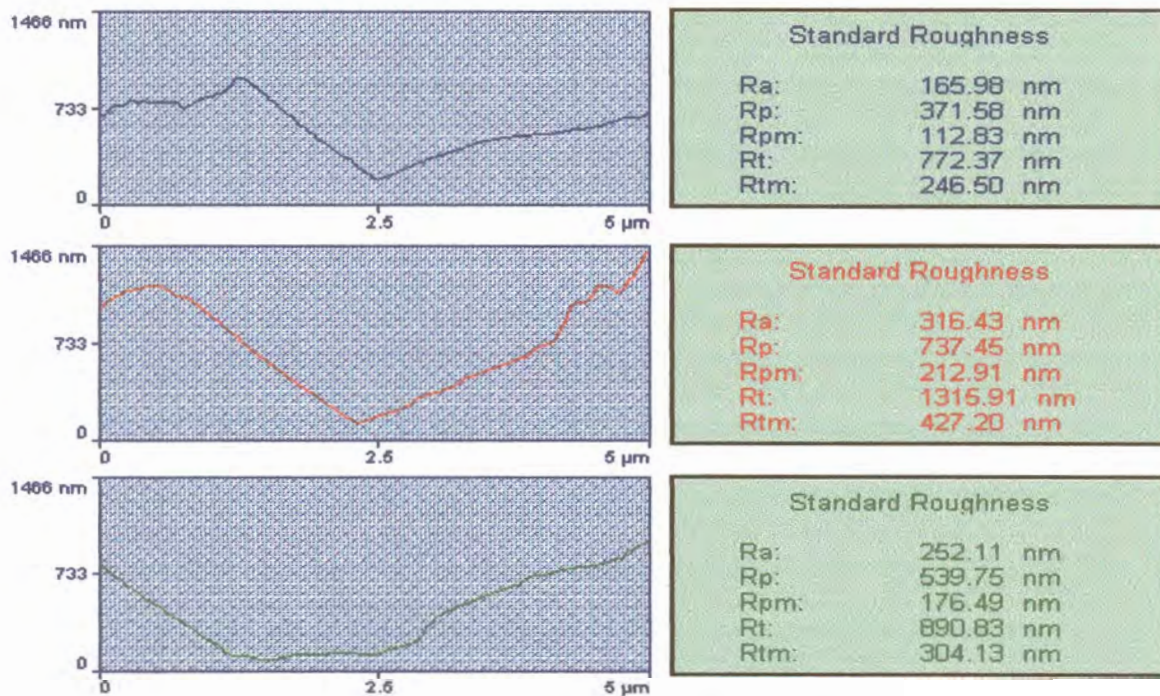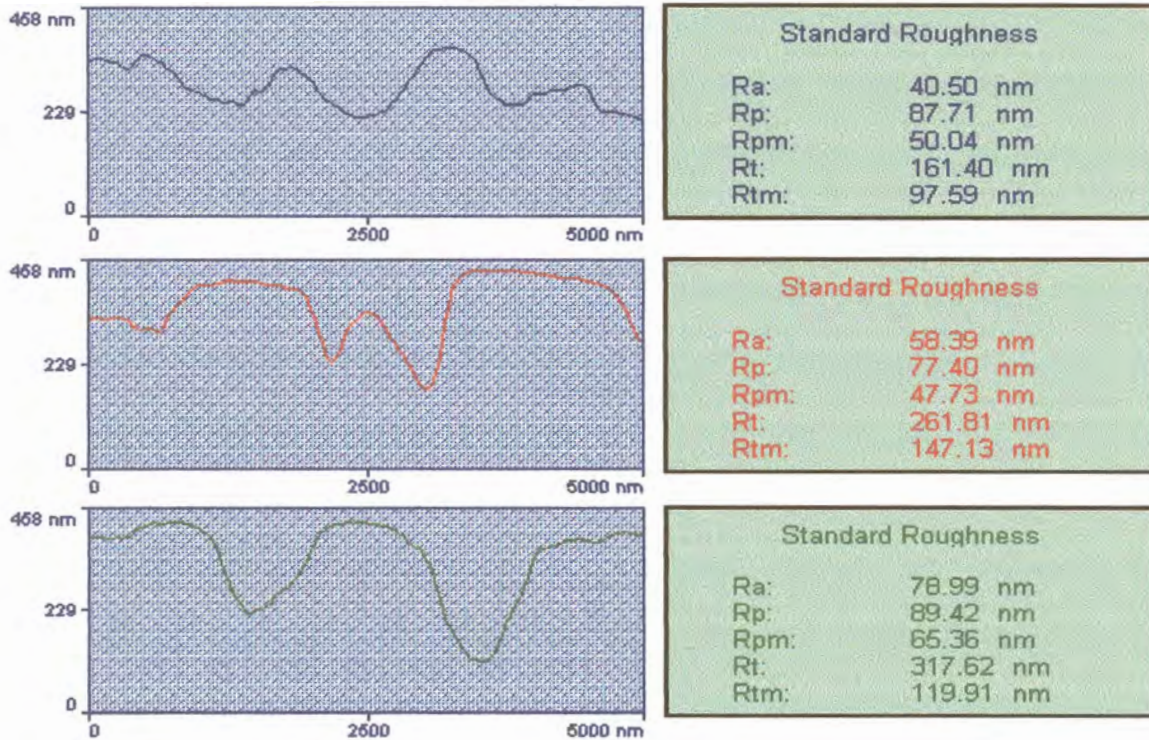| Standard Roughness	
Ra:	93.90 nm
Rp:	208.83 nm
Rpm:	103.28 nm
Rt:	403.30 nm
Rtm:	237.79 nm
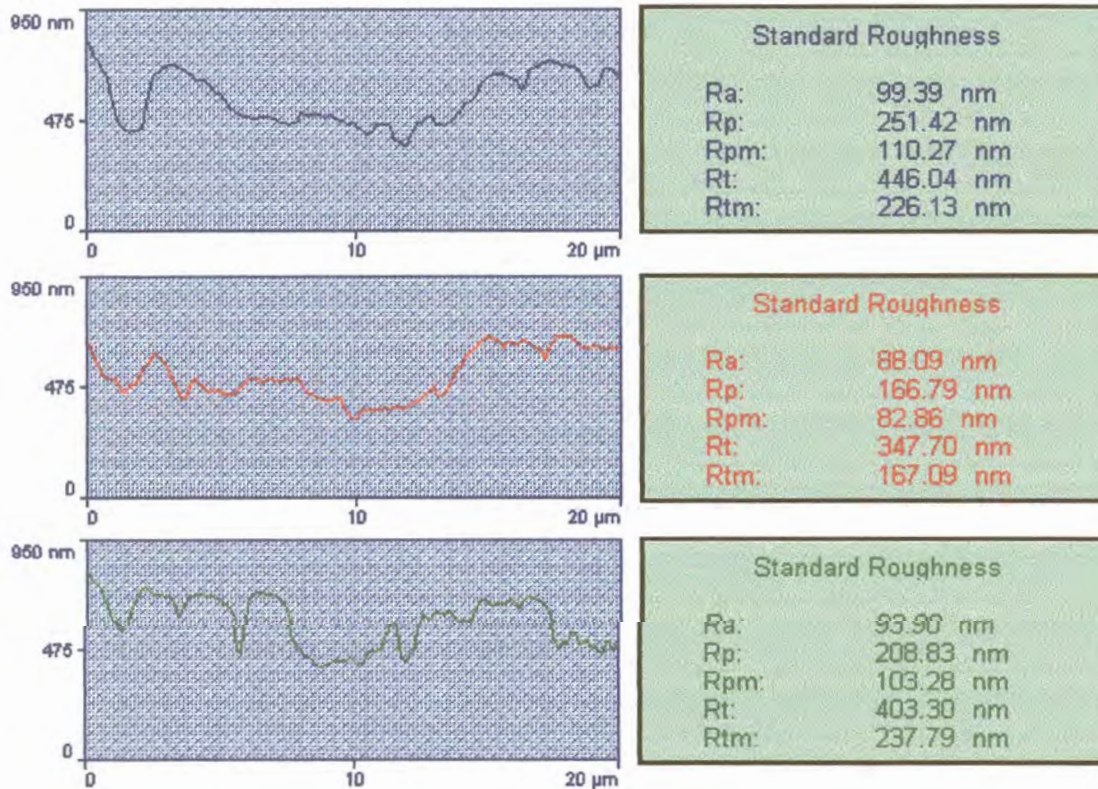
Fig 5-27: Line analysis of the 20µm scans of Ti6Al4V machined control sample surface

100
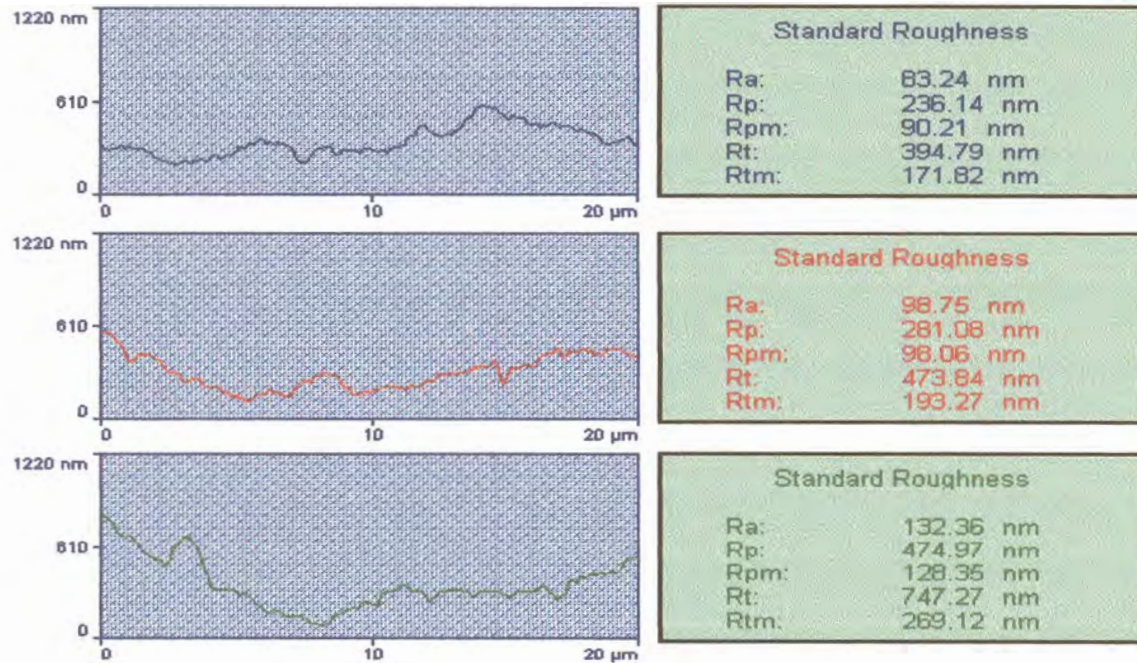
Fig 5-28: Line analysis of the 20μm scans of Ti6Al4V cast control sample surface

For each line drawn that traversed the whole 2D image the computer software produced processed values of Ra, Rtm, Rt, Rpm and Rp, the averages of which are shown in Table 5-8 for the 20μm scans (see Addendum D, p183-187).

Table 5-8: Averages of the line analysis done for the different sample surfaces for the 20μm scan.

Material	Ra	Rtm	Rt	Rpm	Rp
cpTi machined control surface	0.12	0.23	0.56	0.11	0.25
cpTi machined control surface & RFGDT	0.08	0.23	0.47	0.11	0.24
Ti6Al4V machined control surface	0.08	0.19	0.40	0.08	0.18
Ti6Al4V machined control surface & RFGDT	0.12	0.31	0.64	0.15	0.31
cpTi cast control surface	0.40	1.02	2.15	0.50	0.98
cpTi cast control surface & RFGDT	0.59	1.26	2.87	0.63	1.47
Ti6Al4V cast control surface	0.39	0.87	2.00	0.40	0.83
Ti6Al4V cast control surface & RFGDT	0.34	0.87	1.88	0.43	0.98

Similar predetermined lines were drawn for the 5μm scans and the line analyses for the different sample surfaces are shown in Figures 5-29 to 5-32 (see p102-103).

101

Standard Roughness

Ra:	24.21 nm
Rp:	133.13 nm
Rpm:	42.30 nm
Rt:	207.67 nm
Rtm:	75.93 nm

Standard Roughness

Ra:	35.01 nm
Rp:	125.41 nm
Rpm:	50.06 nm
Rt:	182.15 nm
Rtm:	89.66 nm

Standard Roughness

Ra:	52.74 nm
Rp:	99.49 nm
Rpm:	56.42 nm
Rt:	240.86 nm
Rtm:	107.96 nm

Fig 5-29: Line analysis of the 5µm scans of cpTi machined control sample surface

Standard Roughness

Ra:	165.98 nm
Rp:	371.58 nm
Rpm:	112.83 nm
Rt:	772.37 nm
Rtm:	246.50 nm

Standard Roughness

Ra:	316.43 nm
Rp:	737.45 nm
Rpm:	212.91 nm
Rt:	1315.91 nm
Rtm:	427.20 nm

Standard Roughness

Ra:	252.11 nm
Rp:	539.75 nm
Rpm:	176.49 nm
Rt:	890.83 nm
Rtm:	304.13 nm

Fig 5-30: Line analysis of the 5µm scans of cpTi cast control sample surface

Standard Roughness	
Ra:	40.50 nm
Rp:	87.71 nm
Rpm:	50.04 nm
Rt:	161.40 nm
Rtm:	97.59 nm

Standard Roughness	
Ra:	58.39 nm
Rp:	77.40 nm
Rpm:	47.73 nm
Rt:	261.81 nm
Rtm:	147.13 nm

Standard Roughness	
Ra:	78.99 nm
Rp:	89.42 nm
Rpm:	65.36 nm
Rt:	317.62 nm
Rtm:	119.91 nm

Fig 5-31: Line analysis of the 5μm scans of Ti6Al4V machined control sample surface

Standard Roughness	
Ra:	372.59 nm
Rp:	608.32 nm
Rpm:	192.70 nm
Rt:	1287.49 nm
Rtm:	414.96 nm

Standard Roughness	
Ra:	185.82 nm
Rp:	620.01 nm
Rpm:	225.01 nm
Rt:	1102.43 nm
Rtm:	477.32 nm

Standard Roughness	
Ra:	503.63 nm
Rp:	1225.26 nm
Rpm:	341.53 nm
Rt:	2370.21 nm
Rtm:	650.42 nm
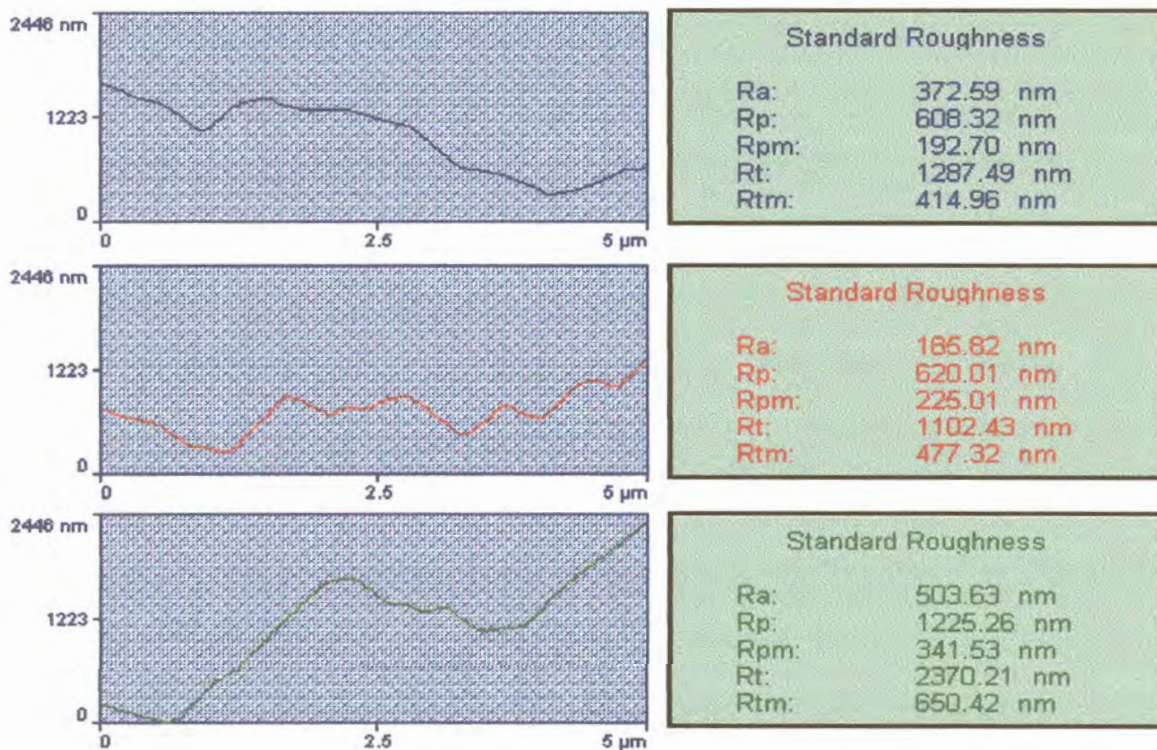
Fig 5-32: Line analysis of the 5μm scans of Ti6Al4V cast control sample surface

103

The means of the different Line analyses values for the 5μm scans are shown in Table 5-9 (see Addendum E, p188-192). Even at a smaller scan the surfaces of cast samples had higher values compared to machined samples.

Table 5-9: Averages of the line analysis done for the different sample surfaces for the 5μm scan.

Material	Ra	Rtm	Rt	Rpm	Rp
cpTi machined control surface	0.05	0.10	0.24	0.04	0.12
cpTi machined control surface & RFGDT	0.05	0.10	0.24	0.04	0.13
Ti6Al4V machined control surface	0.07	0.13	0.29	0.06	0.11
Ti6Al4V machined control surface & RFGDT	0.07	0.15	0.33	0.07	0.18
cpTi cast control surface	0.26	0.37	1.06	0.19	0.58
cpTi cast control surface & RFGDT	0.22	0.35	0.98	0.17	0.48
Ti6Al4V cast control surface	0.24	0.37	1.05	0.18	0.52
Ti6Al4V cast control surface & RFGDT	0.15	0.26	0.66	0.13	0.32

Ra

Ra is the average distance of the profile from the mean line (see 2.6.2.1, p33) Generally a smooth surface will have a very small value, as the distance from the mean is nearly absent. For both scans the Ra value was determined by the fabrication procedure and not by the material employed or treatment rendered. The mean Ra for the 20μm and 5μm scans of surfaces of cast samples was 0.31μm and 0.18μm and this value was significantly higher than that for surfaces of machined samples (0.10μm and 0.06μm).

Rt

The Rt value shows us the distance between the highest peak and lowest valley recorded (see 2.6.2.1, p33). For both the 20µm and 5µm scans there was a significantly higher peak for the surfaces of cast samples (1.66µm and 0.77µm) when compared with machined samples (0.52µm and 0.28µm). No significant differences were observed between the different materials used or the type of treatment rendered.

Rtm

Rtm is a measure of the peak to valley height (see 2.6.2.1, p34). The Rtm value of 0.76µm for the surfaces of cast samples was significantly higher than machined samples (0.24µm) for 20µm scans (p=0.0042). The 5µm scan had a similar significantly higher measure for the surfaces of cast samples (0.29µm) compared to machined surfaces (0.12µm). Rtm was determined solely by the fabrication process.

Rp

Rp is the measure of the single highest peak recorded on the image scan (see 2.6.2.1, p34) and for the 20µm scan it was significantly higher for the surfaces of cast samples (0.77µm) than the machined samples (0.24µm). Interestingly for the 20µm scans RFGDT significantly (p=0.04) increased the Rp value of the surfaces of cast samples to 0.62µm and machined samples to 0.39µm. For the 5µm scan fabrication determined the Rp value which was significantly higher for the surfaces of cast samples (0.40µm) compared to machined samples (0.13µm).

Rpm

Rpm is the measure of the mean peak heights on an image scan (see 2.6.2.1, p34). The Rpm for the surfaces of cast samples was 0.37µm (20µm scan) and 0.14µm (5µm scans) and was

significantly higher than machined samples (0.11µm and 0.05µm).

Fabrication procedures adopted significantly influenced line analyses of sample surfaces for the 20µm scans and a summary of the different values is shown in Fig 5-33.
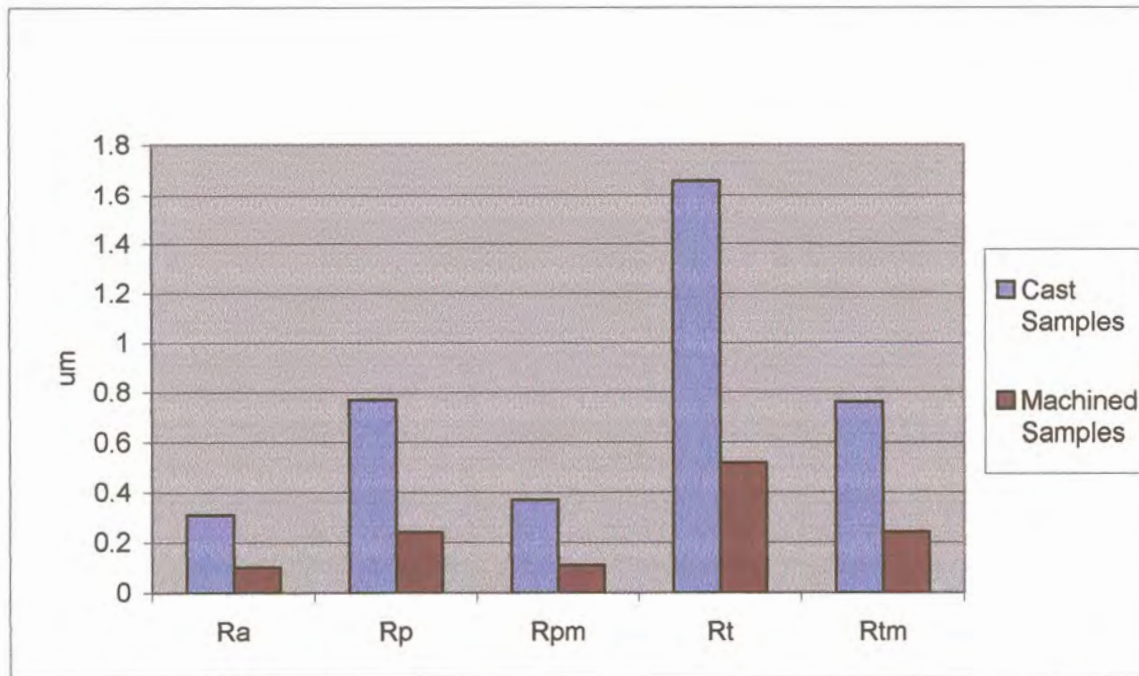
Fig 5-33: Different values of line analysis of sample surfaces as related to fabrication procedures for the 20µm scan

5.1.3   Depth Profile

Depth profiles depict the oxide thickness (see 2.6.3, p35). It is the distance between the outside or exterior of the sample and the bulk material.

Fig 5-34 (see p107) shows a tracing of the depth profile for the Ti6Al4V cast control RFGDT sample. Depth profiles of other samples are shown in Addendum G (see p196-199). As the overlying oxide is sputtered away, the O1s and Ti2p peaks from the oxide decreases and the O1s and Ti2p peaks from the substrate increases. The Oxygen signal from the substrate originates from dissolved Oxygen in the Titanium or Titanium alloy matrix (Louw, 1997).
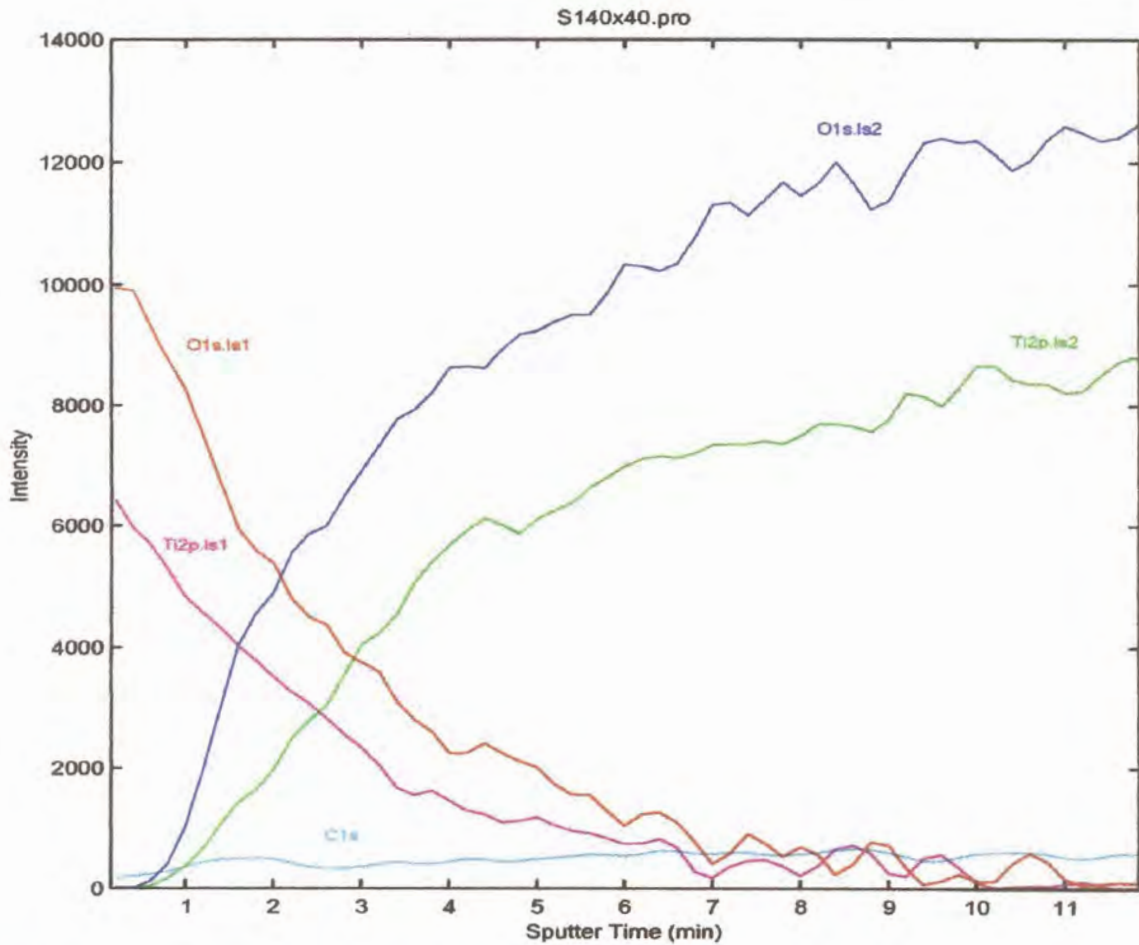
Fig 5-34: Tracing of the depth profile of Ti6Al4V cast control RFGDT sample

From the depth profile tracing the sputter time required for the oxygen peak to reach half its background concentration regardless of its initial intensity was recorded for each sample (see Table 5-10, p108). The oxide thickness was then calculated from the known sputter time of $3.5nm.sec^{-1}$ (see 4.4.3, p65).

Table 5-10: Sputter time and Oxide thickness of samples.

Sample	putter time (min)	Oxide thickness (nm)
cpTi machined control surface	0.8	2.8
cpTi machined control surface RFGDT	1.2	4.2
cpTi machined SI Enhanced	1.2	4.2
cpTi machined SI Enhanced RFGDT	2.2	7.7
cpTi machined ES Enhanced	1.6	5.6
cpTi machined ES Enhanced RFGDT	2.4	8.4
Ti6Al4V machined control surface	0.5	1.9
Ti6Al4V machined control surface RFGDT	0.8	2.8
Ti6Al4V machined SI Enhanced	1.8	6.3
Ti6Al4V machined SI Enhanced RFGDT	1.9	6.7
Ti6Al4V machined ES Enhanced	1.8	6.3
Ti6Al4V machined ES Enhanced RFGDT	2.0	7.0
cpTi cast control surface	1.8	6.3
cpTi cast control surface RFGDT	1.8	6.3
cpTi cast SI Enhanced	1.6	5.6
cpTi cast SI Enhanced RFGDT	2.4	8.4
cpTi cast ES Enhanced	1.5	5.3
cpTi cast ES Enhanced RFGDT	2.4	8.4
Ti6Al4V cast control surface	1.5	6.0
Ti6Al4V cast control surface RFGDT	2.1	7.4
Ti6Al4V cast SI Enhanced	1.2	4.2
Ti6Al4V cast SI Enhanced RFGDT	1.6	5.6
Ti6Al4V cast ES Enhanced	1.7	6.0
Ti6Al4V cast ES Enhanced RFGDT	2.4	8.4

Fig 5-35 (see p109) shows the oxide depth of the different samples analyzed before and after RFGDT. With the exception of the Ti6Al4V machined ES sample all other ES enhanced samples had similar oxide thicknesses of 8.4nm. cpTi cast SI sample also had a similar oxide thickness of 8.4nm.

The analysis showed that the method of fabrication employed had a significant effect on the oxide thickness of samples (p=0.0062) and it was higher for cast samples (6.47nm) than machined samples (5.32nm). Surface enhancement significantly increased the oxide thickness (p=0.0006). Control surfaces had a thinner oxide (4.70nm) compared to enhanced surfaces (SI=6.08nm and ES=6.91nm). On average the oxide thickness was significantly thicker on RFGDT samples (6.77nm) than untreated samples (5.03nm)(p=0.0002). There was an interaction between the method of fabrication and surface enhancement and machined control surfaces had significantly lower oxide thicknesses

(2.93nm) compared to other samples (p=0.0011). Material used for sample preparation had no apparent influence on the oxide thickness.
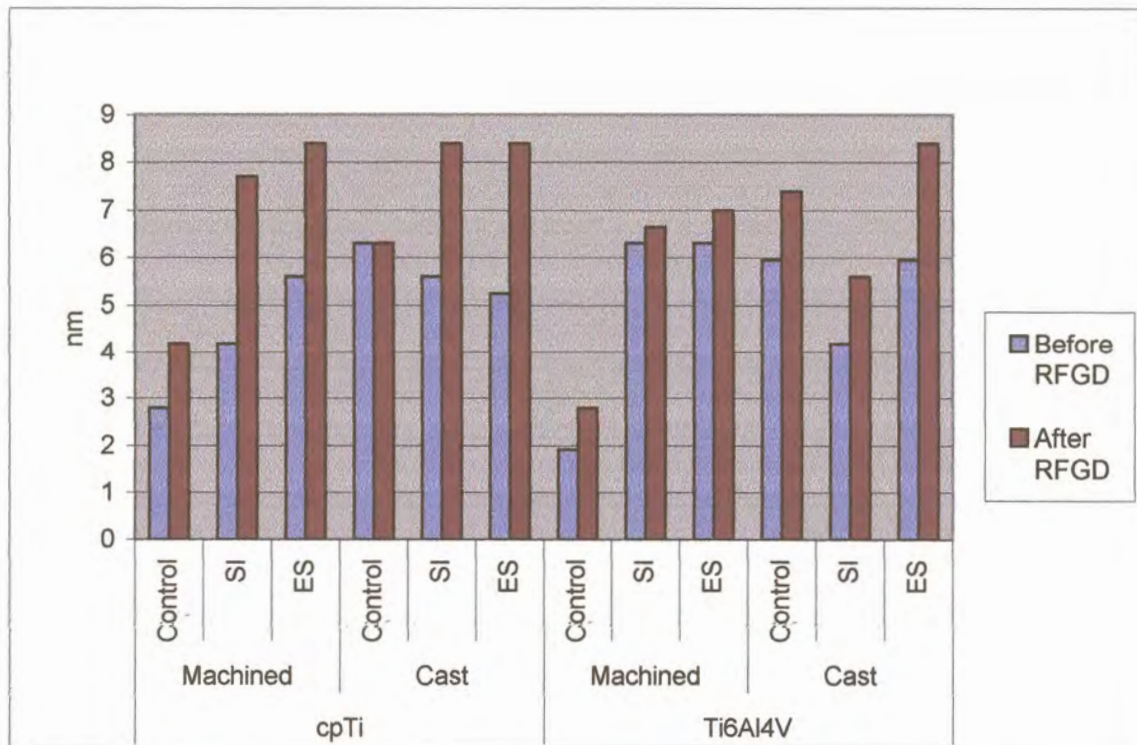
Fig 5-35: Oxide thickness of sample surfaces

5.2   Cell Culturing

5.2.1   Cell Attachment

5.2.1.1   Fibroblasts

At time zero, fibroblasts of $10.58 \times 10^4 cells.ml^{-1}$ concentration were inoculated on cpTi and Ti6Al4V samples and Tissue Culture plastic, as a control. At time intervals of 1 day, 2 days, 14 days and 28 days the cells were counted and their % attachment efficiency and proliferation determined (see Addendum A, p178).

A comparison of the mean % attachment efficiency and proliferation of fibroblasts on samples showed that there was

no significant difference between day 1 (40.21%) and 2 (47.11%), but a significant difference was noted between day 1 and 2 and day 14 (79.94%). Day 14 was also significantly lower than day 28 (130.07%).

When fibroblasts were analyzed for their % attachment efficiency and proliferation on the different surfaces no significant differences were observed between samples regardless of surface characteristics. The machined Ti6Al4V control sample had the highest % attachment efficiency and proliferation for fibroblasts (88.743%) compared even to the control surface of tissue culture plastic (86.55%). The lowest % attachment efficiency and proliferation of fibroblasts was on cpTi cast control surface (58.52%)(p>0.05).

Fig 5-36 shows a line graph for the % attachment efficiency and proliferation for fibroblasts on the different sample surfaces prepared from cpTi by machining. It is seen that fibroblasts behave similarly up to day 14, where the machined cpTi ES samples showed a higher % attachment efficiency and proliferation, even to the control. At 28 days the machined cpTi SI sample had the lowest % attachment efficiency and proliferation compared to the other machined cpTi control and ES samples (p<0.05).
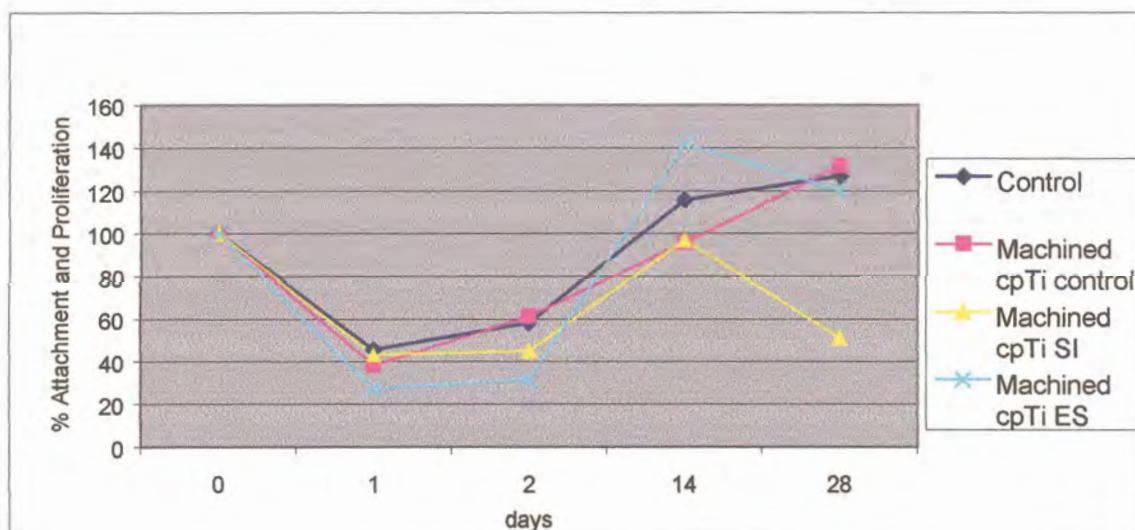
Fig 5-36: Percent attachment efficiency and proliferation of fibroblasts on machined cpTi samples

A line graph of the % attachment efficiency and proliferation of fibroblasts on machined Ti6Al4V samples (see Fig 5-37), shows that the samples had a similar trend, up to day 14, where samples were more or less similar in % attachment and proliferation. At day 28 the machined Ti6Al4V control sample maintained a much higher % attachment efficiency and proliferation that was similar to the control, and about double the % attachment and proliferation rate of the SI and ES samples (p>005).
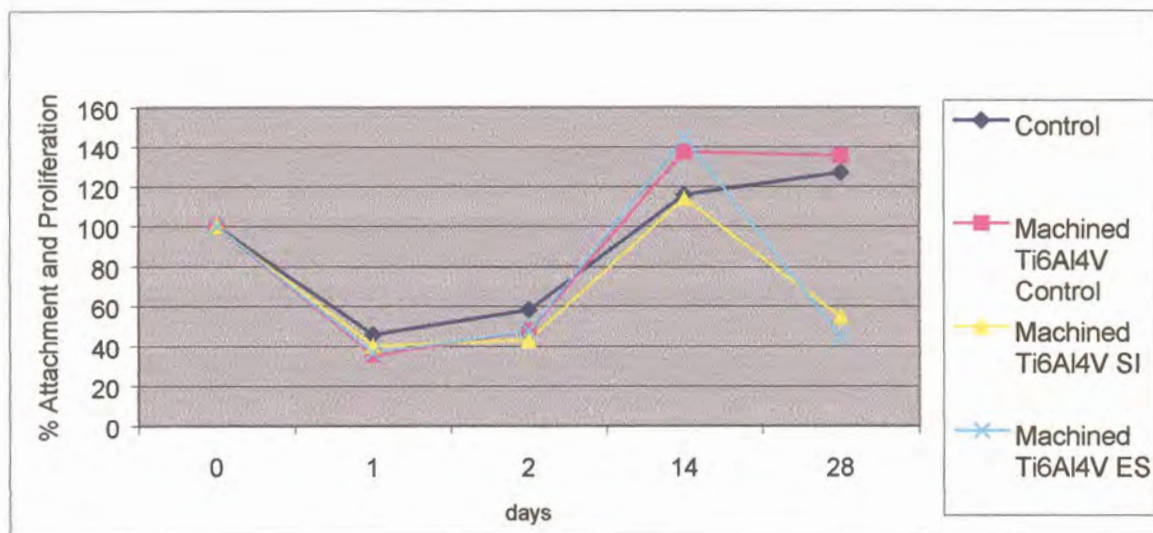
Fig 5-37: Percent attachment efficiency and proliferation of fibroblasts on machined Ti6Al4V samples

Fig 5-38 (see p 112) is a line graph for fibroblast cells exposed to surfaces of cast cpTi samples. No results were reported for the cast cpTi SI surface due to contamination. Cast cpTi control and ES samples had a much lower % attachment efficiency and proliferation than the control, with the cast cpTi control surface having the lowest % attachment efficiency and proliferation (p>0.05).
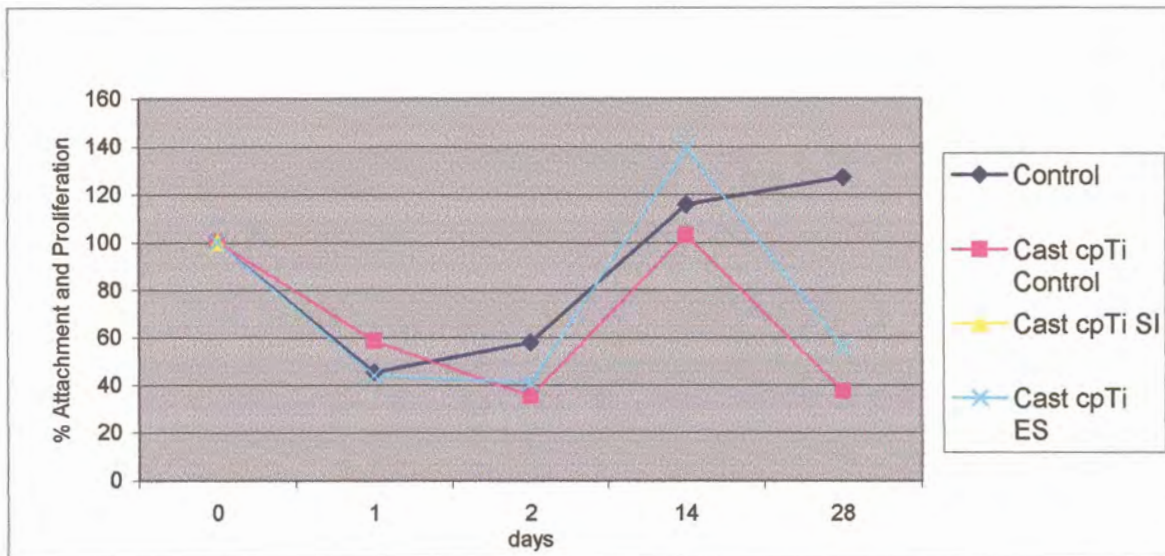
Fig 5-38: Percent attachment efficiency and proliferation of fibroblasts exposed to cast cpTi samples

When surfaces of cast Ti6Al4V samples were analyzed (see Fig 5-39), the % attachment efficiency and proliferation of fibroblasts was seen to be similar up to day 2. At day 14, a spike in % attachment efficiency and proliferation is seen for the cast Ti6Al4V control sample, which is much higher than the control (p>0.05). The cast Ti6Al4V control, SI and ES samples at 28 days had a much lower % attachment efficiency and proliferation of fibroblasts than the control (p>0.05).
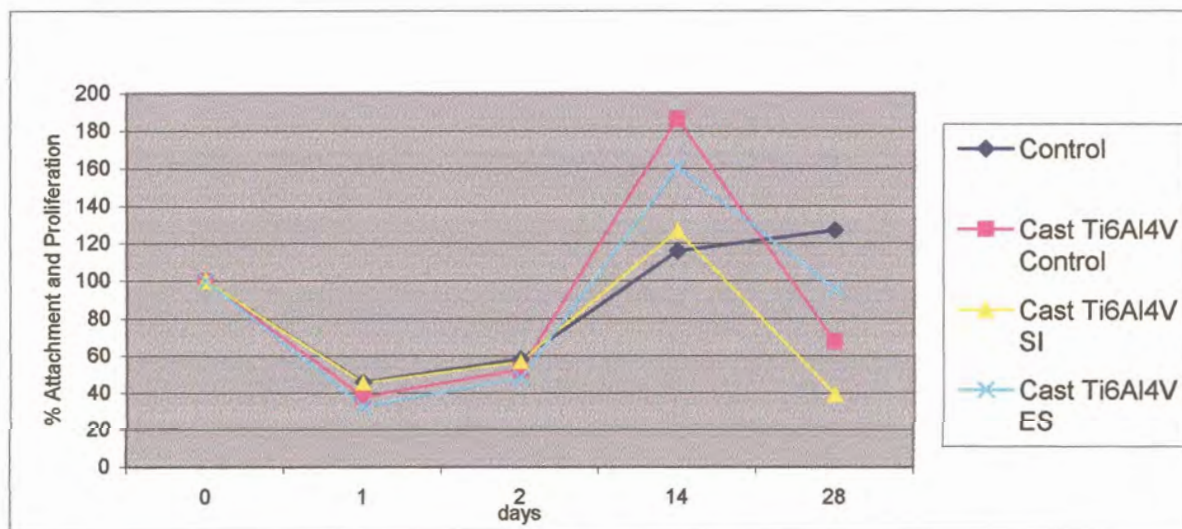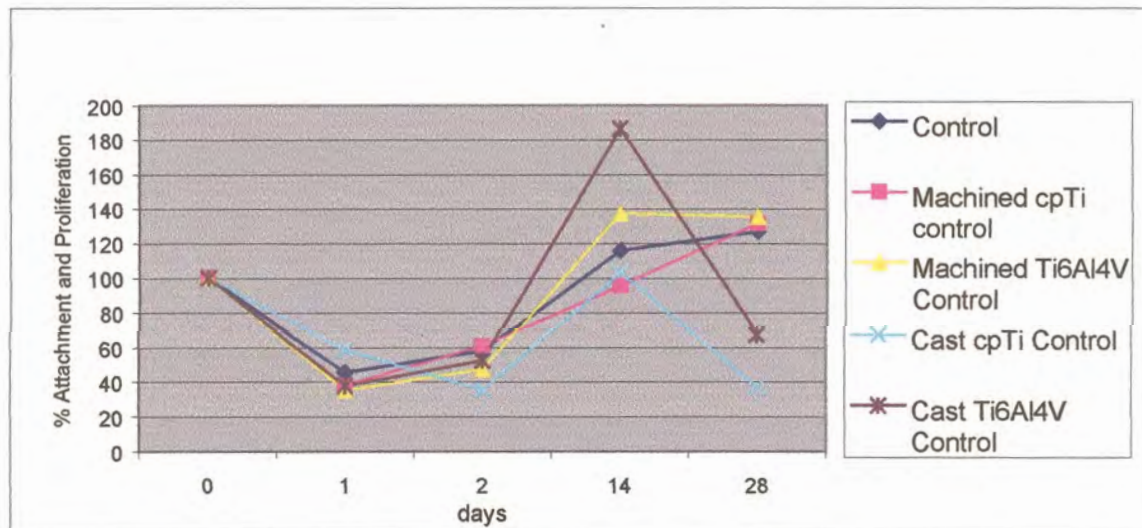

Fig 5-39: Percent attachment efficiency and proliferation of fibroblasts exposed to cast Ti6Al4V samples

Fig 5-40 shows the % attachment efficiency and proliferation of fibroblasts on the surfaces of all machined samples. The % attachment efficiency and proliferation of samples followed a similar trend up to 14 days with different maximum percentages. At 28 days the machined cpTi SI, machined Ti6Al4V SI and machined Ti6Al4V ES samples were observed to have a lower % attachment efficiency and proliferation compared to other samples. The machined cpTi and Ti6Al4V control and the machined cpTi ES samples had a % attachment efficiency and proliferation similar to the control that was much higher than the other samples (p>0.05).
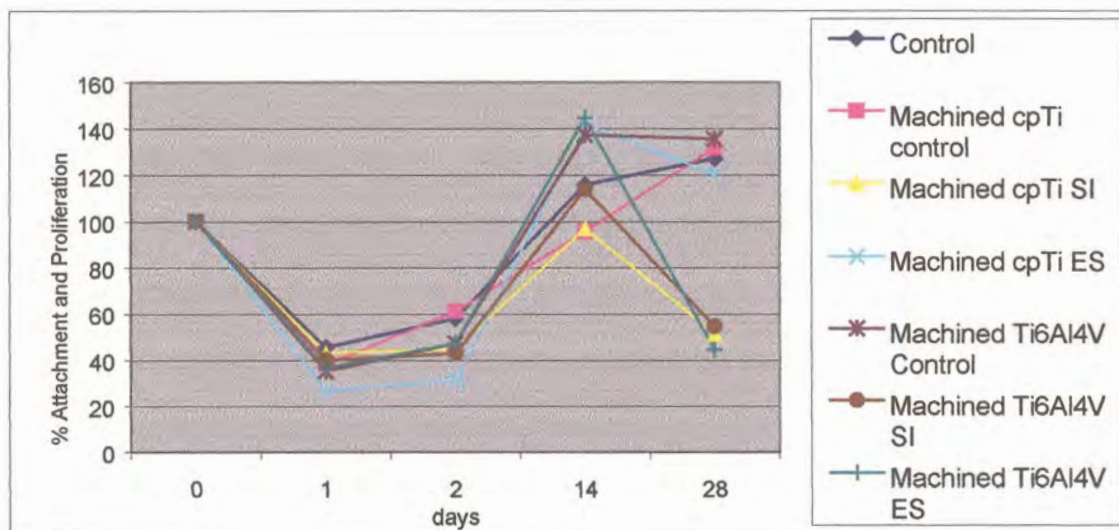
Fig 5-40: Percent attachment efficiency and proliferation of fibroblasts exposed to machined samples

Fig 5-41 (see p114) shows the line graph for fibroblasts on surfaces of cast samples. Cast samples behaved in a similar manner up to day 2. From day 2 to day 14, there was an increased in % attachment efficiency and proliferation of cells, but at different rates. The cast Ti6Al4V control recorded nearly double the % attachment efficiency and proliferation than the cast cpTi control sample (p>0.05). A decline was observed in comparison to the control at 28 days. Cast cpTi control and cast Ti6Al4V SI samples had the lowest % attachment efficiency and proliferation compared to other cast samples (p>0.05).
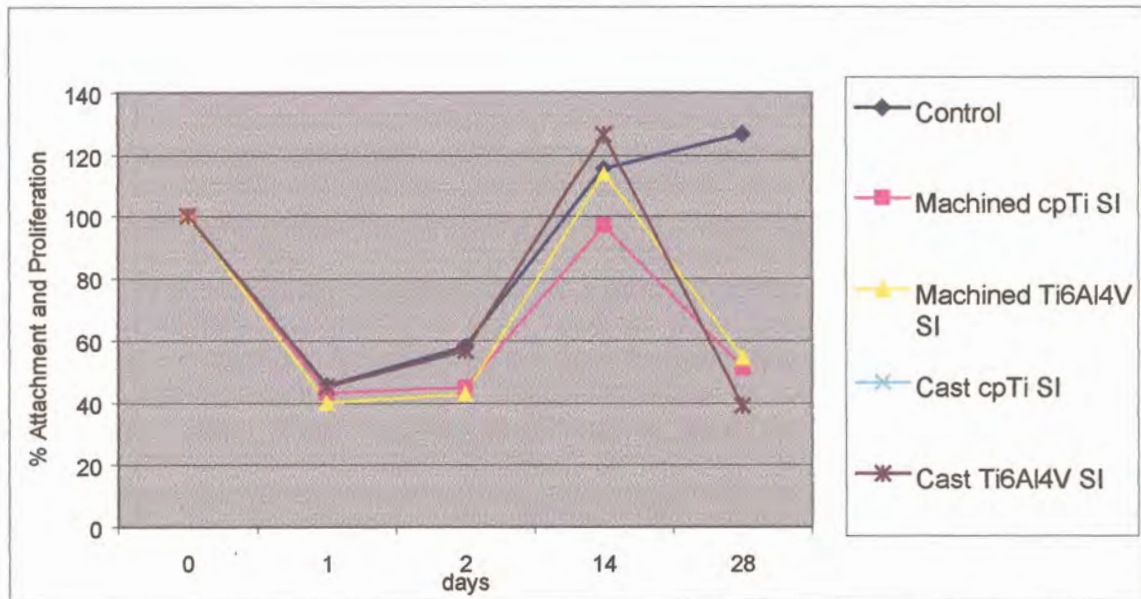
113
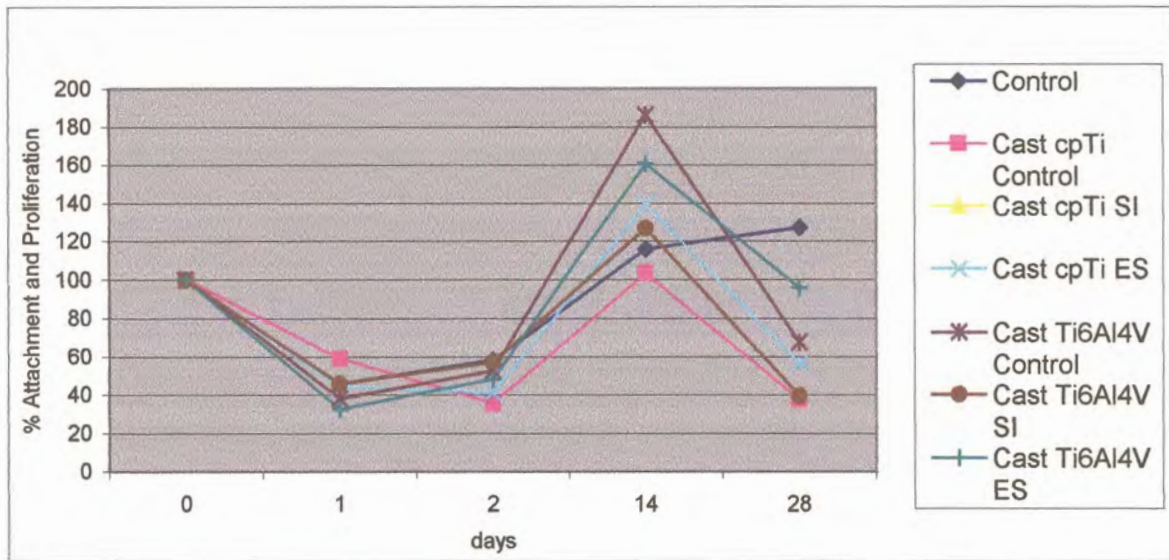
Fig 5-41: Percent attachment efficiency and proliferation of fibroblasts exposed to cast samples

Fig 5-42 shows the % attachment efficiency and proliferation of fibroblasts on fabricated control samples. Though the % attachment efficiency and proliferation was similar for day 1 and 2, at day 14 cast Ti6Al4V samples showed the highest % attachment efficiency and proliferation in comparison to the other samples and the control (p>0.05). At day 28 the % attachment efficiency and proliferation for the machined control samples was higher than the cast control samples (p>0.05).

Fig 5-42: Percent attachment efficiency and proliferation of fibroblasts exposed to different control samples

Fig 5-43 shows the % attachment efficiency and proliferation of fibroblasts on surfaces of SI enhanced samples. Regardless of the material or fabrication procedure, the SI enhanced samples showed a similar trend, but at 28 days they had a much lower % attachment efficiency and proliferation compared to the control (p>0.05).

Fig 5-43: Percent attachment efficiency and proliferation of fibroblasts exposed to SI enhanced samples

The % attachment efficiency and proliferation of fibroblasts on surfaces of ES samples is shown in Fig 5-44 (see p116). The samples had a similar trend of % attachment efficiency and proliferation up to day 2. At day 14 all samples had a higher % attachment efficiency and proliferation than the control (p>0.05). The cast Ti6Al4V ES had a higher % attachment efficiency and proliferation than the control (p>0.05). The machined cpTi ES sample was closer in % attachment efficiency and proliferation to the control than the other samples at 28 days (p>0.05).
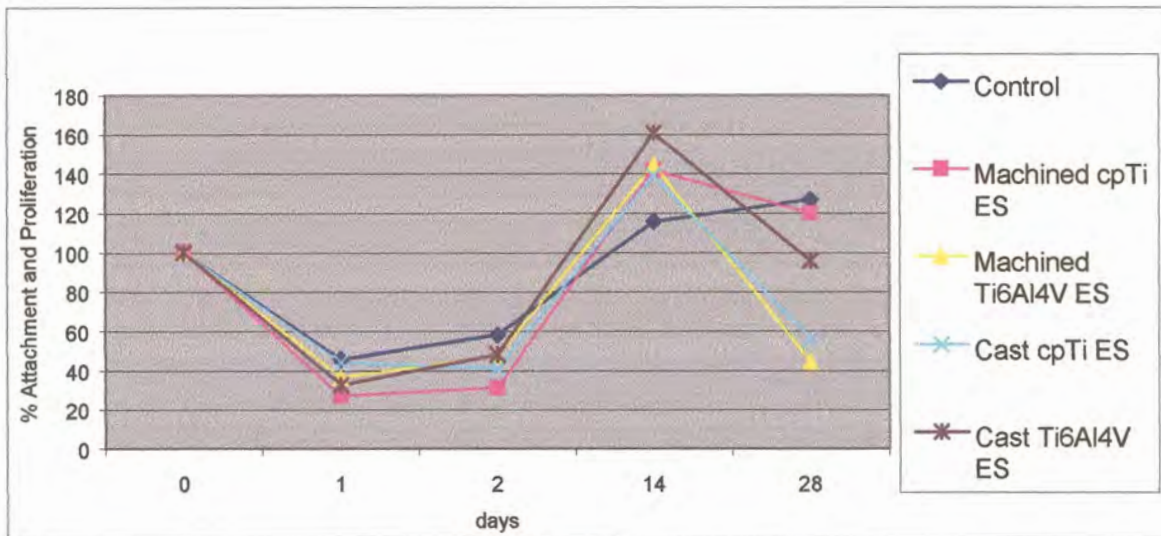
Fig 5-44: Percent attachment efficiency and proliferation of fibroblasts exposed to ES samples

5.2.1.2 Osteoblast-like Cells

At time zero osteoblasts-like cells of 11.0 X 10^4 cells.ml^{-1} concentration were inoculated on cpTi and Ti6Al4V samples and Tissue Culture plastic, as a control. At time intervals of 2 days, 14 days and 28 days the cells were counted and their % attachment efficiency and proliferation determined. Counts of day 1 were lost due to infection (see Addendum B, p179).

A comparison of mean % attachment efficiency and proliferation showed that day 14 (163.75%) was significantly higher than day 2 and day 28 (p=0.0004). Day 2 (98.05%) and day 28 (79.00%) showed no differences (p>0.05).

When surfaces were analyzed for their % attachment efficiency and proliferation for osteoblasts-like cells, no significant differences were observed between the different samples regardless of surface characteristics, but the % attachment efficiency and proliferation on the surface of cast cpTi control sample (77.37%) was about half that on machined Ti6Al4V SI sample (145.09%) (p>0.05). The osteoblasts-like cells on different samples were observed to have a % attachment efficiency and proliferation that was either higher or lower than the control (109.58%) (p>0.05).

116

Fig 5-45 shows the % attachment efficiency and proliferation of osteoblasts-like cells on the surfaces of machined cpTi samples. The machined cpTi SI and ES samples maintained more or less a steady growth from day 2 to day 14. The machined cpTi control sample had a much higher % attachment efficiency and proliferation than the other machined cpTi samples but lower than the control surface (p>0.05). The % attachment efficiency and proliferation of osteoblasts-like cells on machined cpTi SI sample was stable to day 28 unlike other samples that showed a decline at day 28 (p>0.05). At day 28 samples were still having a higher % attachment efficiency and proliferation than the control (p>0.05).
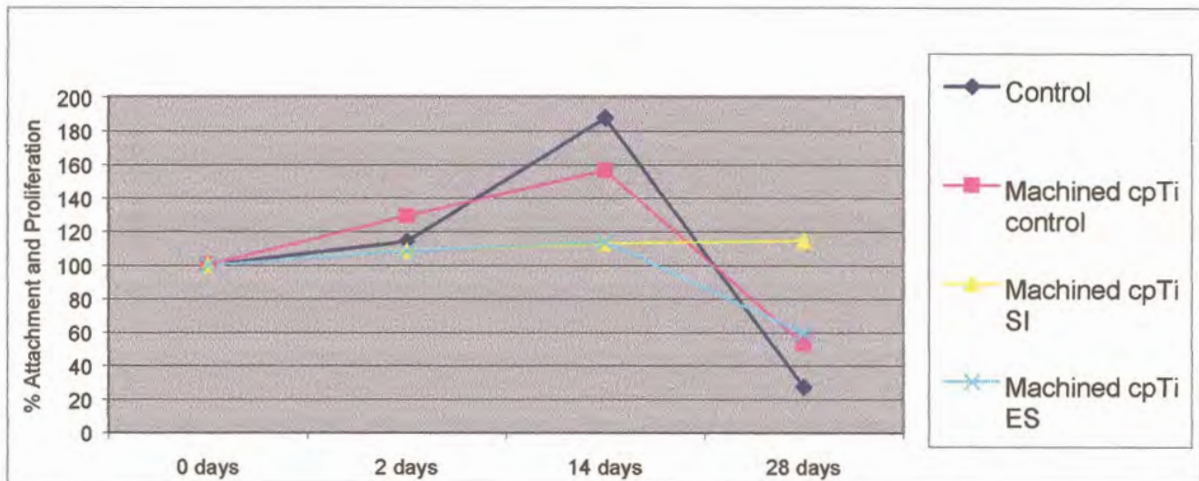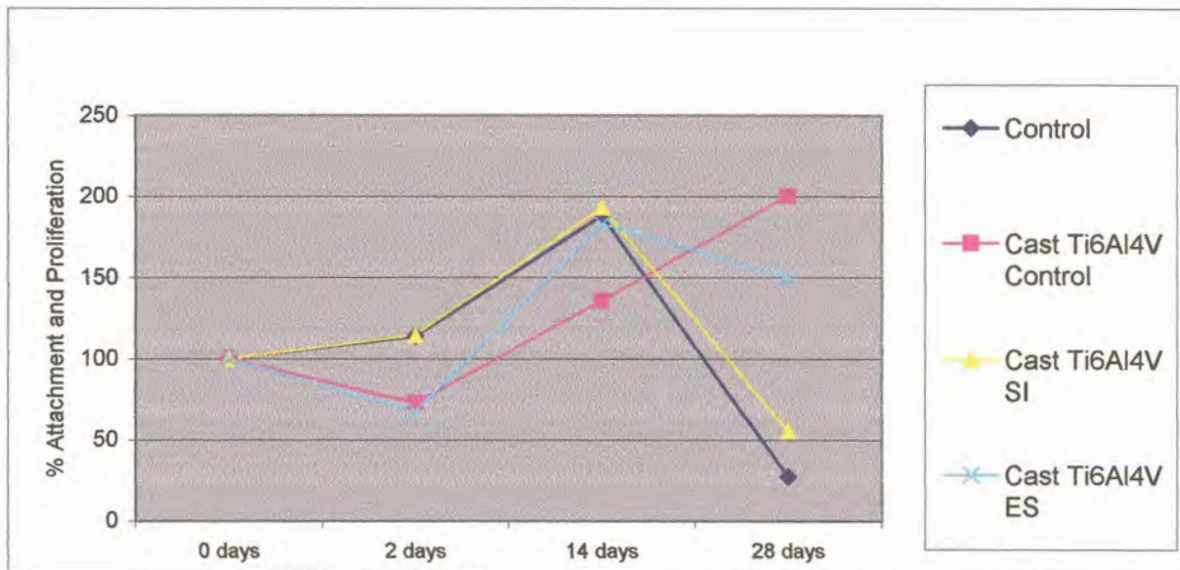

Fig 5-45: Percent attachment efficiency and proliferation of osteoblasts-like cells exposed to machined cpTi samples

Fig 5-46 (see p118) shows the % attachment efficiency and proliferation of osteoblasts-like cells on surfaces of machined Ti6Al4V samples. The % attachment efficiency and proliferation varied between samples at day 2. At day 14, there was an increase in % attachment efficiency and proliferation for all samples with the machined Ti6Al4V SI sample having a similar count as the control (p>0.05). At day 28 the machined Ti6Al4V SI sample was about 10 fold higher in % attachment efficiency and proliferation than the other

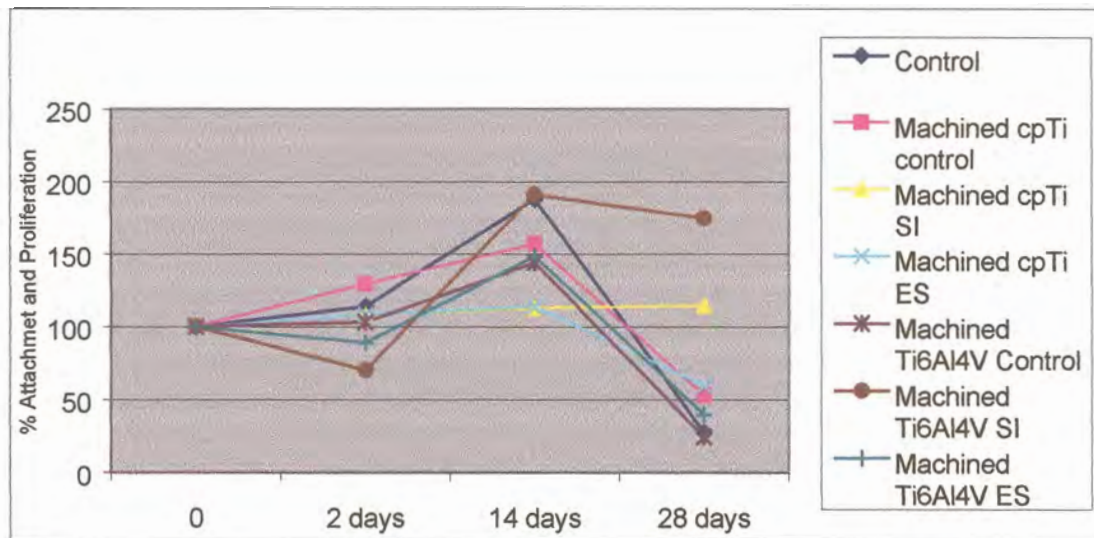samples that showed a decline in % attachment efficiency and proliferation to below 50% (p>0.05).
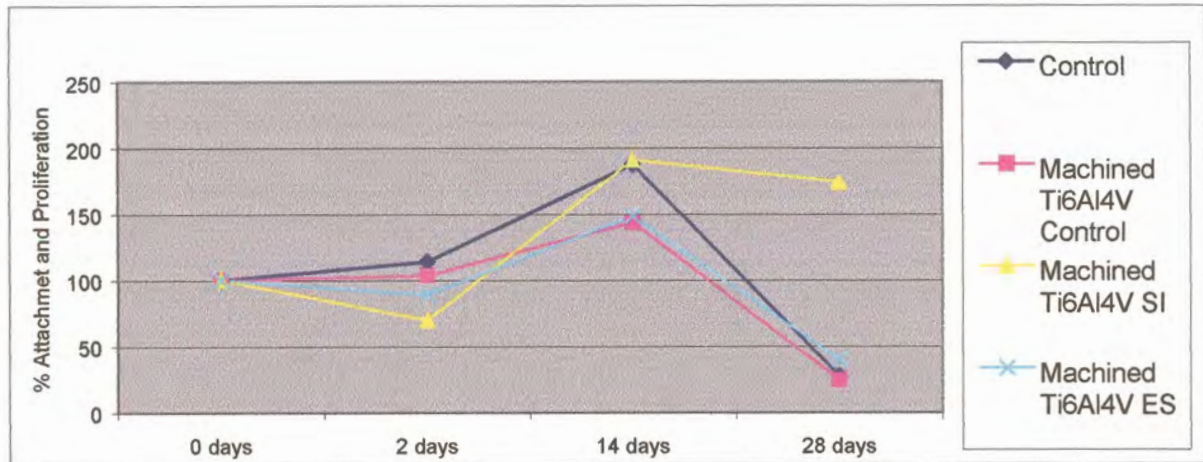
Fig 5-46: Percent attachment efficiency and proliferation of osteoblasts-like cells exposed to machined Ti6Al4V samples

The % attachment efficiency and proliferation of osteoblasts-like cells on surfaces of cast cpTi samples is shown in Fig 5-47. Although samples behaved more or less the same at day 2, at day 14, other samples and the control had a higher % attachment efficiency and proliferation compared to cast cpTi control sample which was more or less similar to day 2 (p>0.05). All samples showed a decline in % attachment efficiency and proliferation at day 28 (p>0.05).
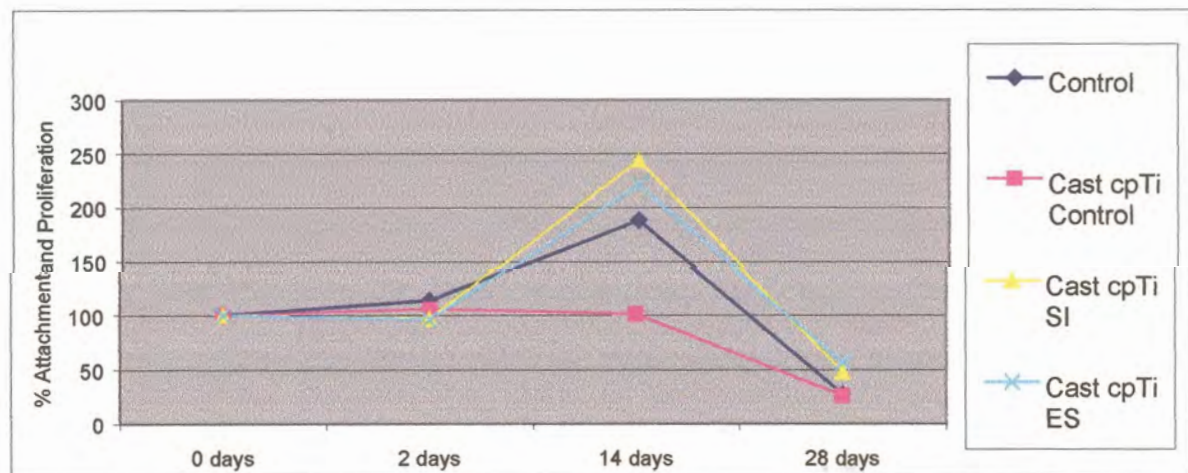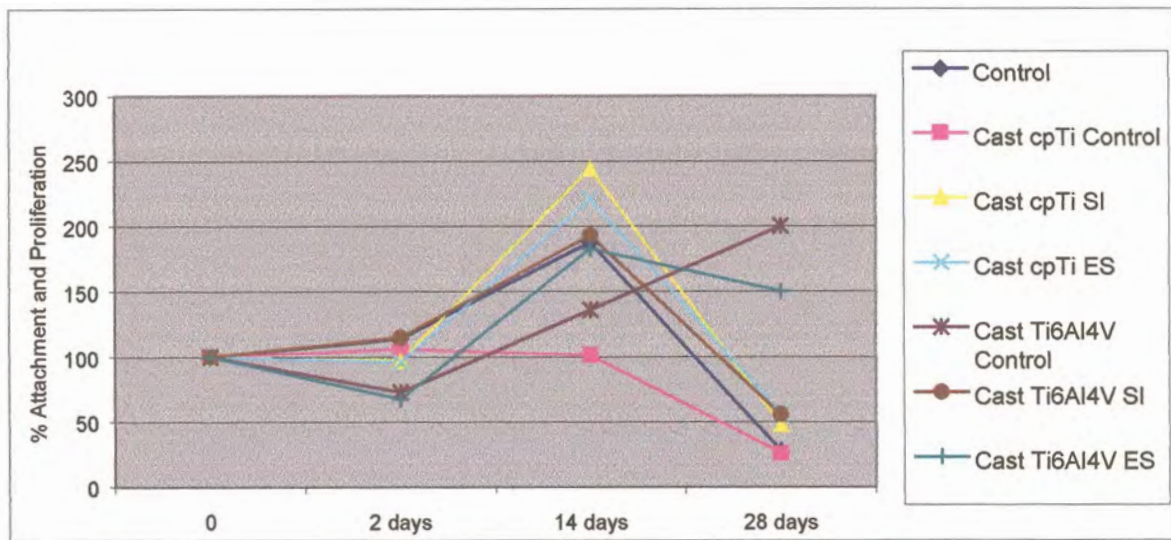

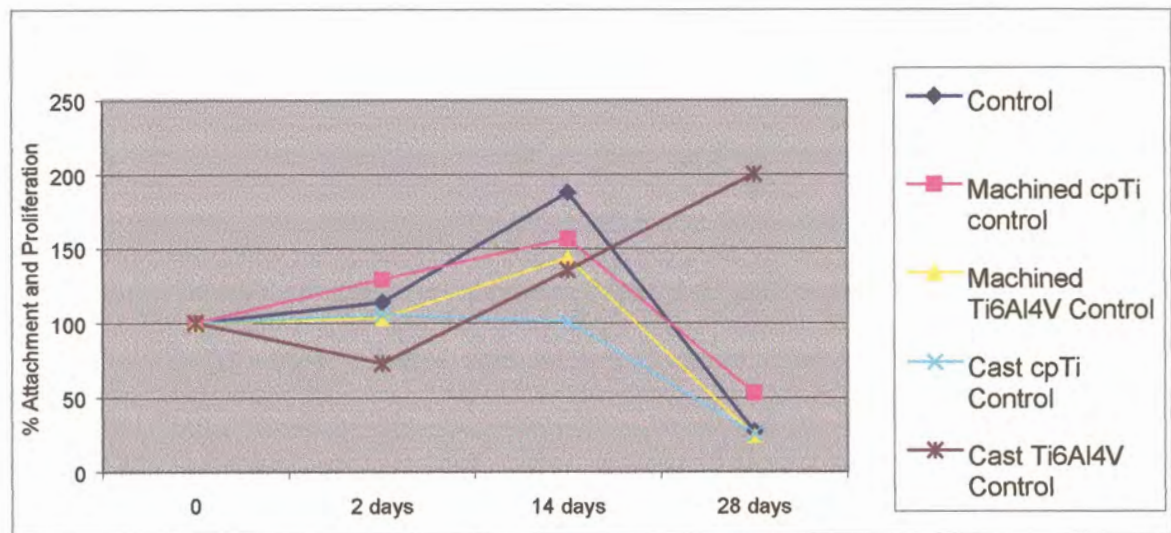Fig 5-47: Percent attachment efficiency and proliferation of osteoblasts-like cells exposed to cast cpTi samples

Fig 5-48 shows the % attachment efficiency and proliferation of osteoblasts-like cells on surfaces of cast Ti6Al4V samples. The cast Ti6Al4V control sample showed an increase in % attachment efficiency and proliferation over time. The cast Ti6Al4V SI declined similar to the control at day 28. The cast Ti6Al4V ES sample maintained a % attachment efficiency and proliferation of over 150% at day 28 that was much higher than the control and cast Ti6AL4V SI samples (p>0.05).

Fig 5-48: Percent attachment efficiency and proliferation of osteoblasts-like cells exposed to cast Ti6Al4V samples

Fig 5-49 (see p120) shows the % attachment efficiency and proliferation of osteoblasts-like cells on surfaces of machined samples. The machined Ti6Al4V SI sample had the lowest % attachment efficiency and proliferation at day 2 compared to other samples. At day 14 it had increased to the same % as the control and at day 28 it still had the highest % attachment efficiency and proliferation of over 150% (p>0.05). The machined cpTi SI sample maintained a steady % attachment efficiency and proliferation over time. All other samples including the control dropped in % attachment efficiency and proliferation at 28 days (p>0.05).
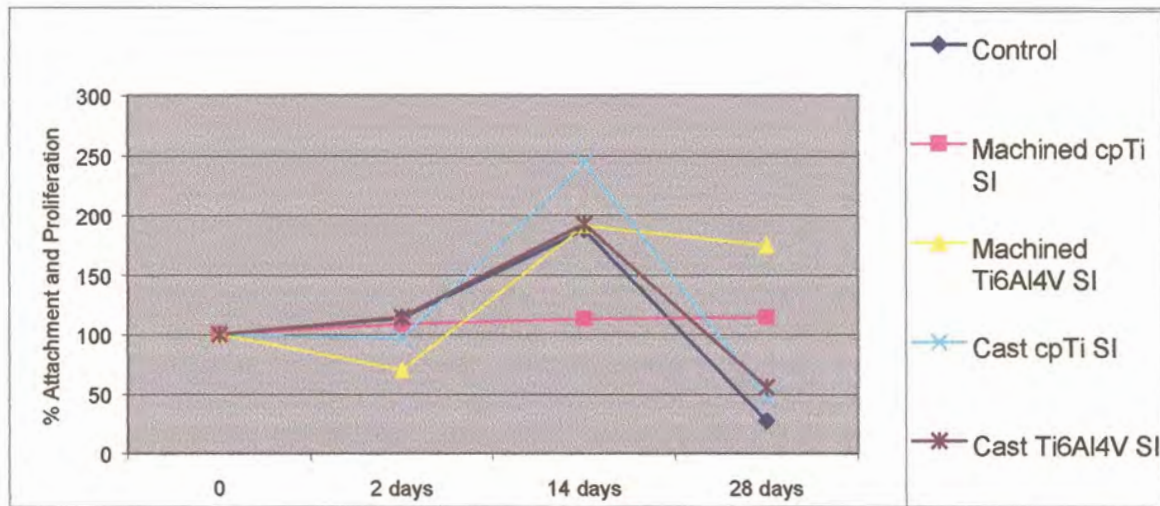
Fig 5-49: Percent attachment efficiency and proliferation of osteoblasts-like cells exposed to machined samples

Fig 5-50 (see p121) shows the % attachment efficiency and proliferation of osteoblasts-like cells on surfaces of cast samples. Cast cpTi control sample maintained a constant % attachment efficiency and proliferation to day 14 after which it declined to have the lowest % attachment efficiency and proliferation at day 28 (p>0.05). At day 14, the cast cpTi SI surface had the highest % attachment efficiency and proliferation compared to other samples and showed a decline in % attachment efficiency and proliferation at 28 days (p>0.05). At day 28, the cast Ti6Al4V control sample had the highest proliferation rate followed by the cast cpTi ES surface though both showed an initial decrease in % attachment efficiency and proliferation at day 2 (p>0.05).

Fig 5-51 (see p121) shows the % attachment efficiency and proliferation for osteoblasts-like cells on control surfaces of samples. The cast Ti6Al4V control had an initial decline at day 2, followed by a steady increase to day 14 and day 28. At day 28, it had the highest % attachment efficiency and proliferation of 200% compared to other surfaces (p>0.05). All other samples had a low % attachment efficiency and proliferation at day 28 (p>0.05).

Fig 5-50: Percent attachment efficiency and proliferation of osteoblasts-like cells exposed to cast samples

Fig 5-51: Percent attachment efficiency and proliferation of osteoblasts-like cells exposed to control surfaces of samples

Fig 5-52 (see p122) shows the % attachment efficiency and proliferation of osteoblasts-like cells on surfaces of SI samples. A steady % attachment efficiency and proliferation was maintained over time on machined cpTi SI samples. The machined Ti6Al4V SI sample had an initial decrease in percent attachment efficiency and proliferation at day 2 but the highest at day 28 (p>0.05). At day 14, cast cpTi SI samples had the highest % attachment efficiency of over 200% but decreased to about 50% by day 28 (p>0.05).

Fig 5-52: Percent attachment efficiency and proliferation of osteoblasts-like cells exposed to SI samples

Fig 5-53 shows the % attachment efficiency and proliferation of osteoblasts-like cells on surfaces of ES samples. The cast Ti6Al4V ES sample had the highest % attachment efficiency and proliferation at 28 days compared to other samples, but initially showed a decline at day 2. The cast cpTi ES sample had the highest % attachment efficiency and proliferation of over 200% at day 14 but declined to about 50% at day 28. Results show that up to day 14 machined cpTi ES samples maintained a constant % attachment efficiency and proliferation after which a declined was observed at day 28.
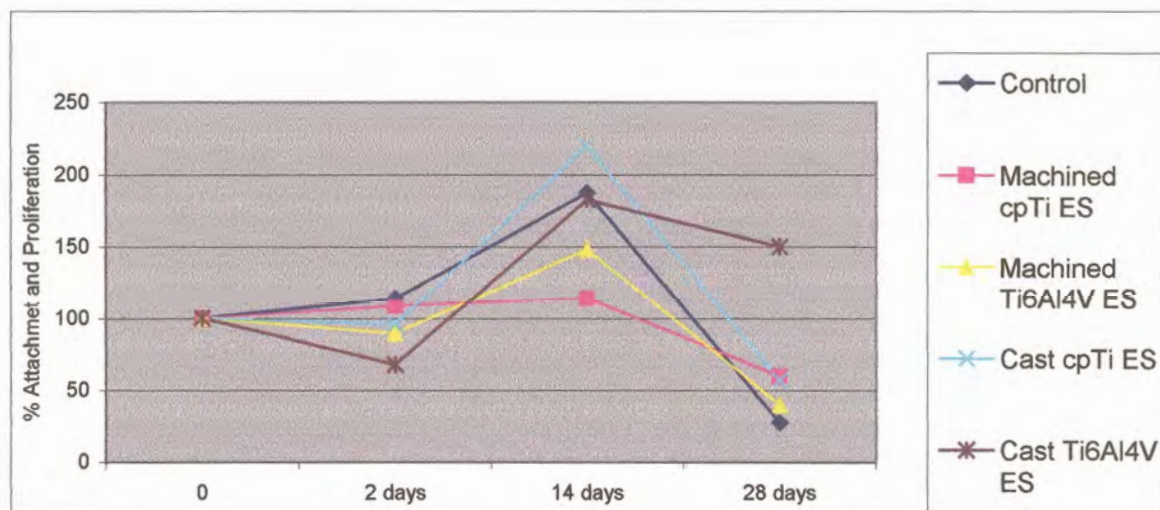
Fig 5-53: Percent attachment efficiency and proliferation of osteoblasts-like cells exposed to ES samples

5.2.2   Scanning Electron Microscope Analysis

5.2.2.1   Fibroblasts

Two days

Following seeding, the fibroblasts were seen to attach and spread, displaying an extremely flat configuration, in an apparent attempt to colonize the entire substrate surface (see Fig 5-54 and 5-55, p124). The cells were seen to be in close contact with the surface of the sample discs and though a network of cells is seen over the surface, there are still areas where cells have not spread or attached. The neighboring cells maintained contact with one another in a haphazard manner through multiple extensions, varying from extremely short to relative long extensions. The machined Ti6Al4V control sample was the only sample that had a monolayer of cells on its surface after 2 days and it appeared more intense than the control sample (see Fig 5-55, p124). With the proliferation and spreading of cells it was difficult to identify individual cells within the continuous sheet.
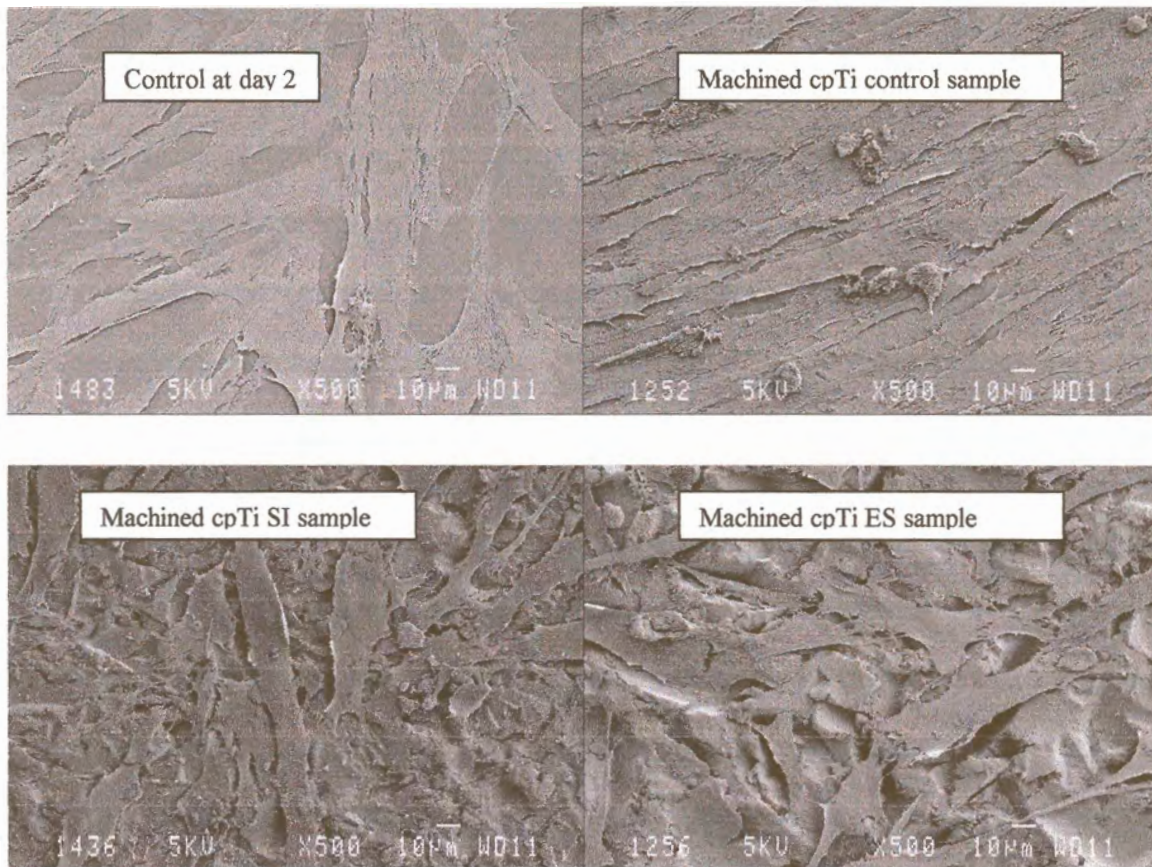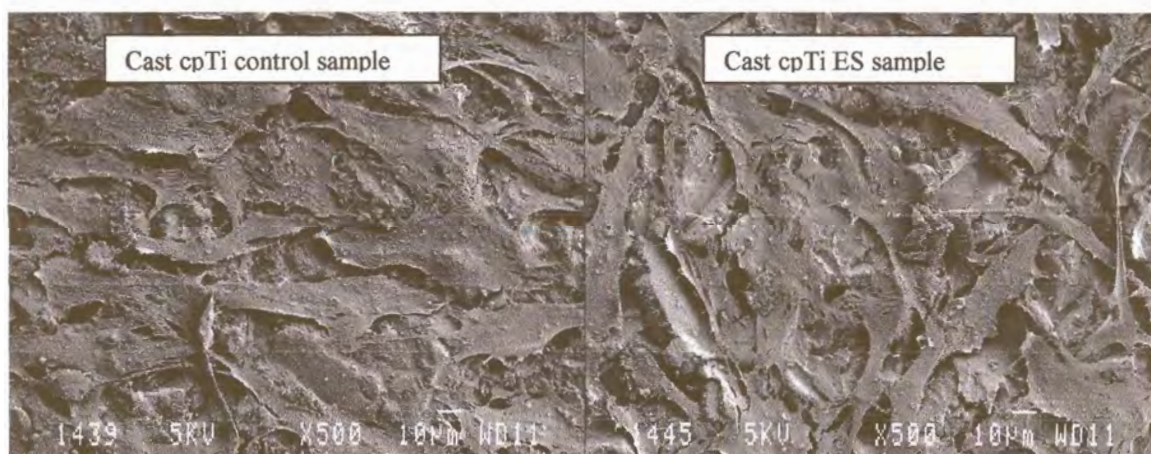
Fig 5-54: Growth of fibroblasts on surfaces of machined cpTi samples after 2 days incubation
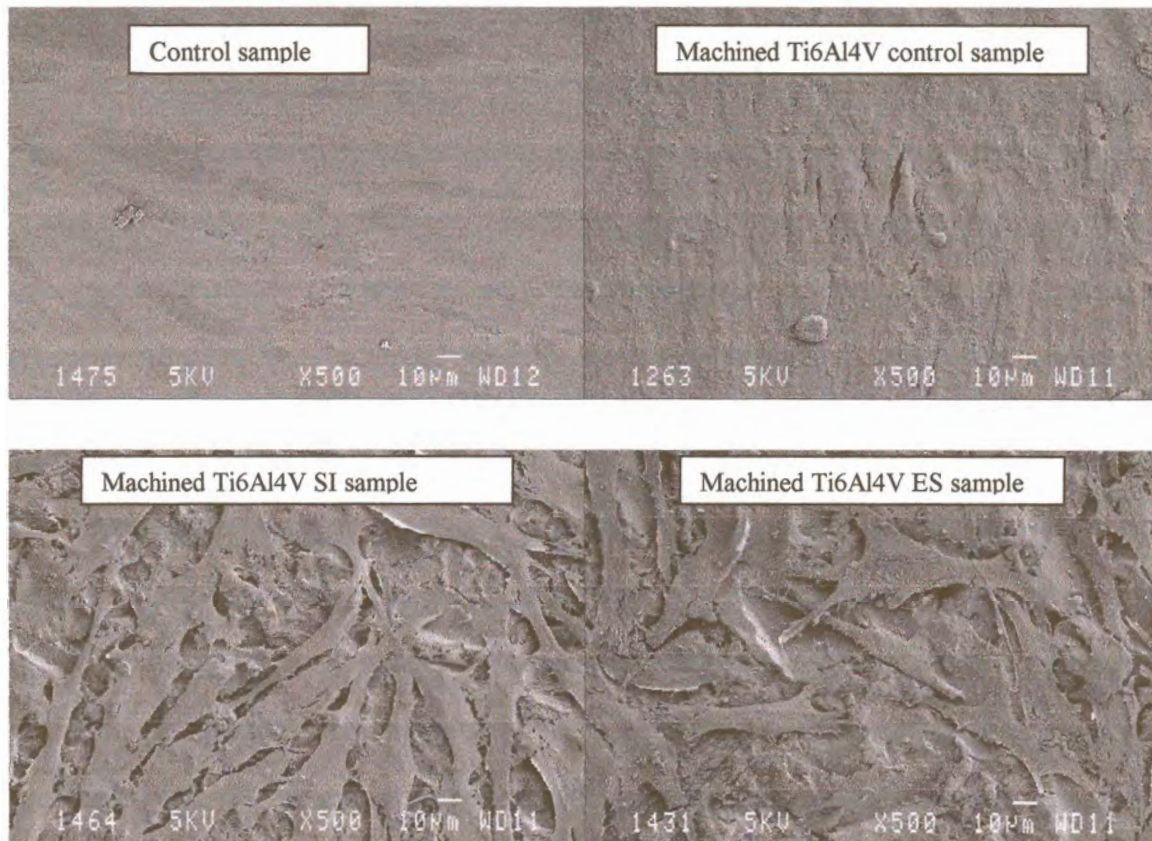
Fig 5-55: Growth of fibroblasts on surfaces of machined Ti6Al4V samples after 2 days incubation

On machined control surfaces fibroblasts were observed to have spread at a much faster rate and appeared to follow the topography created by the machining grooves (see Fig 5-56).
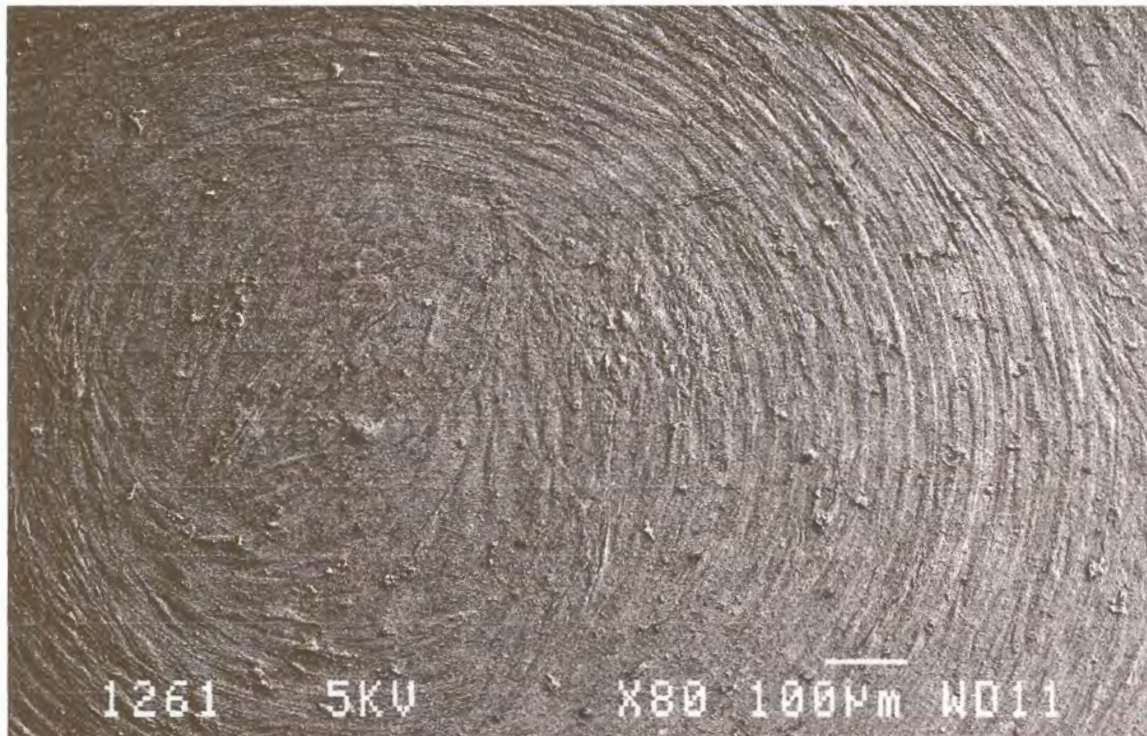
Fig 5-56: Fibroblasts aligned according to the grooves created by machining on surface of machined Ti6Al4V control sample

Fibroblasts on cast samples had a similar appearance to the machined enhanced samples (see Fig 5-57). Cells were flattened and polygonal in shape. Some parts of the surface were still visible between the spread cells.
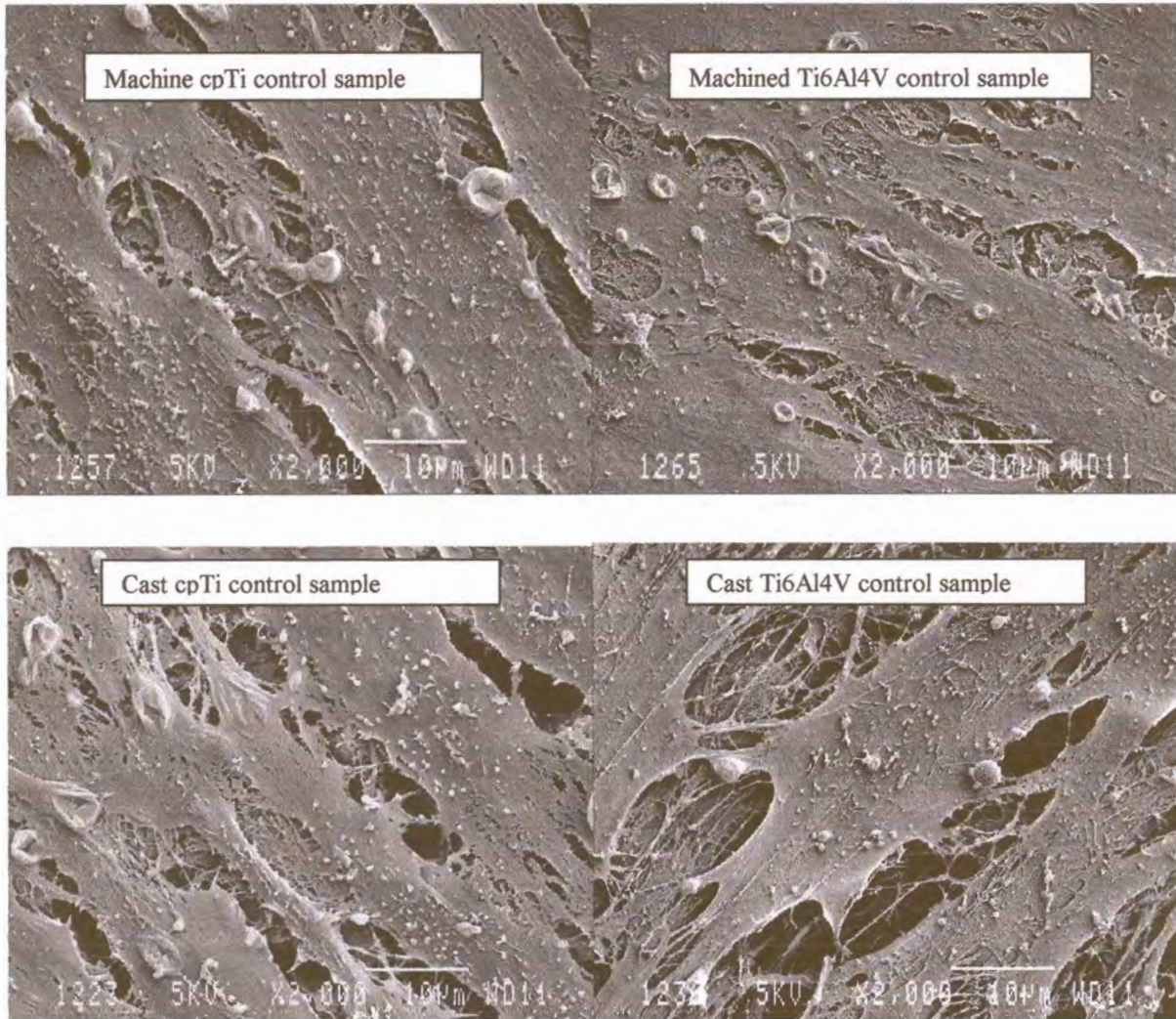

Fig 5-57: Growth of fibroblasts on surfaces of cast cpTi samples after 2 days incubation

Fig 5-58 shows fibroblasts on the surfaces of cast Ti6Al4V and the control samples. Regardless of type of surface preparation, fibroblasts spread on all surfaces with a similar intensity. On the cast Ti6Al4V ES sample long filopodial extensions are seen amidst the spread cells.
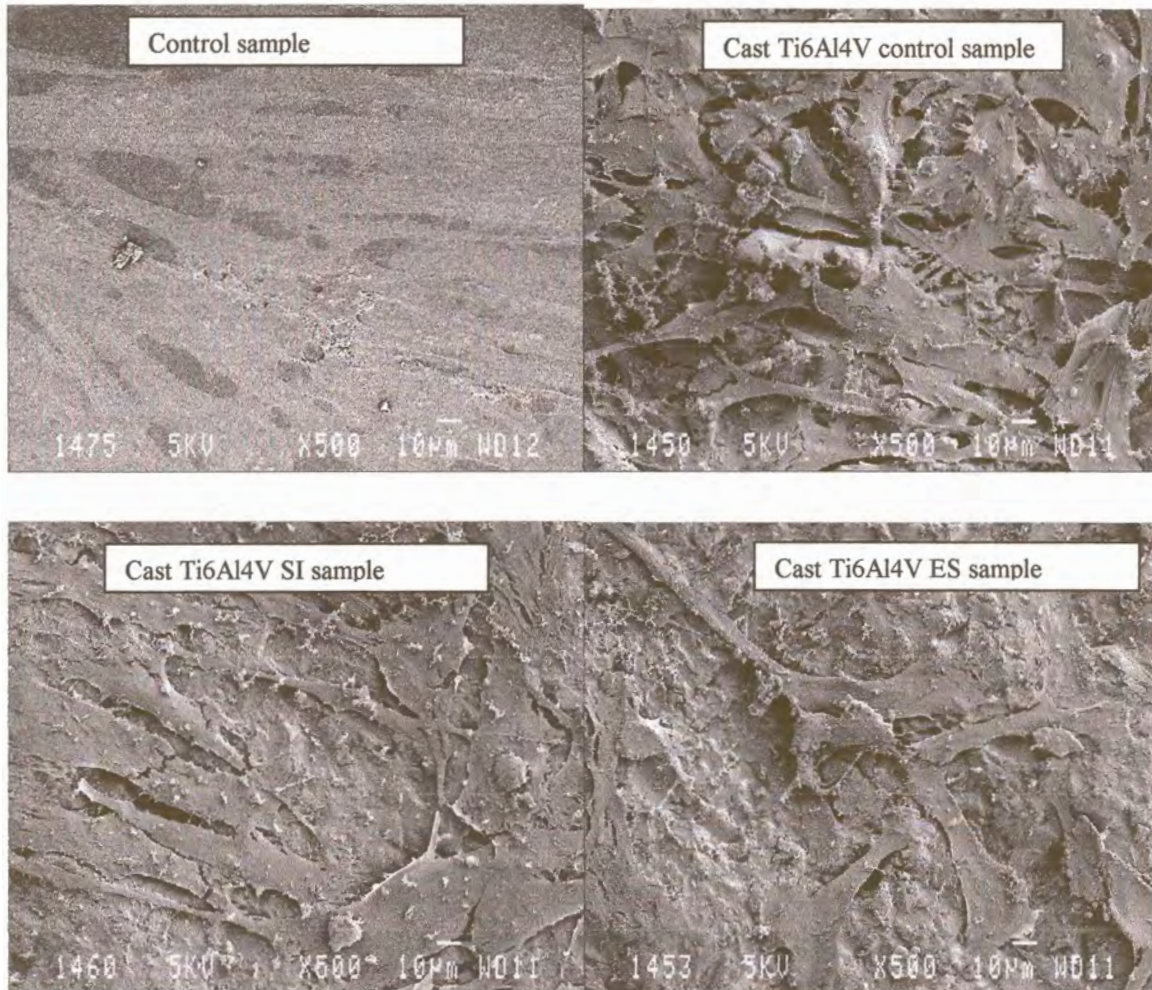
Fig 5-58: Growth of fibroblasts on surfaces of cast Ti6Al4V samples after 2 days incubation

Twenty-eight days

When the control samples are viewed together (see Fig 5-59, p127) no obvious difference can be seen between the fibroblasts. All surfaces are made up of more than a layer of cells and an intercellular matrix of interconnecting fibrils. On the surface cells are seen in the process of dividing and spreading.

Fig 5-59: Growth of fibroblasts on surfaces of control samples after 28 days incubation

Fig 5-60 (see p128) shows fibroblasts on the surfaces of experimentally enhanced samples. An intense monolayer of cells is seen on all surfaces resulting in failure to distinguish the underlying surface topography of samples. After the formation of a cellular layer, the valleys are completely obliterated as can be seen from the image of the machined Ti6Al4V ES sample whose cell layer was torn, probably during processing.
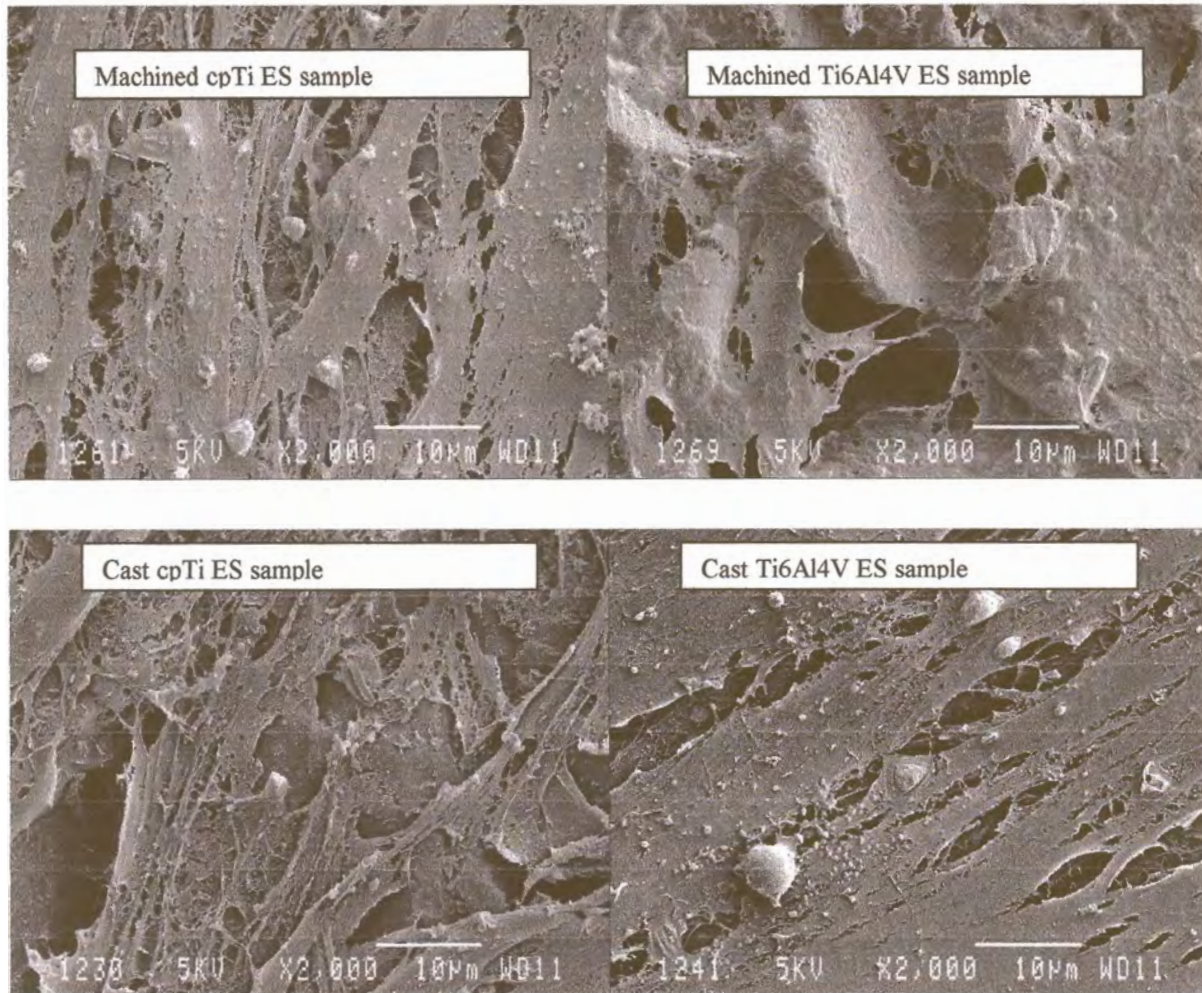
Fig 5-60: Growth of fibroblasts on surfaces of enhanced samples after 28 days incubation

The surfaces of SI enhanced samples also have a similar appearance to experimentally enhanced surfaces (see Fig 5-61, p129). The surface topography is completely obliterated by a carpet of cells. Dividing and spreading cells are seen over the surface. On the control sample a fibroblast is seen with a thickened rounded filopodia extending away from the body of the cell, while on the other samples cells display a flatter appearance of attached filopodia.
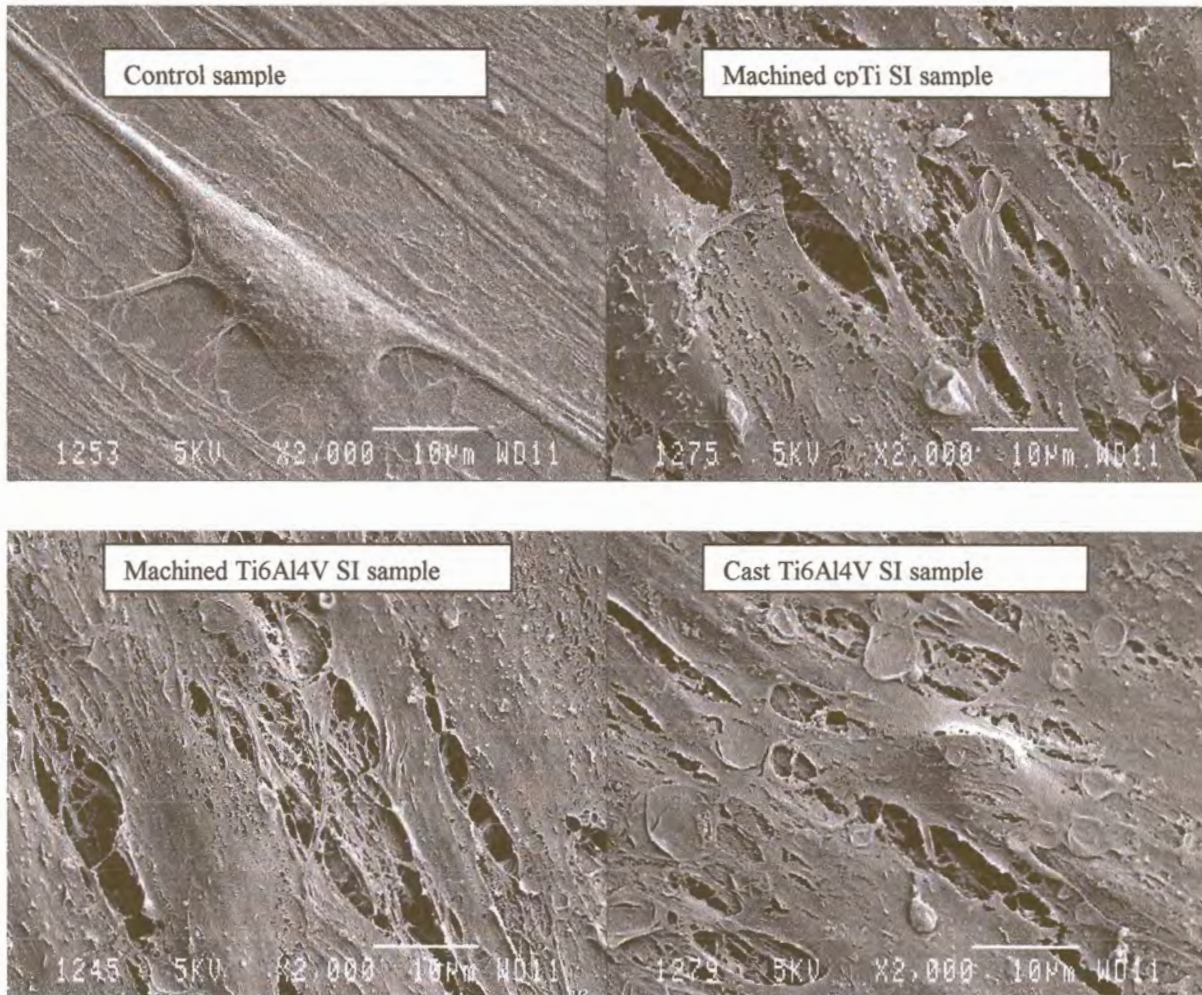
Fig 5-61: Growth of fibroblasts on surfaces of SI enhanced samples after 28 days incubation

5.2.2.2   Osteoblast-like Cells

Two days

Fig 5-62 (see p130) shows the surface of machined cpTi and Ti6Al4V control samples with osteoblasts-like cells completely covering the surface. Flattened cells together with cells that have divided and in the process of attachment and spreading are seen covering the surfaces. The underlying surface topography of machining grooves is displayed.
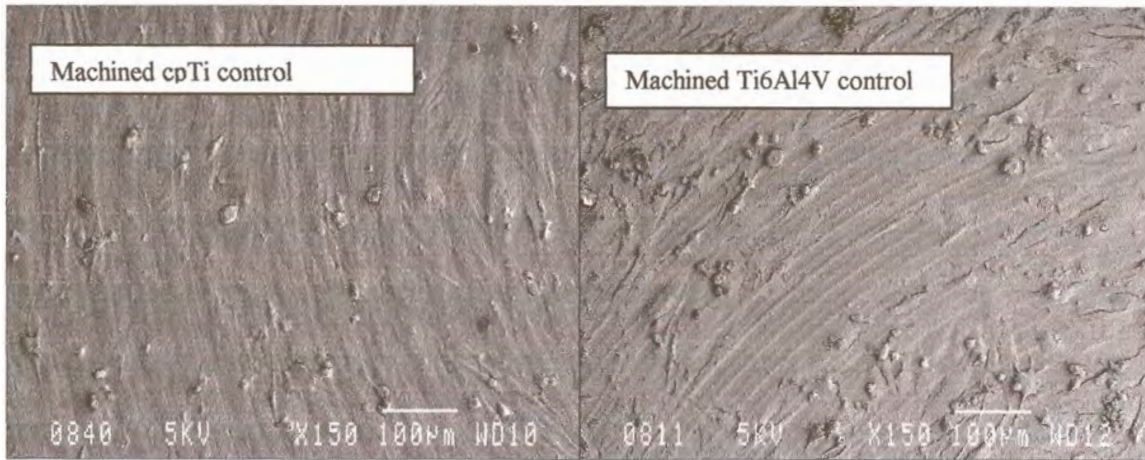
Fig 5-62: Osteoblast-like cells have completely covered the surface of the machined cpTi and Ti6Al4V control sample after 2 days incubation

Regardless of material or surface preparation, machined samples had a similar cell presentation (see Fig 5-63, p131). Osteoblast-like cells had already spread after 2 days as was evidenced by the absence of visible nuclei body within flattened cells. The flattened cells appear polygonal to irregular in shape with complete cytoplasmic extensions of the cell body on the surface (very heterogeneous in appearance). The osteoblasts-like cells spanned across pits and depressions, mostly contacting prominent features of the surface before flattening. Cells that have divided are in the process of attachment as seen over the spread cells.
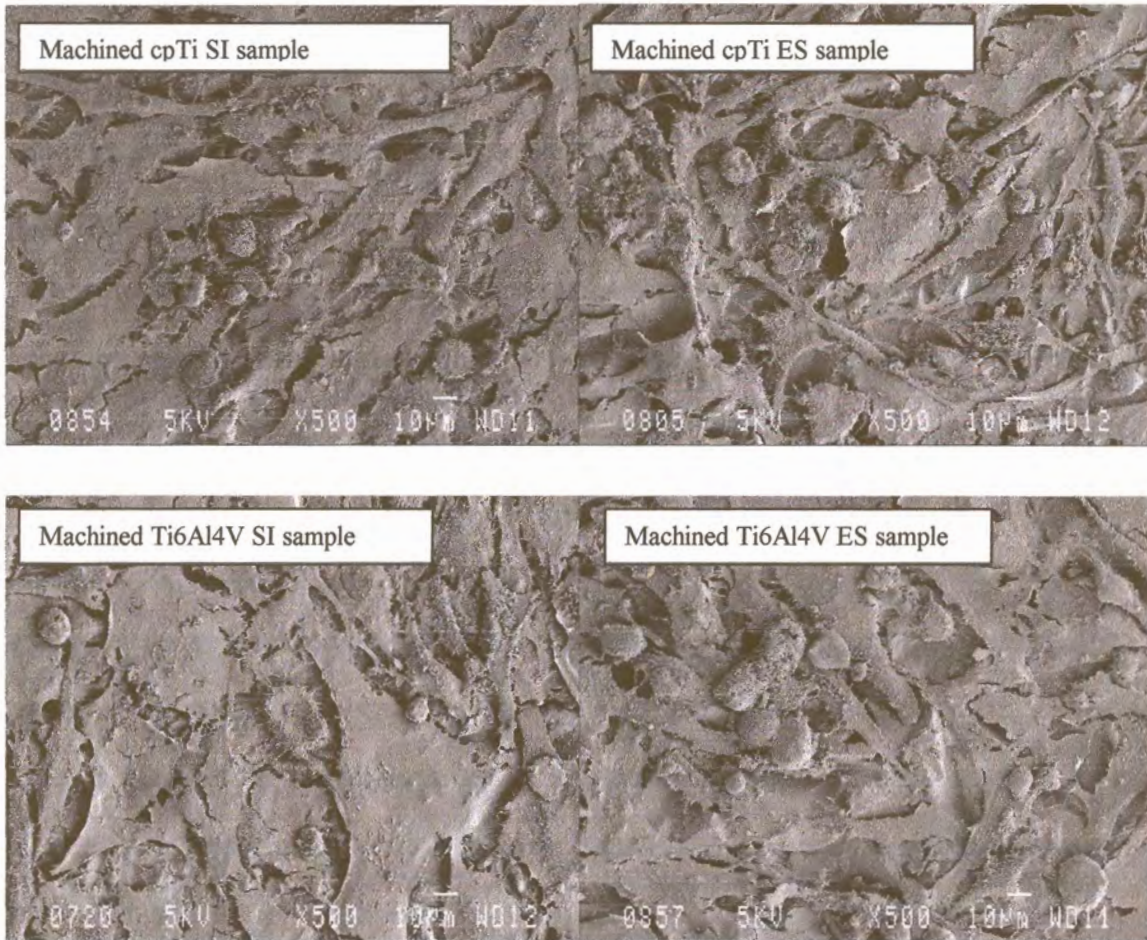
Fig 5-63: Growth of osteoblasts-like cells on surfaces of machined enhanced samples after 2 days incubation

Fig 5-64 shows the surfaces of cast control samples. Osteoblast-like cells are seen to have spread and attached to the peaks. The cell bodies are lifted from the underlying depressions to form a carpet of cells at the surface.
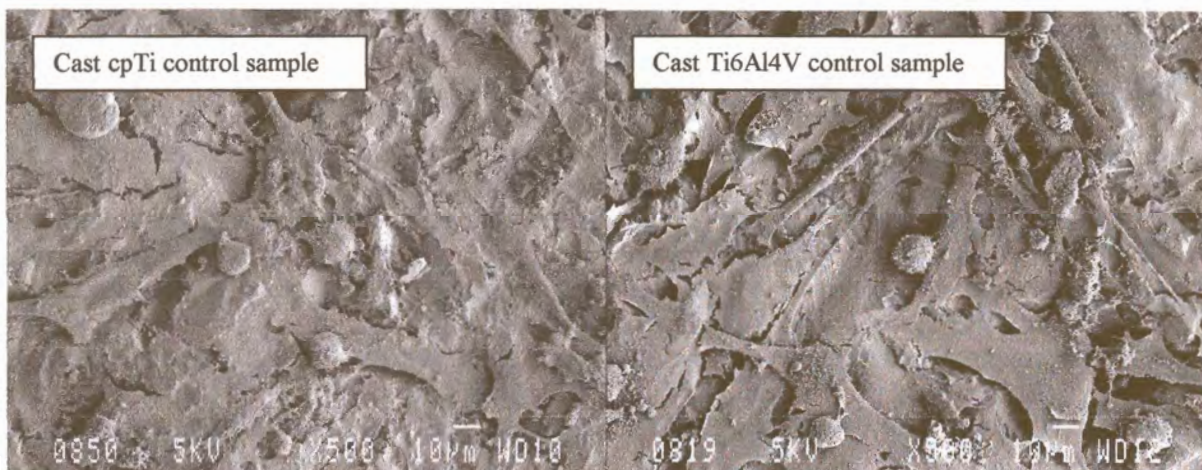
Fig 5-64: Growth of osteoblasts-like cells on surfaces of cast control samples after 2 days incubation

131

Osteoblast-like cells on surfaces of cast enhanced samples are also seen to adhere to peaks and lift off the base to form a layer of cells at the surface (Fig 5-65).
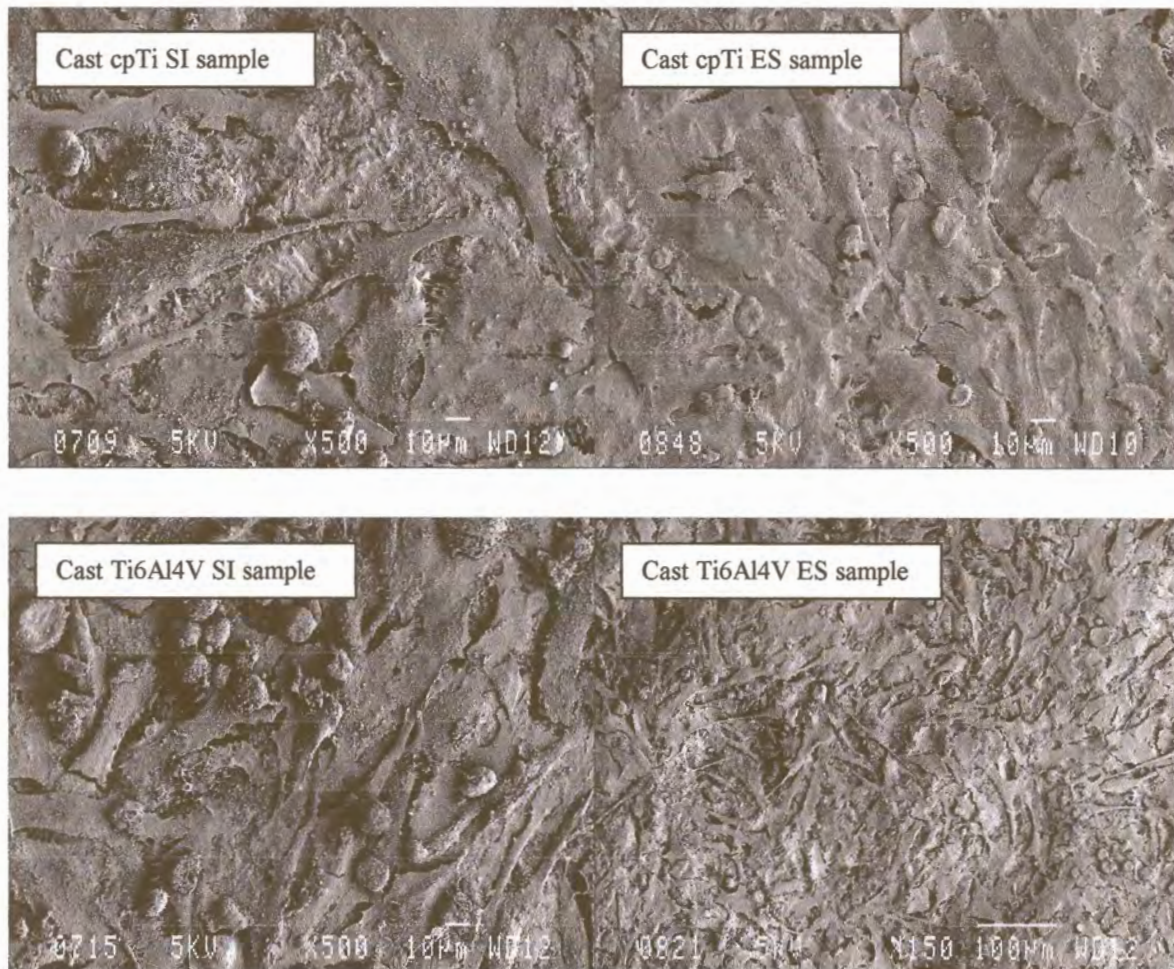

Fig 5-65: Growth of osteoblasts-like cells on surfaces of cast enhanced samples after 2 days incubation

Fig 5-66 (see p133) shows an individual osteoblasts-like cell attached to the surfaces of different samples. Regardless of the surface it is in contact with, the cell has a similar appearance. It is spherical in appearance with its nucleus still very prominent. The cell surface appears rough with foldings and displays numerous microvilli-like projections that anchor the cell to the surfaces. Some of the cells show extensive branching with many smaller filopodia extending in all directions.
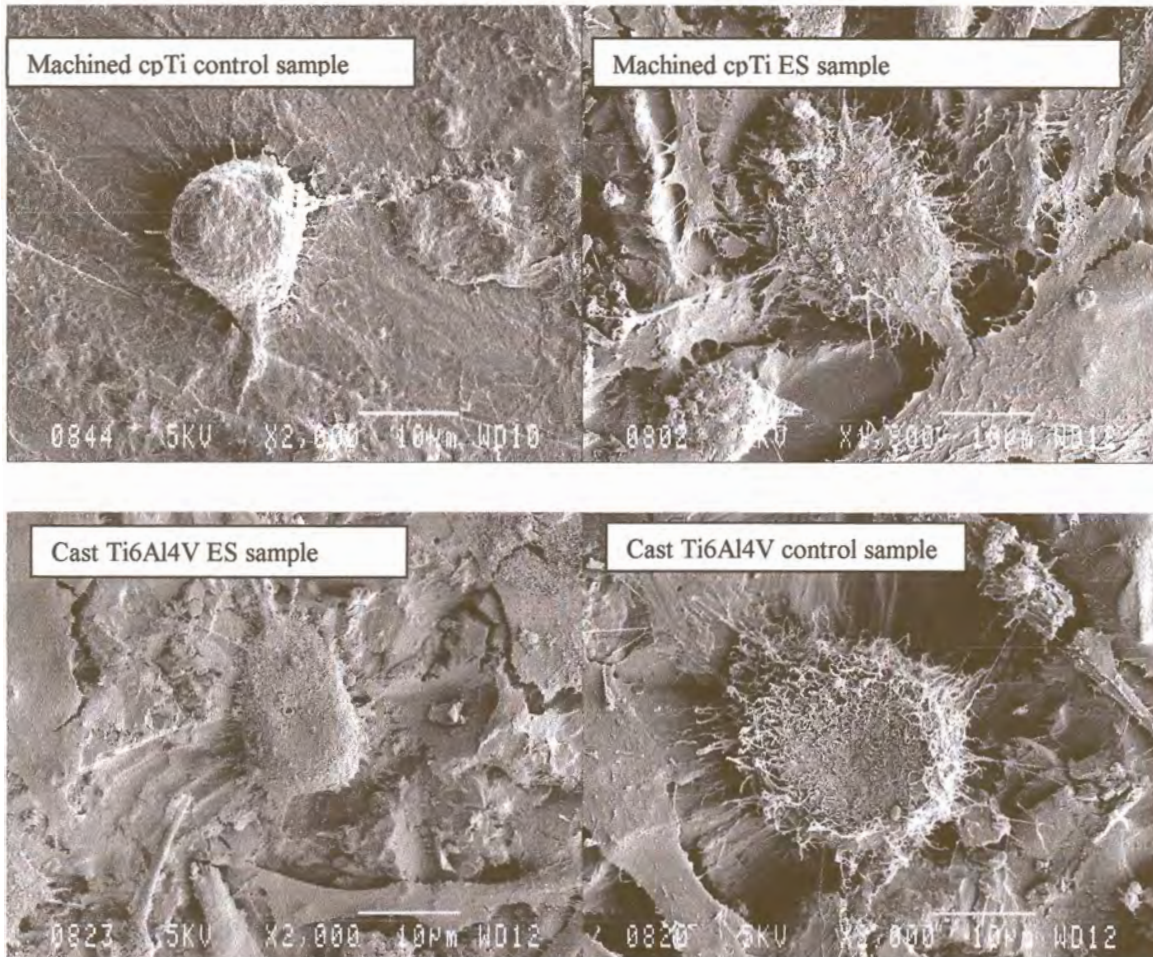
Fig 5-66: Attached osteoblasts-like cell seen on the different Titanium surfaces

Twenty-eight days

Though the cell counts showed a decline in cell growth at 28 days, SEM images shows that the osteoblasts-like cells on surfaces of either machined or cast samples are still in abundance and one surface can not be told apart from another (see Fig 5-67 and 5-68, p134-135). There is a mixture of attached and unattached cells seen over the surfaces. With the exception of the machined control surfaces where cells appeared to lay over the surface in a longitudinal manner, other samples have cells that appear polygonal. While some surfaces are observed to have lots of extracellular deposits (cast cpTi ES and Ti6Al4V SI and machined cpTi SI and Ti6Al4V SI) other samples appear to have numerous cells lying over the surface with some in the process of attachment. More than one layer of cells is obvious.
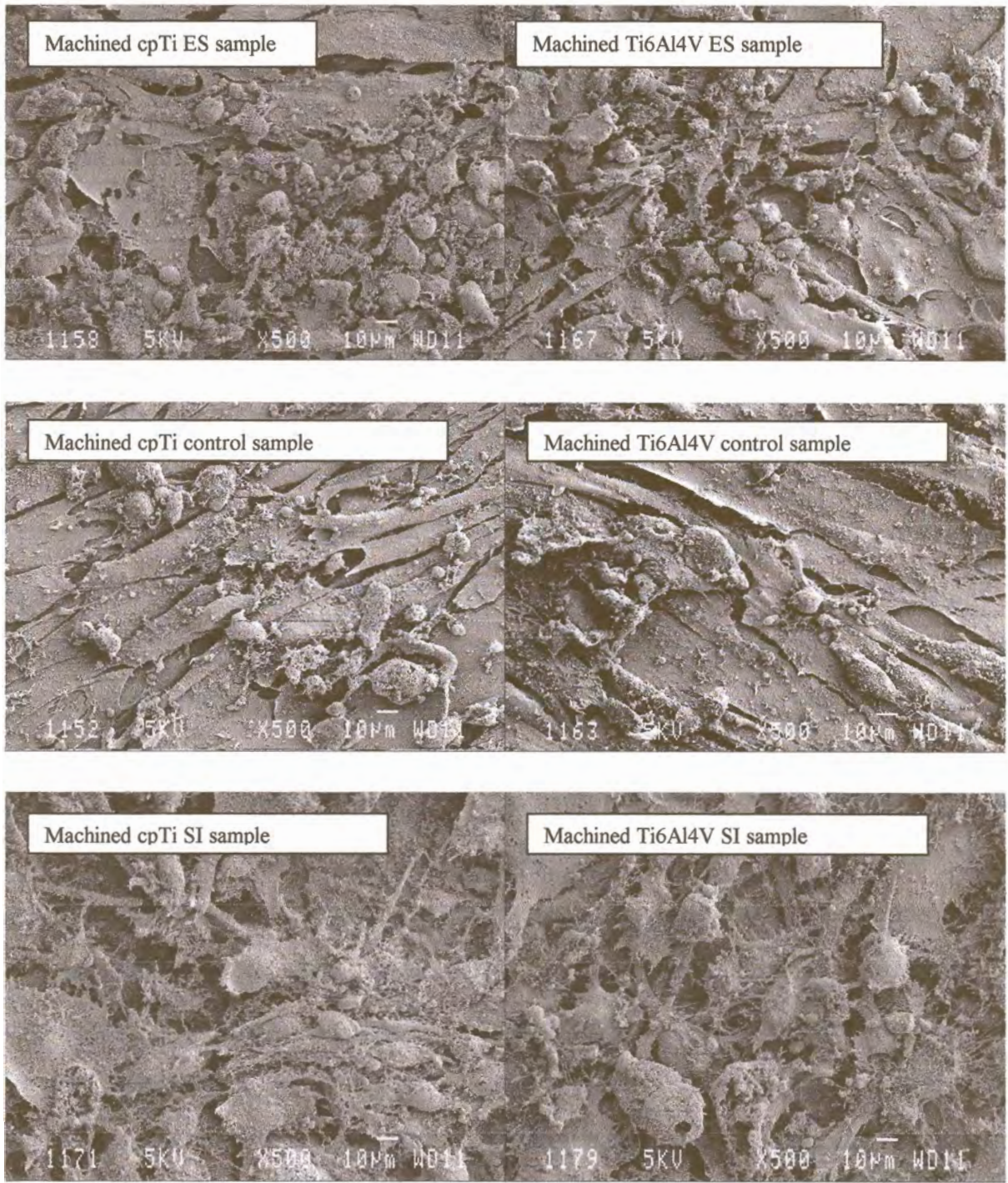
133

Fig 5-67: Growth of osteoblasts-like cells on surfaces of machined samples after 28 days incubation
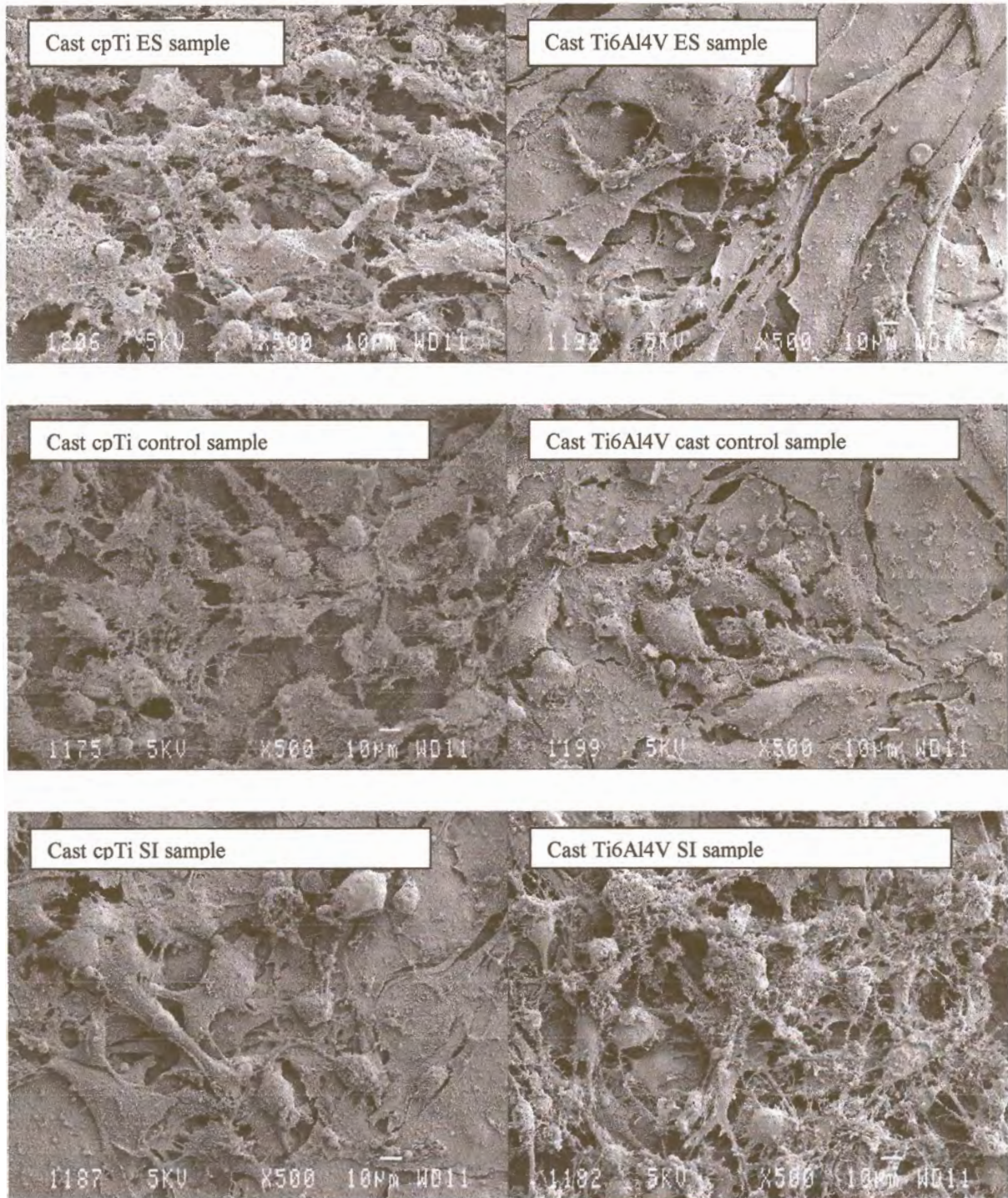
Fig 5-68: Growth of osteoblasts-like cells on surfaces of cast samples after 28 days incubation

In an attempt to migrate on the surface, cells overlapped and superimposed not only with their borders, but often with more extensive involvement of their cell bodies (see Fig 5-69, p136). A network of cell bodies spanned the surface forming a carpet of intertwined cells.
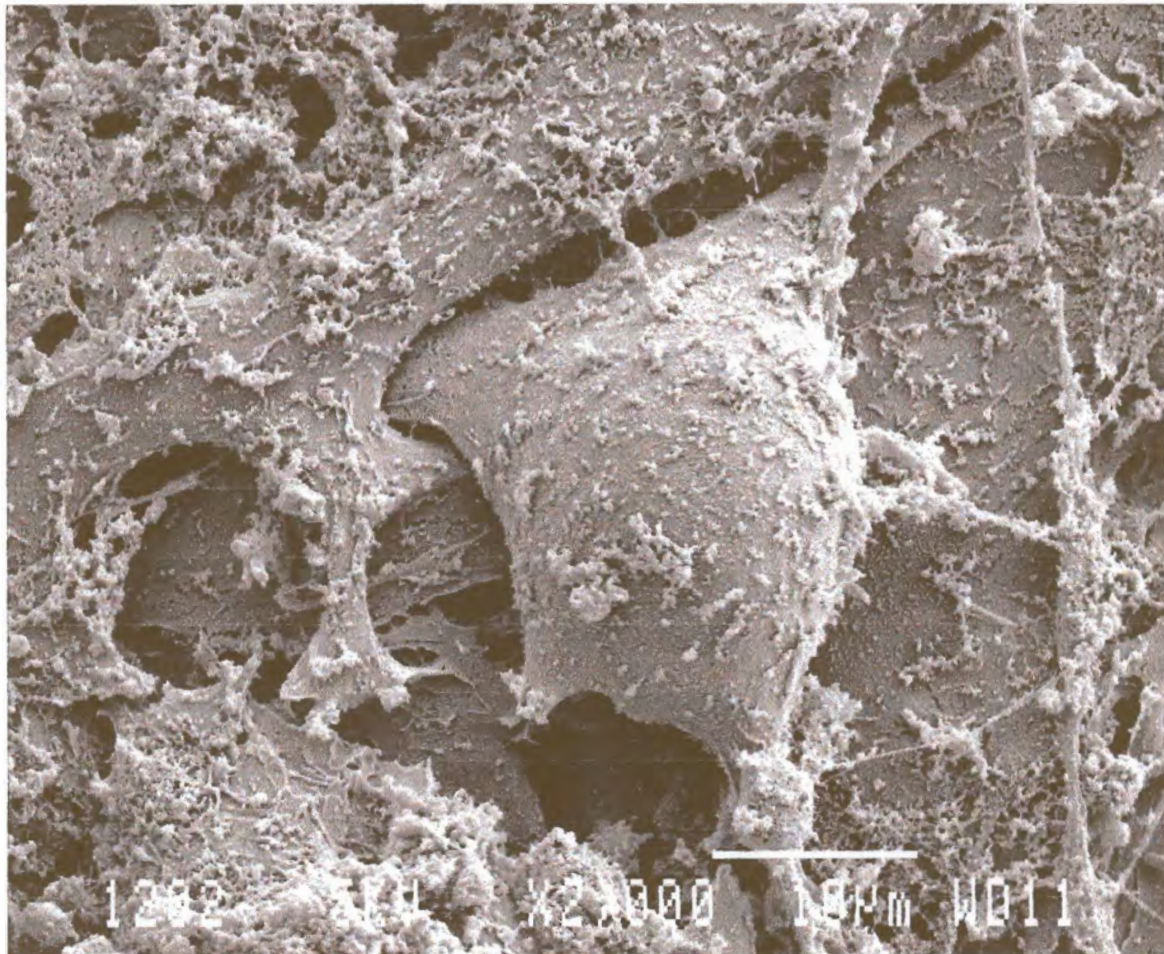
Fig 5-69: Network of osteoblasts-like cells formed on surface of cast Ti6Al4V control samples after 28 days incubation